Sociedade Brasileira de Vácuo

XLVI CBRAVIC
São Carlos – SP
2025

Caderno de Resumos

XLVI Congresso Brasileiro de Aplicações de Vácuo na Indústria e na Ciência

São Carlos - SP

8 a 12 de Novembro de 2025

Dados Internacionais de Catalogação na Publicação (CIP)

C749 Congresso Brasileiro de Aplicações de Vácuo na Indústria e na Ciência (46: 2025: São Carlos, SP).

Caderno de resumos do XLV CBrAVIC [recurso eletrônico] / organizadores: Pedro Augusto de Paula Nascente...[et al.]. – São Carlos: Universidade Federal de São Carlos, 2025.

96 p. : il.
ISBN: 978-65-02-12623-3
DOI: 10.17563/cbravic.2025

1. Ciências aplicadas. 2. Indústria. 3. Tecnologia. I. Nascente, Pedro Augusto de Paula. II. Mastelaro, Valmor Roberto. III. Camargo, Emerson Rodrigues de. IV. Gonçalves, Renato Vitalino. V. Kliauga, Andréa Madeira. VI. Título.

CDU 6
CDD 60

Ficha elaborada pela bibliotecária Priscila Rodrigues dos Santos CRB1/3381

Comitê Organizador

Pedro Augusto de Paula Nascente (Chair) -UFSCar/CCET/DEMa

Valmor Roberto Mastelaro - USP/IFSC/FCM

Emerson Rodrigues de Camargo - UFSCar/CCET/DQ

Renato Vitalino Gonçalves - USP/IFSC/FCM

Andréa Madeira Kliauga - UFSCar/CCET/DEMa

Coordenação técnica

Marcos Dorigão Manfrinato, da FATEC de Sorocaba-SP

Coordenação administrativa

Rejeane Cassia de Luca - Laboratório de Caracterização Estrutural do DEMa/CCET/UFSCar.

Diretoria da Sociedade Brasileira de Vácuo
Presidente: Julio César Sagás (UDESC)
1º Vice-Presidente: Luciano do Nascimento Batista (INMETRO)
2º Vice-Presidente: Márcio Mafra (UTFPR)
1ª Secretária: Luciana Sgarbi Rossino (FATEC-Sorocaba)
2ª Secretária: Júlia Karnopp (UDESC)
1º Tesoureiro: Francisco Alfaro (Biopark)
2º Tesoureiro: Diego Rafael Nespeque Corrêa (UNESP-Bauru)
Diretor Científico: Felipe Carneiro da Silva (FATEC-Cotia)
Diretora Cultural: Denize Kalempa (USP-Lorena)

UFSCar

Sociedade Brasileira de Vácuo

AVACO
TECNOLOGIA EM VÁCUO

ohmini

THORLABS
Compra em dólar e em real
Calibração de Sensores no Brasil

DEMa
UFSCar

ppgcem
Programa de Pós-Graduação em Ciência e Engenharia de Materiais

IFSC
USP

CNPq

FAPESP

CAPES

AVS

JVSS

CPqMAE
Centro de Pesquisas em Materiais Avançados e Energia

Programação do XLVI Congresso Brasileiro de Aplicações de Vácuo na Ciência e na Indústria (CBrAVIC) – São Carlos – novembro de 2025

Os minicursos serão realizados no sábado (08/11) e domingo (09/11) nas dependências do Departamento de Engenharia de Materiais (DEMa), localizado na Área Norte do câmpus São Carlos da UFSCar.

As palestras, comunicações orais e apresentação de pôsteres ocorrerão na segunda-feira (10/11), terça-feira (11/11) e quarta-feira (12/11) no do Centro de Pesquisas em Materiais Avançados e Energia (CPqMAE), localizado na Área Norte do câmpus São Carlos da UFSCar.

08 (sábado) - manhã

08:00 - 12:00
Minicurso: Introdução à Ciência e Tecnologia do Vácuo.
Instrutores: Prof. Francisco Tadeu Degasperi (FATEC-SP) e Dr. Marcelo Juni Ferreira (ESS, Suécia).
Local: Seminários da Chefia do DEMa.

09:00 - 12:00
Minicurso: Caracterização de materiais por microscopia eletrônica de transmissão (TEM) e microscopia de sonda de varredura (SPM).
Instrutores: Profa. Andréa M. Kliauga (UFSCar), Prof. Daniel M. Ugarte (Unicamp) e Prof. Abner de Siervo (Unicamp).
Local: Auditório do LCE.

09:00 - 12:00
Minicurso: Ciência e Tecnologia de Filmes Finos.
Instrutor: Prof. Julio César Sagás (UDESC).
Local: Auditório do PPGCEM.

08 (sábado) - tarde

13:00 – 15:00
Minicurso: Introdução à Ciência e Tecnologia do Vácuo (continuação).
Instrutores: Prof. Francisco Tadeu Degasperi (FATEC-SP) e Dr. Marcelo Juni Ferreira (ESS, Suécia).
Local: Sala de Seminários da Chefia do DEMa.

14:00 – 17:00
Minicurso: Caracterização de materiais por microscopia eletrônica de transmissão (TEM) e microscopia de sonda de varredura (SPM) (continuação)
Instrutores: Profa. Andréa M. Kliauga (UFSCar), Prof. Daniel M. Ugarte (Unicamp) e Prof. Abner de Siervo (Unicamp)
Data: 08 de novembro de 2025.
Horário: 09:00 às 12:00 e 14:00 às 17:00.
Local: Auditório do LCE.

14:00 – 17:00
Minicurso: Ciência e Tecnologia de Filmes Finos (continuação).
Instrutor: Prof. Julio César Sagás (UDESC).
Local: Auditório do PPGCEM.

16:00 – 19:00
Minicurso: Modelagem e Cálculo de Sistemas de Vácuo.
Instrutores: Prof. Dr. Nilberto H. Medina (USP) e Prof. F. Tadeu Degasperi (FATEC-SP).
Local: Sala de Seminários da Chefia do DEMa.

09 (domingo) - manhã

08:00 - 12:00
Minicurso: Caracterização de materiais por espectroscopia de fotoelétrons excitados por raios X (XPS) em ultra-alto vácuo e pressão próxima à ambiente (NAP-XPS).
Instrutores: Prof. Pedro A. P. Nascente (UFSCar), Prof. Fabiano Bernardi (UFRGS), Prof. Valmor R. Mastelaro (USP) e Prof. Renato V. Gonçalves (USP).
Local: Auditório do LCE.

08:30 - 12:00
Minicurso: Introdução à Dinâmica dos Gases Rarefeitos: Teoria e Aplicações aos Sistemas de Vácuo.
Instrutor: Prof. Felix Sharipov (UFPR).
Local: Sala de Seminários da Chefia do DEMa.

09:00 - 12:00
Minicurso: Ciência e Tecnologia de Plasmas.
Instrutores: Prof. Julio César Sagás (UDESC) e Dra. Júlia Karnopp (UDESC).
Local: Auditório do PPGCEM.

09 (domingo) – tarde

13:00 - 15:30
Minicurso: Introdução à Metrologia do Vácuo.
Instrutores: Dr. Luciano do Nascimento Batista (INMETRO) e Prof. F. Tadeu Degasperi (FATEC-SP).
Local: Sala de Seminários da Chefia do DEMa.

14:00 – 17:00
Minicurso: Ciência e Tecnologia de Plasmas (continuação).
Instrutores: Prof. Julio César Sagás (UDESC) e Dra. Júlia Karnopp (UDESC).
Local: Auditório do PPGCEM.

14:00 – 18:00
Minicurso: Caracterização de materiais por espectroscopia de fotoelétrons excitados por raios X (XPS) em ultra-alto vácuo e pressão próxima à ambiente (NAP-XPS) (continuação).
Instrutores: Prof. Pedro A. P. Nascente (UFSCar), Prof. Fabiano Bernardi (UFRGS), Prof. Valmor R. Mastelaro (USP) e Prof. Renato V. Gonçalves (USP).
Local: Auditório do LCE.

Obs.: almoço na Cozinha do Lobo (ADUFSCar) e coffee breaks de manhã e à tarde no saguão do DEMa.

XLVI CBrAVIC

As palestras, comunicações orais e apresentação de pôsteres ocorrerão na segunda-feira (10/11), terça-feira (11/11) e quarta-feira (12/11) no do Centro de Pesquisas em Materiais Avançados e Energia (CPqMAE), localizado na Área Norte do câmpus São Carlos da UFSCar.

10 (segunda-feira) - manhã

08:00 – 9:00 Registro dos participantes do XLVI CBrAVIC.
09:00 – 10:15 Cerimônia de Abertura.
Mestre de Cerimônia: Me. Maria Estela A. P. Canevarolo.
Componentes da Mesa:

Profa. Dra. Maria de Jesus Dutra dos Reis, Vice-Reitora da UFSCar;

Prof. Dr. Moacir Rossi Forim, Pró-Reitor Adjunto de Pesquisa da UFSCar;

Prof. Dr. Luiz Fernando de Oriani e Paulillo, Diretor do Centro de Ciências Exatas e de Tecnologia (CCET) da UFSCar;

Prof. Dr. Osvaldo Novais de Oliveira Júnior, Diretor Instituto de Física de São Carlos (IFSC) da USP;

Prof. Dr. Luiz Antonio Pessan, Diretor de Programas e Bolas da Coordenação de Aperfeiçoamento de Pessoal de Nível Superior (CAPES);

Prof. Dr. Guilherme Zepon, Coordenador do Programa de Pós Graduação em Ciência e Engenharia de Materiais (PPGCEM) do CCET/UFSCar.

Prof. Dr. Guilherme Y. Koga, Chefe do Departamento de Engenharia de Materiais (DEMa) do CCET/UFSCar;

Prof. Dr. Ernesto A. Urquieta-Gonzalez, Coordenador Geral do Centro de Pesquisa em Materiais Avançados e Energia (CPqMAE) do CCET/UFSCar;

Prof. Dr. Julio César Sagás, Presidente da Sociedade Brasileira de Vácuo e professor associado do Departamento de Física do Centro de Ciências e Tecnologia (CCT) da Universidade do Estado de Santa Catarina (UDESC), Joinville, SC;

Prof. Dr. Pedro Augusto de Paula Nascente, Coordenador Geral do XLVI Congresso Brasileiro de Aplicações de Vácuo na Indústria e na Ciência (CBrAVIC 2025) e professor titular do DEMA/CCET/UFSCar.

10:15 – 10:35 Coffee Break.

10:35 – 12:30 Sessão Oral 1. Coordenador: Prof. Pedro A. P. Nascente, Vice-Coordenador: Profa. Andréa M. Kliauga.
10:35 – 11:20 Palestra Convidada 1. Prof. Tim Schäfer, representante da AVS, University of Göttingen, Alemanha, “Molecular Beam Scattering on Oxidized Metal Surfaces: Dynamics and Interactions“.
11:20 – 12:00 Palestra Convidada 2. Prof. Fabiano Bernardi, UFRGS, Porto Alegre, RS, “Probing nanostructures in action: how do they transform during reactions?”
12:00 – 12:30 Comunicação Oral Convidada 1. Profa. Danieli A. P. Reis, Unifesp, São José dos Campos, SP. “Unraveling the Creep Behavior: a Mechanical Assessment of Advanced Thermal Barrier Coatings for Aerospace Applications”.

12:30 – 14:15 Almoço.

14:15 – 17:00 Sessão Oral 2. Coordenador: Dr. Marcelo Juni Ferreira, Vice-Coordenador: Prof. F. Tadeu Degasperi.
14:15 – 15:00 Palestra Convidada 3. Prof. Junichiro Kamiya, Japan Atomic Energy Agency, Japão, “Social Implementation of Vacuum Technology Derived from Accelerators”.
15:00 – 15:30 Comunicação Oral Convidada 2. Profa. Elidiane C. Rangel, Unesp, Sorocaba, SP, “Sputtering on Liquids for the Production of Multimetallic Nanoparticles”.
15:30 – 15:50 Comunicação Oral Selecionada 1. Prof. Francisco Alfaro, Laboratório de Biomateriais e Bioengenharia, Biopark Educação, Toledo, PR. “Plasma-Assisted Optimization of PDMS Surface Functionalization for Durable Chitosan-Based Biofunctional Coatings”.
15:50 – 16:10 Comunicação Oral Selecionada 2. Prof. Felix Sharipov, Universidade Federal do Paraná, Departamento de Física, Curitiba, PR. “Photophoretic Levitation of Perforated Structures in Near-Space Conditions”.

16:10 – 16:30 Coffee Break.
16:30 – 18:30 Sessão de Pôsteres 1. Coordenadores: Prof. Fabiano Bernardi e Prof. Valmor R. Mastelaro.

11 (terça-feira) - manhã

08:00 – 10:00 Sessão Oral 3. Coordenadora: Profa. Maria Luiza Rocco, Vice-Coordenadora: Profa. Elidiane C. Rangel.
08:00 08:45 Palestra Convidada 4. Prof. André A. Pasa, Universidade Federal de Santa Catarina, Florianópolis, SC, "Potassium Intercalation in Prussian Blue Thin Films for Sustainable Battery Applications".
08:45 – 09:30 Palestra Convidada 5. Prof. Miguel D. Sánchez, Universidad Nacional del Sur, Bahia Blanca, Argentina, "Metal-Support Interaction Synergy in Low-Loaded Palladium Catalysts".
09:30 – 10:00 Comunicação Oral Convidada 3. Prof. Konstantin Kostov, Unesp, Guaratinguetá, SP, "Explanation of Temperature Distribution in Helium Streams Expanding in Atmospheric Air".

10:00– 10:20 Coffee Break.

10:20 – 12:20 Sessão Oral 4. Coordenadora: Dra. Nazir Monteiro dos Santos, Vice-Coordenador: Prof. Jeferson A. Moreto.
10:20 – 11:05 Palestra Convidada 6. Profa. Lúcia Vieira, Univap, São José dos Campos, SP, "Reparo de Feridas Usando Curativos Eletrofiados de PVA-CA e Plasma Frio In Vivo".
11:05 – 11:35 Comunicação Oral Convidada 4. Profa. Maria Luiza Rocco, Universidade Federal do Rio de Janeiro, Rio de Janeiro, RJ, "The Interplay of Electronic Structure, Morphology and Charge Transfer Dynamics of Semiconductors with Application in Organic Solar Cells".
11:35 – 11:55 Comunicação Oral Selecionada 3. Prof. Rodrigo S. Pessoa, Instituto Tecnológico de Aeronáutica, São José dos Campos, SP. "Plasma-Activated Liquids: Generation, Characterization and Applications in Biomedicine and Materials Science".
11:55 – 12:25 Comunicação Oral Selecionada 4. Dra. Thaisa B. F. Moraes, Universidade de São Paulo, Escola de Engenharia de Lorena. "Viologen-Based Films Electrodeposited on ITO: a Stable and Conductive Platform for Immobilizing Molecular Catalysts".

12:25 – 14:15 Almoço.

14:15 – 16:00 Sessão Oral 5. Coordenador: Prof. Julio C. Sagás, Vice-Coordenador: Prof. Luis C. Fontana.
14:15 – 15: 00 Palestra Convidada 7. Prof. Marcelo Maia da Costa (PUC-Rio, Rio de Janeiro, RJ), "Obtaining Two-Dimensional Materials for Sensor Applications".
15:00 – 15:30 Comunicação Oral Convidada 5. Dr. Marcelo Juni Ferreira, European Spallation Source, Lund, Suécia, "ESS Proton Beam Commissioning on Dump and Vacuum System Operation for Beam on Target".
15:30 – 16:00 Comunicação Oral Convidada 6. Diego Mantovani, Laval University, Quebec, Canada. "Low-Vacuum Glow Discharge for the Innovation in Biomaterials and Implants for Health, Food, and Agriculture".

16:00 – 16:25 Coffee Break.
1
16:25 – 18:25 Sessão de Pôsteres 2. Coordenadores: Profa. Elidiane Rangel, Prof. Carlos R. Grandini e Prof. Diego R. N. Corrêa.

12 (quarta-feira) - manhã
08:00 – 10:30 Sessão Oral 6: Vácuo na Indústria. Coordenador: Prof. F. Tadeu Deagsperi (organizador), Vice-Coordenador: Dr. Álvaro J. Damião.
Abertura, escopo e objetivos.
08:00 – 08:30Sr. Fernando Zappelline, AHETEST Ltda., Cotia, SP. "Detecção de Vazamentos em Sistemas de

Vácuo Industriais".
08:30 – 09:00 Sr. Fernando J. Arroyo, FCA Usinagem, Campinas, SP. "Aspectos Construtivos de Sistemas de Vácuo".
09:00 – 09:30 Dr. Luciano do Nascimento Batista, LAPRE-INMETRO, Xerém, RJ. "A Necessidade da Metrologia de Vácuo na Indústria e na Ciência".
09:30 – 10:00 Sr. Maurício Oliveira Costa, TEX Equipamentos Eletrônicos, Itupeva, SP. "Instrumentação à Determinação de Estanqueidade e à Medição de Quantidade de Gás em Sistemas Industriais".
10:00 – 10:30 Sr. Hugo A. Garrido Aguiar, Centro Tecnológico de Metrologia, São Paulo, SP. " A Metrologia de Vácuo; Serviços de Metrologia de Pressão e Vácuo com Quantidade de Gás".

10:30– 10:50 Coffee Break.

10:50 – 12:10 Sessão Oral 7. Coordenador: Prof. Marcos Dorigão Manfrinato, Vice-Coordenador: Prof. Konstantin G. Kostov.
10:50 – 11:10 Comunicação Oral Selecionada 5. Dra Júlia Karnopp, Universidade do Estado de Santa Catarina, Centro de Ciências Tecnológicas, Joinville, SC. "Exploring the Individual and Combined Effects of Long-Lived Reactive Species on Plasma-Activated Water".
11:10 – 11:30 Comunicação Oral Selecionada 6. Sr. Otávio A. M. Silva, Universidade Federal de Lavras, Escola de Engenharia, Departamento de Engenharia Química e de Materiais, Lavras, MG. "Functionalization of Ti by Cold Plasma with Silver Nanoparticles and Adhesion Analysis".
11:30 – 11:50 Comunicação Oral Selecionada 7. Dra. Nazir Monteiro dos Santos, Instituto de Estudos Avançados, São José dos Campos, SP. "Structural Characterization of Thermal Barrier Coatings under Extreme Thermal Loading in Subsonic Plasma Flow for Atmospheric Reentry Applications".
11:50 – 12:10 Comunicação Oral Selecionada 8. Prof. Conrado R. M. Afonso, Universidade Federal de São Carlos, Departamento de Engenharia de Materiais, São Carlos, SP. "Processing of Ti-33Zr-33Nb Beta Alloy Processed by Casting, Laser 3D Printing, and Severe Plastic Deformation".

12 (quarta-feira) – tarde

12:10 – 14:00 Almoço.

14:00 – 16:0 Sessão de Pôsteres 3. Coordenadores: Prof. Rogério P. Mota e Prof. Emerson Camargo.
16:00 – 16:20 Coffee Break.
16:20 – 16:40 Informações sobre a Revista Brasileira de Aplicações de Vácuo.
16:40 - 18:00 Assembleia, Encerramento e Premiações.

CVD DIAMOND FILM FROM METHANE GAS ON P-TYPE SILICON SUBSTRATE: CHARACTERIZATION AND APPLICATIONS IN INDUSTRY

Yago dos Santos Campos[1]*, Evaldo Chagas Gouvêa[1], Teófilo Miguel de Souza[1]
[1]*UNESP - Faculdade de Engenharia e Ciências - Guaratinguetá Campus*

1. Introduction

Diamond exhibits exceptional properties such as hardness, chemical inertness, and high thermal conductivity, making it highly valued in various industrial sectors [1]. This work aims to characterize CVD diamond thin films deposited on a P-type silicon substrate and explore their potential industrial applications, with particular emphasis on the oil and gas industry, where durability is crucial in severe environments.

2. Experimental

Initially, a literature review on diamond properties and applications was conducted. Thin films were synthesized using the HFCVD method on P-type and intrinsic silicon substrates, using a mixture of methane and hydrogen. The HFCVD reactor operated at a pressure of 20 Torr, with a gas mixture of 1.5% CH_4 and 98.5% H_2. The substrate was maintained at approximately 800 °C, with heated tungsten filaments responsible for methane dissociation. The samples were characterized by optical microscopy, SEM, and EDS.

3. Results and Discussions

Optical microscopy with linear polarization (Fig. 1) revealed a uniform, polycrystalline surface with good coverage of the silicon substrate. SEM revealed homogeneous microstructures with diamond crystals exhibiting a varied particle size distribution, demonstrating good growth on both substrate types (Fig. 2). EDS analysis confirmed high purity (>98% carbon), with trace amounts of tungsten from the filaments (HFCVD).

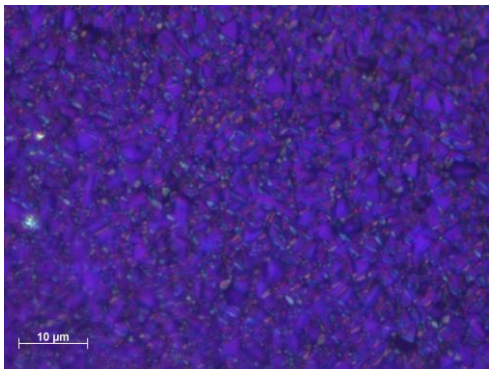

Fig. 1. *Image of CVD diamond sample by optical microscopy.*

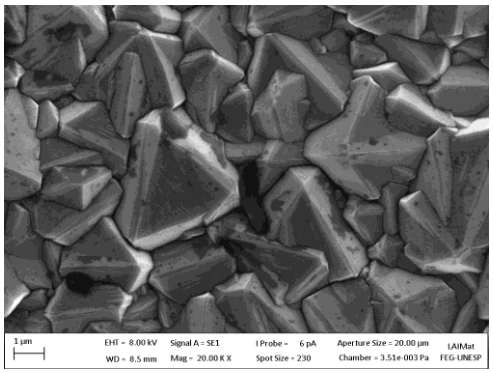

Fig. 2. *Image of CVD diamond sample on P-type substrate by SEM, with 20,000 X magnification.*

The observed properties of diamond films, combined with their hardness, high thermal conductivity, and low friction coefficient, make these films promising industrial applications. These include: valve and mechanical seal coatings in corrosive environments [2]; thermal dissipation in high-power transistors [3]; and optical windows for harsh environments [1], such as in oil extraction and refining processes.

4. References

[1] R. M. Nor *et al.*, "Diamond: Synthesis, characterisation and applications," *Advanced Structured Materials,* vol. 5, pp. 195–217, 2010. [Online]. Available: http://dx.doi.org/10.1007/8611_2010_17. [Accessed: Jul. 30, 2025].
[2] D. W. Wheeler, "Applications of diamond to improve tribological performance in the oil and gas industry," *Lubricants,* vol. 6, no. 3, 2018. [Online]. Available: https://www.mdpi.com/2075-4442/6/3/84. [Accessed: Aug. 7, 2025].
[3] M. Chernykh *et al.*, "GaN-based heterostructures with CVD diamond heat sinks: A new fabrication approach towards efficient electronic devices," *Applied Materials Today,* vol. 26, 2022. [Online]. Available: https://doi.org/10.1016/j.apmt.2021.101338. [Accessed: Jul. 30, 2025].

Acknowledgments

We gratefully acknowledge the financial support from the Programa de Formação de Recursos Humanos da ANP – PRH 34.1/FEG/UNESP (ANP Human Resources Development Program), which enabled the development of this work and participation in the conference. We also thank Professor Luís Rogério de Oliveira Hein for his valuable assistance in obtaining the diamond film images at LAIMat.
*Corresponding author: yago.campos@unesp.br

ATOMIC LAYER DEPOSITION OF AL_2O_3 ON PLA: IMPROVING RESISTANCE TO ATOMIC OXYGEN IN LOW-EARTH ORBIT

T. M. Vieira[1], M.P. Gomes[1], N.K.A.M. Galvão[2], F.C. Dalan[1], A.S.S. Sobrinho[1], H.S. Maciel[1*] and R.S. Pessoa[1]
[1]*Plasmas and Processes Laboratory (LPP), Aeronautics Institute of Technology (ITA), 12228-900, São José dos Campos-SP, Brazil*
[2] *Instituto Nacional de Pesquisas Espaciais (INPE), 12227-010, São José dos Campos-SP, Brazil*

1. Introduction

Polylactic acid (PLA) is a biodegradable polymer widely used in additive manufacturing due to its low cost and easy processing [1]. Despite its potential for Aerospace application, PLA has poor thermal stability, low environmental resistance, and degrades under harsh conditions. In low-Earth orbit, atomic oxygen (AO) accelerates surface erosion of PLA [7]. To mitigate this effect, protective coatings such as aluminum oxide (Al_2O_3) deposited by atomic layer deposition (ALD) was studied. Results show ALD Al_2O_3 provides lightweight, uniform protection, improving PLA durability in space.

2. Experimental

PLA samples (20 × 20 × 2 mm³) were 3D-printed with PLA PREMIUM HT filament and coated with Al_2O_3 films by thermal ALD at 100 °C using trimethylaluminum (TMA) and deionized water as precursors. Five coating thicknesses (100, 250, 500, 750, and 1000 cycles) were prepared and immersed into low-pressure oxygen plasma, so being exposed to neutral AO and energetic ion conditions. AO density was measured by optical emission actinometry, while SEM, ellipsometry, and gravimetric analysis evaluated structural and mass changes.

3. Results and Discussions

Even ultrathin films (16.5 nm) effectively protected against neutral AO exposure, while thicker coatings (101 nm) prevented erosion entirely, even under energetic ion conditions. These findings highlight ALD-deposited Al_2O_3 as a lightweight and efficient strategy to enhance PLA durability in harsh LEO environments.

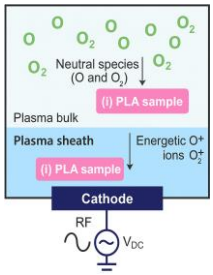

Fig. 1. *Schematic of the RIE setup with PLA samples in two positions.*

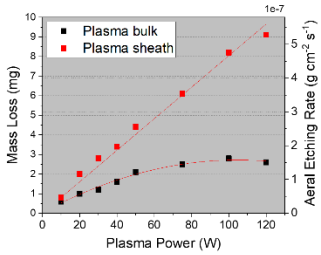

Fig. 2. *Δm (left) and etching rate (right) of uncoated PLA after 1800 s O_2 plasma vs. RF power, for bulk (black) and sheath (red).*

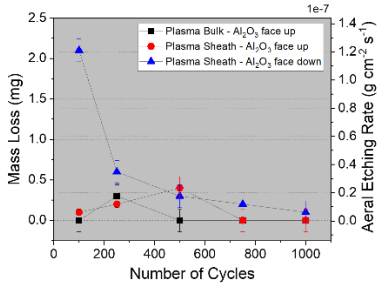

Fig. 3. *Δm (left) and etching rate (right) of Al_2O_3-coated PLA vs. ALD cycles (100–1000). Conditions: 100 W, 1800 s, O_2 plasma at 2×10^{-2} Torr.*

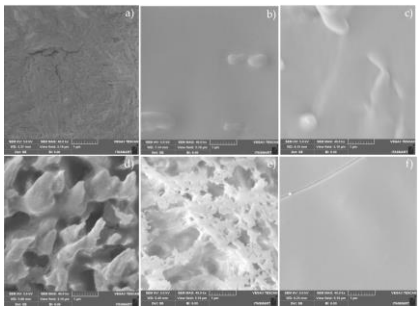

Fig. 4. *SEM micrographs of PLA: (a–c) uncoated, 100 ALD cycles, 1000 ALD cycles; (d–f) same samples after O_2 plasma (100 W, 1800 s, 2×10^{-2} Torr).*

4. References

[1]- P. Favia and R. D'Agostino, Surf. & Coat. Tech., **98**, 1102-1106, (1998).
[2]- H. Yasuda *"Plasma Polymerization"*, 2nd edition, Academic Press, USA, (1980).

Acknowledgments
FAPESP (2022/11544-0), CNPq AEB–Uniespaço (405637/2022-5), CAPES, CNPq and CNPq PCI (300217/2024-2).

CHARACTERIZATION OF A HOME-MADE DC SPUTTER SYSTEM

Henrique Moreira Pinto[1], David Amorin Silva[1], Giuseppe Antonio Cirino[1]*
[1] *Depto Eng Elétrica - CCET - UFSCar*

1. Introduction

The semiconductor industry uses a wide range of materials in the form of thin films, obtained from a multitude of techniques. This work reports the performance characterization of a low-cost home-built planar direct current (DC) sputter system. This characterization was carried out concerning the discharge electric breakdown for argon at low pressure, as well as the limits of operation of the DC power supply.

2. Experimental

Figure 1 shows a home-built parallel plate DC sputter system [1]. It comprises a 5 mm- thick borosilicate glass tube (150 mm height and 150 mm inner diameter), sealed by two 316-L stainless steel flanges. The water-cooled cathode comprises the top electrode, and the anode is at the bottom. The cathode diameter is 120 mm and a variable inter electrode distance, D, within the range 30 < D < 80 mm is allowed. Experiments were carried out for argon plasma, with copper target.

3. Results and Discussions

The electric breakdown characterization of our DC sputter system was carried out by determining its Paschen's curve, fig. 2. The equation showed inset fig.2 was fitted over the experimental data, enabling one to estimate the constants A = 15 [Torr-1·cm-1], B = 210 [V·Torr-1·cm-1] and γe = 0.012 [electrons / incident ion] [2]. For most DC sputtering systems γe is in the range 0.01 < γe < 0.1, so at the target, the dominating fraction of the discharge current is due to ions towards the cathode.

Fig. 3 shows a typical I_{AK} - V_{AK} characterization of the discharge, for a multitude of combination of pressure and inter electrode distance. The maximum power hyperbole (dot- trace line) is plotted together. The deposition process must operate inside the rectangular area delimited by 85 mA and 1.5 kV.

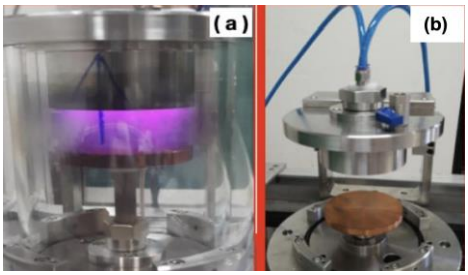

Fig. 1. *DC sputter system. (a) argon plasma at 100 mTorr; (b) anode (bottom) and water-cooled cathode (top).*

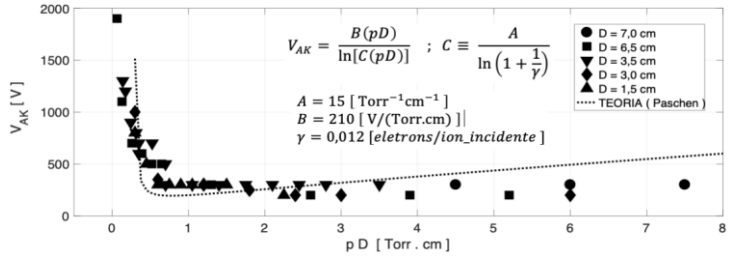

Fig. 2. *Paschen's curve obtained from the sputter system used in this work, for argon plasma and copper target.*

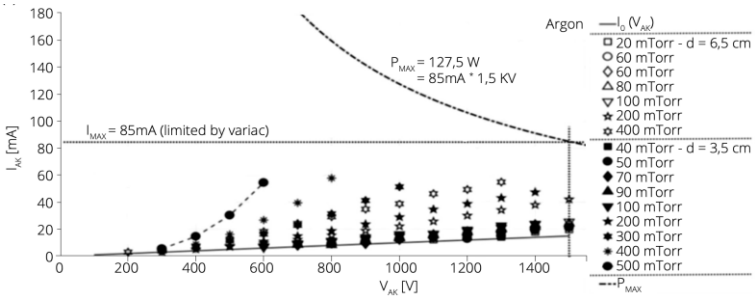

Fig. 3. *I-V characterization of the discharge. The maximum power hyperbole (dot- trace line) is plotted together. The deposition process must operate inside the rectangular area delimited by 85 mA and 1.5 kV.*

4. References

[1] H.M. Pinto, MSc Thesis, UFSCar, (2022).
[2] H.M. Pinto and G.A. Cirino, Rev. Bras. Apl. Vac., 42, e0423 (2023).
*Corresponding author: gcirino@ufscar.br

COLD PLASMA AS A SUSTAINABLE TOOL FOR REMOVING SULFAMETHOXAZOLE-TYPE ANTIBIOTICS FROM WATER

Luan Pereira Goussain Filippo[1]*, Bruno Henrique da Silva Leal[1], Karla Virginia Leite Lima[2], David Luiz Arruda da Silva[2], Konstantin Georgiev Kostov[1], Raquel Fernandes Pupo Nogueira[2], William Chiappim Junior[1]
[1]*São Paulo State University (UNESP), Guaratinguetá, São Paulo*
[2]*São Paulo State University (UNESP), Araraquara, São Paulo*

1. Introduction

Water pollution by emerging contaminants has become a major concern, with about 26% of rivers containing concentrations above safety thresholds for common compounds such as caffeine, nicotine, analgesics, and antibiotics [1]. As an eco-friendly alternative, the design and optimization of non-thermal atmospheric pressure plasma (NTAPP) systems are crucial, since they provide significant benefits over conventional chemical treatments, especially by avoiding solvents potentially harmful to the environment [2]. In this context, this study introduces the Affordable Plasma Device (APD), a modular parallel-plate dielectric barrier discharge reactor, proposed as a low-cost and sustainable solution for resource-limited settings.

2. Experimental

The APD was tested under multiple configurations, with power and water treatment efficiency assessed as criteria to identify the most effective operating mode. Pharmaceutical degradation was examined using sulfamethoxazole (SMX), a common antibiotic in medicine, through quantification of its removal rate in water and evaluation of possible degradation pathways. The study employed ultraviolet-visible (UV-Vis) spectroscopy, detection of reactive oxygen and nitrogen species (RONS), and high-performance liquid chromatography (HPLC).

3. Results and Discussions

The plasma device showed capacity to generate RONS in NTAPP with limited resources, operating under high voltages supplied by an adapted source. Its modular design enables use in different configurations, including systems with liquid or gas flow, yielding a low-cost technology. In PAW production, the reactor worked indirectly in water treatment, promoting notable acidification, with a decrease of up to 2.88 pH units in 60 minutes, linked to H+ release via RONS dissociation at the gas–liquid interface. Moreover, strong nitrate incorporation in water was detected, while ozone formation stayed confined to the air interface, with the RONS produced illustrated in figure 1. In pharmaceutical degradation assays, SMX exhibited 88 ± 7% removal without catalysts, mainly ascribed to superoxide radicals, while hydrogen peroxide contribution was minor. The degradation profile appears in figure 2.

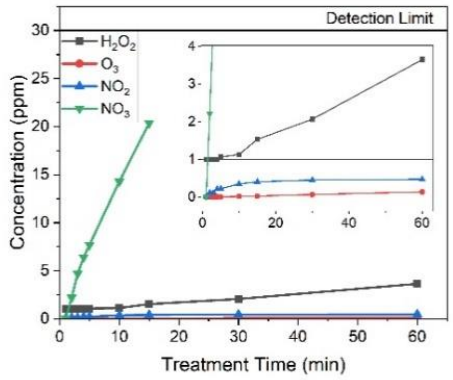

Fig. 1. *RONS Generation in Deionized Water*

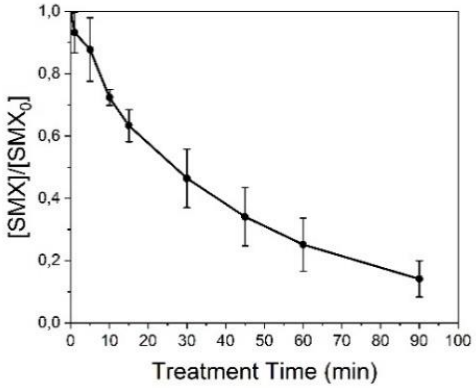

Fig. 2. *SMX Degradation by Treatment Time*

4. References

[1]- WILKINSON, J. et al. Proceedings of the National Academy of Sciences of the United States of America, 2022.
[2]- SINGH, M.; VAJPAYEE, M.; LEDWANI, L. Materials Today: Proceedings, v. 43, p. 2868–2871, 2021.

Acknowledgments

This work wouldn't be possible without the collaboration of the team at LPP a
*Corresponding author: luan.filippo@unesp.br

CHARACTERIZATION OF ATMOSPHERIC PRESSURE PLASMA TORCH

David Amorin Silva[1], Heitor Vinicius Mercaldi[1], Giuseppe Antonio Cirino[1]*
[1] *Depto Eng Elétrica - CCET – UFSCar*

1. Introduction

The use of atmospheric plasma torch has increased exponentially in several knowledge domains, from medicine [1] to agriculture [2]. Theses benefits occur due to the generation of reactive oxygen species (ROS), hydrogen-containing ROS (H-ROS) and reactive nitrogen species (RNS) in the vicinity of the plasma torch. This work reports the electrical, optical and thermal characterizations of a DBD-like atmospheric-pressure plasma torch prototype.

2. Experimental

Our prototype consists of two borosilicate concentric tubes, with electrodes whereby we apply high voltage pulses, fig.1. A home-made high-voltage pulses controller was developed and used to supply high-voltage between the inner electrode and the outer ring electrode by means of a PWM signal. Argon at a flow rate of 8 l/min was applied to break down the discharge. OES spectra were collected by using a USB4000 unity from Ocean Optics®. Thermal imaging was collected by using a thermal camera model C4 from FLIR®.

3. Results and Discussions

Figure 2 shows (right) a typical waveform applied to the electrodes in order to ignite the discharge. Pulses period is T=1us, but still with strong oscillations, which tends to increase the discharge temperature. At left it shows the linear behaviour of the pulse amplitude applied to the electrodes as a function of the duty cycle of the PWM modulator.

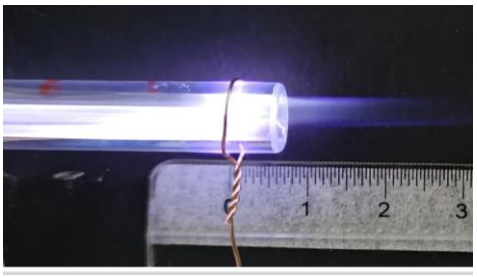

Fig. 1. *Prototype of the DBD-like atmospheric-pressure plasma torch: internal filament with external ring shape electrode.*

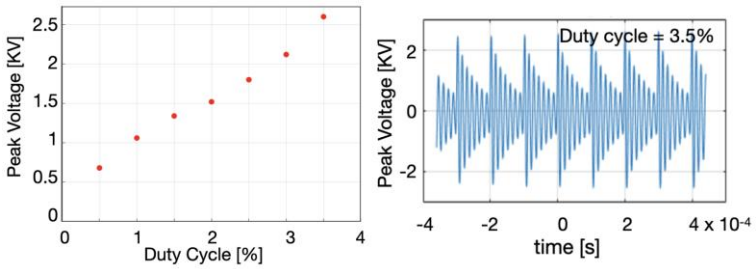

Fig. 2. *(right) Waveform applied to the electrodes in order to ignite the discharge; (left) Peak voltage applied to the electrodes as a function of the duty cycle of the PWM modulator.*

Thermal imaging were collected when the plasma plume impinges a paper sheet target (75 g/cm2) located 1 cm away from the tube end, fig. 3. The target temperature increases with the duty cycle, but still bellow 36 oC. OES characterization identified the presence of hidroxil (OH, 308 nm) radicals as well as other nitrogen species, fig.4. The high oxidation potential of OH show its strong oxidizing properties in melanoma treatment [1].

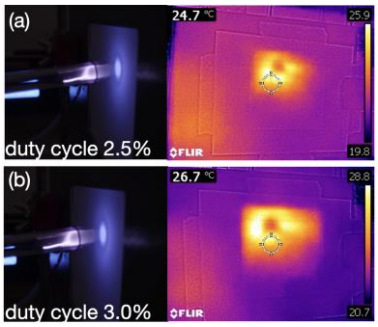

Fig. 3. *Thermal images of the plasma plume impinging a paper sheet at 1 cm from the tube end.*

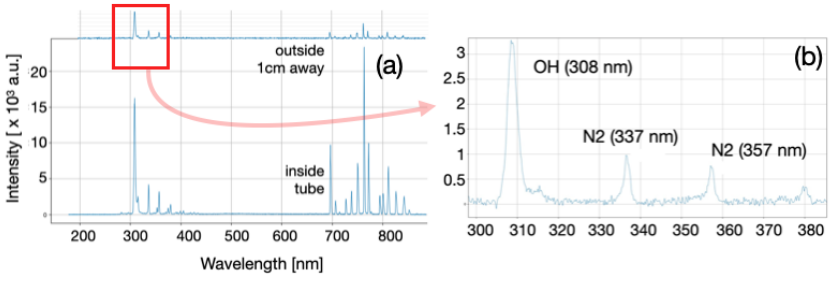

Fig. 4. *(a) Optical emission spectra from argon plasma at two different regions of the plasma: Tube interior and generated torch/ (b) zooming in the 300nm region, The presence of hidroxil (OH, 308 nm) radicals as well as other nitrogen species was identified.*

4. References

[1] A. Rafiei *et al*, Clinical Plasma Medicine, 19–20, 100102, (2020).
[2] D. Yan *et al*, Plasma, 5, 98-111, (2022).
*Corresponding author: gcirino@ufscar.br

CATALYTIC STUDY OF THE CONVERSION OF MICROBIAL BIO-OIL INTO GREEN DIESEL

Ana Barbara Azevedo Gomes Goular*, Thainá Barbosa de Lima Cordeiro, José Geraldo da Cruz Pradella, Lucia Vieira
University of the Paraíba Valley

1. Introduction

Efficient catalysts are essential for the conversion of biomass into sustainable fuels, such as green diesel. However, supports such as γ-Al_2O_3 exhibit limitations in acidity and thermal stability, compromising the dispersion of active phases and the overall catalyst durability [1,2]. The addition of small amounts of niobium oxide (Nb_2O_5) to the support enhances activity, selectivity, and stability due to metal–support interactions and the presence of Lewis and Brønsted acid sites, which are important in hydrocarbon cracking and hydrocracking reactions [3,4]. In this context, the Nb_2O_5-modified support is subsequently impregnated with nickel (Ni), aiming to produce bifunctional catalysts suitable for hydrodeoxygenation (HDO) reactions of microbial bio-oil.

2. Experimental

The study, developed as part of the master's qualification, followed previously established experimental procedures for the preparation and evaluation of the catalyst. The catalytic support was thermally treated and subsequently impregnated with Ni. The material was then characterized by porosimetry N_2 physisorption (BET) to determine the surface area and pore volume according to ASTM C1069−09 (2014); energy-dispersive X-ray spectroscopy (EDX); and X-ray diffraction (XRD) for identification of the support structure. After these characterizations, the catalyst was applied in the HDO reaction of vegetable oil to obtain Hydrotreated Vegetable Oil (HVO).

3. Results and Discussions

The characterization results of the support calcined at 600 °C indicate that the addition of Nb_2O_5 improves the textural properties of alumina. EDX analysis confirmed the presence of Nb in the support structure, indicating that the oxide was efficiently incorporated. XRD patterns showed the retention of the γ-alumina phase, with no detectable crystalline Nb_2O_5 phases, suggesting that the oxide is well dispersed within the alumina matrix. After Ni impregnation, the catalyst was applied in HDO reaction of vegetable oil, and the analysis of the obtained product is currently ongoing. This procedure will subsequently be applied to microbial bio-oil if the results with vegetable oil prove satisfactory, allowing the evaluation of the catalyst's performance with more complex substrates.

4. References

[1] K. Tanabe, Z. Chen, T. Iizuka. Chemtech, 21, p. 628, (1991).
[2] K. Tanabe. Catal. Today, 8, p. 1, (1990).
[3] Moreno, E.L.; Rajagopal, K. Desafios da acidez na catálise em estado sólido. Quim. Nova, 32, 538–542, (2009).
[4] K. Tanabe, ChemTech. Review Various catalyzed by niobium compounds and materials. Elsevier.p. 202, (1995).

Acknowledgments

We would like to thank CNPq (Scholarship No. 384356/2025-7) and CNPq (Project No. 407946/2022-5), Brazil, for financial support.
*Corresponding author: anabarbaragoulart@gmail.com

COMPOSITE DEVELOPMENT FOR REUTILIZATION OF METAL CONTAMINATED POLYMER

Alana M. Corá[1]*, Jane M. F. de Paiva[2], Elidiane C. Rangel[3], Silvia P. Irazusta[1]

[1]*Faculdade de Tecnologia de Sorocaba (Fatec)*
[2]*Universidade Federal de São Carlos (UFSCar) - Campus Sorocaba*
[3]*Instituto de Ciência e Tecnologia (UNESP) - Campus de Sorocaba*

1. Introduction

In the field of civil construction, the reuse of waste materials in the production of composites is a common practice. With the increasing use of polymers for soil remediation, another type of waste is generated. Thus, the development of composites as a means of reusing this waste has become a growing practice, in which residues are incorporated into a different matrix and employed as reinforcement in the composite [1].

2. Experimental

The potential application of the sodium polyacrylate (PAS) after its use in a soil remediation of metallic contaminants was conducted by evaluate its incorporation in a composite as constructive material. For the preparation of the specimens, samples were produced with and without PASe, in triplicate, using cement and sand (1:3) with 2% PAS. The samples were molded into PVC cylinders measuring Ø5×10 cm and cured for 7, 14, and 28 days. The tests followed the ABNT 7215 standard for Portland cement to compressive strength test and were analyzed by Scanning Electron Microscopy (SEM).

3. Results and Discussions

The control preparation without PAS addition, exhibited a progressive increase in compressive strength (Fig. 1), as curing time advanced. In contrast, the PAS composite showed a reduction in strength,as compared with the control cement. However, when comparing the compressive strength of the composite at 28 days with the control at 7 days, the values were comparable. These findings suggest that composite with the PAS may require extended curing times in order to achieve compressive strength levels equivalent to those reached by standard preparation at shorter curing times. The SEM analysis, represented by the Fig. 2, 3, and 4, of the control and composite samples (40x) reveals differences in microstructure over time. In the 7 and 14 day samples, the composite (Fig. 2b and 3b) exhibits greater heterogeneity and porosity compared to the control (Fig. 2a 3a), associated with the presence of PAS. After 28 days, the composite surface becomes similar to that of the control samples. In short, the reuse of the waste generated in remediation in another production process, such as the one presented here, offers the closing of the PAS cycle, in accordance with the principles of circularity.

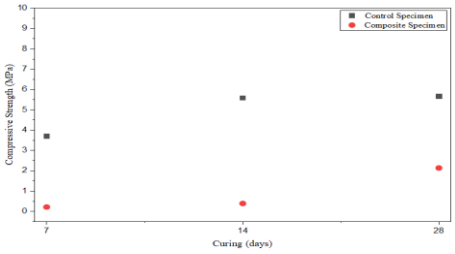

Fig. 1. *Compressive strength of control and composite samples at different curing times.*

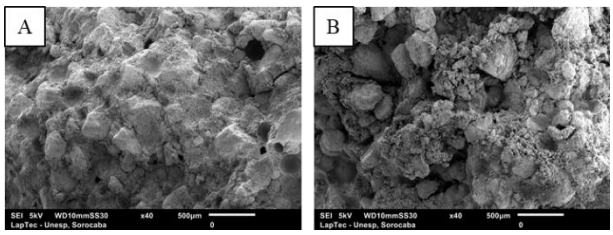

Fig. 2. *SEM images of the 7 days specimens, where A. represents the control and B. the composite*

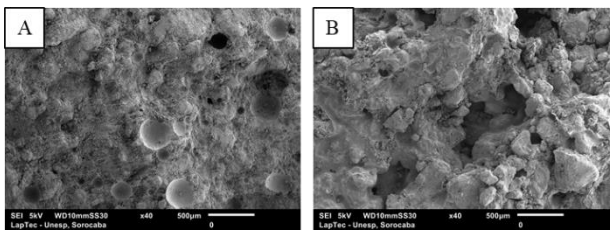

Fig. 3. *SEM images of the 14 days specimens, where A. represents the control and B. the composite*

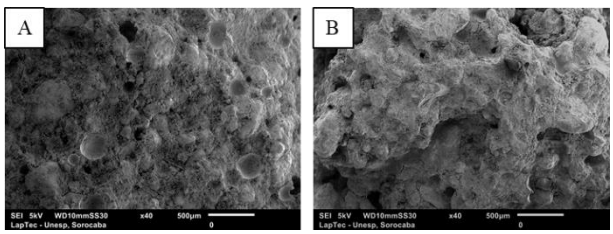

Fig. 4. *SEM images of the 28 days specimens, where A. represents the control and B. the composite*

4. References

[1] – N. T. A, Filho *et al*. Rev. Bras. de Eng. Agrícola e Ambiental, **16**, 894-902 (2012).

Acknowledgments

To FAPESP for the Process No. 2022/49136-3.
*Corresponding author: alana.cora@gmail.com

COMPUTACIONAL FLUID DYNAMICS SIMULATION OF A CONICAL PLASMA JET OPERATING AT ATMOSPHERIC PRESSURE

Ana Carla de Paula Leite Almeida[1]*, Fellype do Nascimento[1], and Konstantin Georgiev Kostov[1]
[1]*Universidade Estadual Paulista "Julio de Mesquita Filho", campus de Guaratinguetá – UNESP*

1. Introduction

The investigation of plasmas plays a central role in applications ranging from industrial processes to fusion research. However, experiments in this field are often complex, costly, and time-consuming. In this context, computational simulations emerge as an essential tool, as they enable the efficient exploration of a wide range of operating conditions. These models make it possible to analyze the interactions between charged particles and electromagnetic fields, providing a deeper understanding of plasma dynamics and assisting in the optimization of experiments [1]. In this work, we present a computational simulation performed in *COMSOL Multiphysics 6.2*, dedicated to the study of an atmospheric pressure plasma jet (APPJ) with a funnel-shaped geometry, as proposed in [2], with a focus on the preliminary characterization of the hydrodynamic behavior inside the device.

2. Experimental or Theory

The geometry of the dielectric barrier discharge (DBD)-based plasma jet using argon at atmospheric pressure is illustrated in Fig. 1a. The APPJ (Fig. 1b) investigated in this work is currently operated by the Plasma and Applications Laboratory (LPA) at UNESP, Guaratinguetá. The beneficial properties of this device can be attributed to the effective confinement of reactive species within the conical jet, which can be achieved with very short sample-to-nozzle distances (a few millimeters) and moderate gas flow rates [2,3]. A two-dimensional (2D) axisymmetric laminar flow model with an argon flow rate of 2 L/min, coupled with a diluted species transport module, was employed for the hydrodynamic study of the APPJ. This model serves as a platform for future work in which the simulated reactor will be applied to different plasma jet applications.

3. Results and Discussions

In the lower region of the domain, near the funnel outlet (Fig. 2), the formation of a vortex was observed because of the interaction between the argon jet and the system geometry. This flow generates a recirculation zone that enhances mixing with the surrounding atmospheric air, leading to a concentration gradient at the jet boundaries.

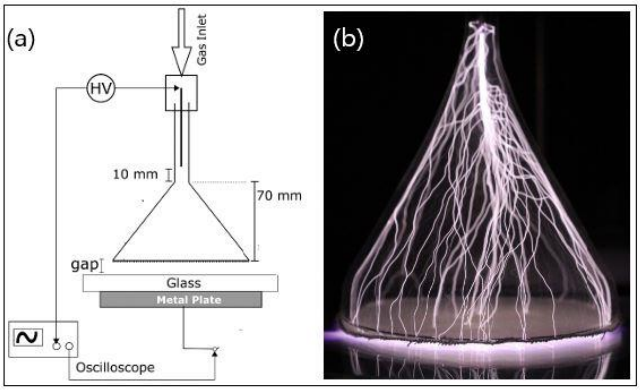

Fig. 1. (a) *Schematic drawing of the plasma jet configuration;* **(b)** *Conical Plasma Jet with Argon. [2] .*

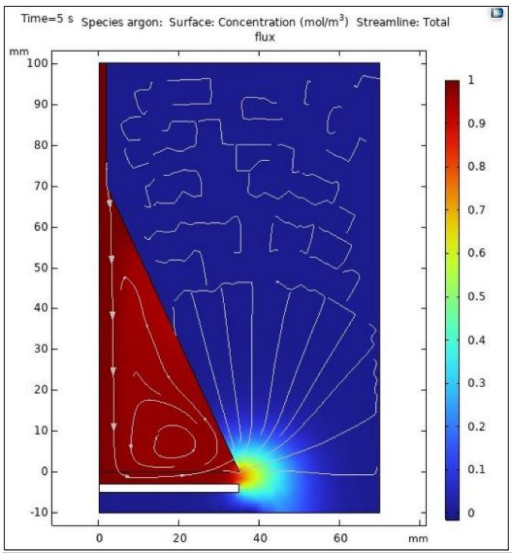

Fig. 2. *Spatial distribution of Ar concentration (mol·m⁻³) in the conical APPJ, obtained with COMSOL.*

4. References

[1]- M. Hamidieh and M. Ghassemi, IEEE Access, **12**, 104688–104707 (2024).
[2]- F.V.P. Kodaira et al., Polymers, **15**, 3344 (2023).
[3]- T.S.M. Mui et al., Surf. Coat. Technol., **352**, 338–347 (2018).

Acknowledgments

The authors acknowledge the financial support of CAPES (Grant No. 88887.924842/2023-00) and FAPESP.
* Corresponding author: ana.c.almeida@unesp.br

DEVELOPMENT AND CHARACTERIZATION OF A NEW MULTICOMPONENT ALLOY BASED ON 30TI-30NB-5FE-30MN-5AL (%AT) FOR BIOMEDICAL APPLICATIONS

Luccas Nunes C. da Silva[1]*, Diego R. Nespeque Correa[2], Jhuliene M. Elen Torrento[3], Carlos Roberto Grandini
[1] *Faculty of Engineering of Bauru, São Paulo State University (UNESP), Bauru-SP, Brazil.*
[2] *Faculty of Sciences, São Paulo State University (UNESP), Bauru, SP, Brazil;*
[3] *Faculty of Sciences, São Paulo State University (UNESP), Bauru, SP, Brazil;*

1. Introduction

In recent years, materials science has driven significant advancements in the field of biomedical engineering. In this context, titanium alloys have established themselves as the most successful class of materials, with vast applications in dental implants, joint replacements, trauma devices, and cardiovascular implants [1]. It is in this scenario that the emergence of High-Entropy Alloys (HEAs) has revolutionized the field of biomedical materials. Unlike conventional alloys, their approach of incorporating multiple principal elements results in a remarkable combination of mechanical, biological, and chemical properties [2]. In this context, the present work aims to develop a multicomponent alloy of the Ti-Nb-Fe-Mn-Al system with potential for biomedical applications.

2. Experimental

For the preparation of the ingot, commercially pure metals were used in the following atomic proportions: Ti (30%), Nb (30%), Fe (5%), Mn (30%), and Al (5%). The alloy was melted in an arc melting furnace under an inert argon atmosphere. Subsequently, part of the ingot was subjected to a homogenization heat treatment, conducted in a vacuum of 10^{-5} Torr at 1000 °C for 12 hours, followed by slow cooling. Finally, both samples were characterized through chemical, physical, structural, microstructural, mechanical, and biological analyses.

3. Results and Discussions

The experimental density obtained for the alloy was 6.75 ± 0.01 g/cm³, a value higher than that of Ti-6Al 4V (4.43 g/cm³) but lower than that of 316L stainless steel (7.99 g/cm³). These results place the alloy within an intermediate range between the main metallic biomaterials. Fig. 1 depicts that the elastic modulus of the TiNbFeMnAl system is comparable to that of 316L stainless steel and higher than that of the Ti 6Al-4V alloy. Regarding Vickers microhardness, the value obtained for the system is significantly higher than that of conventional biomaterials, which confirms the theoretical prediction of high hardness for such alloys. Fig. 2 shows the characteristic X-ray diffractogram of a multiphase crystalline structure. The major phase was identified as Body-Centered Cubic (BCC). In addition to the BCC phase, additional peaks are observed, indicating the presence of secondary phases. Preliminary MTT and crystal violet tests yielded positive results, with adhesion and cell viability exceeding 70%, indicating that the material exhibits low cytotoxicity.

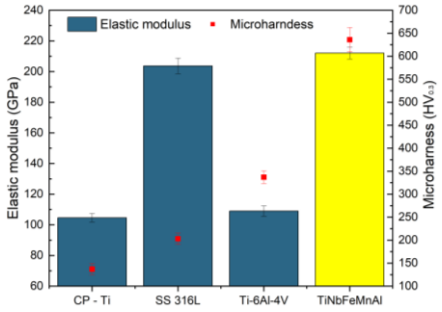

Fig. 1. *Elastic modulus (E) and Vickers microhardness ($HV_{0,3}$) of the heat-treated sample.*

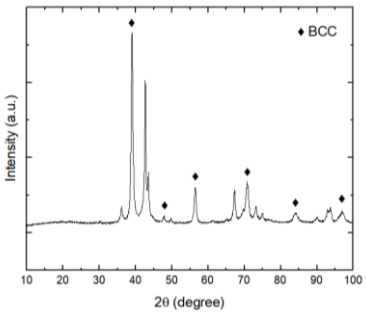

Fig. 2. *XRD patterns of the heat-treated sample.*

4. References

[1] Marin, E., Lanzutti, A. (2023). Biomedical applications of titanium alloys: a comprehensive review. Materials, 17(1), 114.
[2] de Oliveira, T. G., Fagundes, D. V., Capellato, P., Sachs, D., & da Silva, A. A. A. P. (2022). A Review of Biomaterials Based on High-Entropy Alloys. Metals 2022, 12, 1940.

Acknowledgments

The authors would like to thank the Conselho Nacional de Desenvolvimento Científico e Tecnológico (CNPq) for the financial support through the PIBIC fellowship (Project 14390), and UNESP, Bauru and Botucatu campuses, for providing the necessary infrastructure
*Corresponding author: luccas.nunes@unesp.br

ECONOMIC VIABILITY OF PVD FILMS IN STAMPING TOOLS

Jullia Pironato Amaro[1*], Pedro Augusto de Brito Inácio[1], Rogério Varavallo[2], Marcos Dorigão Manfrinato[1]
[1]*FATEC Sorocaba*
[2]*Escola Técnica Estadual Sylvio de Mattos Carvalho*

1. Introduction

The application of PVD coatings on stamping tools began as an alternative to increase their service life, especially in cold forming operations in metals that constitute sliding systems with high load demands, reducing costs such as machine downtime, increasing press occupancy rate, reducing stops for tool changes, allowing greater efficiency and effectiveness [1]. Tooling performance can be affected not only by the layer application, but also by the choice of the chemical composition of the PVD film [2]. The objective of this study is to test two types of stamping tool suppliers with TiN PVD coatings and define purchasing criteria based on service life, cost, and microscopic analysis of the coating.

2. Experimental

Two tool suppliers were selected: Supplier A, with a quenched and tempered tool steel tool with a TiN PVD coating, and Supplier B, with a high-speed steel tool with a TiN PVD coating. Each supplier submitted 10 tools for testing and lifespan verification. For cost analysis, Supplier A's tool cost R$5,000.00 and Supplier B's R$7,000.00. After use, the stamping tools were analyzed with SEM/EDS to verify the base metal and TiN PVD film.

3. Results and Discussions

The service life tests showed that Supplier A's tool lasted 450,000 +- 15,450 cycles and Supplier B's 1,200,000 +- 23,976 cycles. Supplier B's tool had a longer service life, 266.66% longer than Supplier A's. Analyzing the cost/hour worked ratio of Supplier A's tool, which is R$38.00, while Supplier B's is R$18.00, Supplier B's cost is 211.11% lower than Supplier A's tool (**Fig. 1**). Although the acquisition cost of Supplier B's tool was higher than that of Supplier A, the analyses performed demonstrated that Supplier B's tool had a longer service life and a lower cost per hour of use than Supplier A's, making Supplier B the better purchasing option. Regarding the tool metallurgy, Supplier A's PVD layer is 5 microns thick (**Fig. 2(a)**), while Supplier B's was 15 microns thick, consisting of a layer composed of Al_2O_3 and TiN (**Fig. 2(b)**). The greater thickness and the presence of a PVD composite layer for Supplier B's tool led to its greater wear resistance and, consequently, a longer service life.

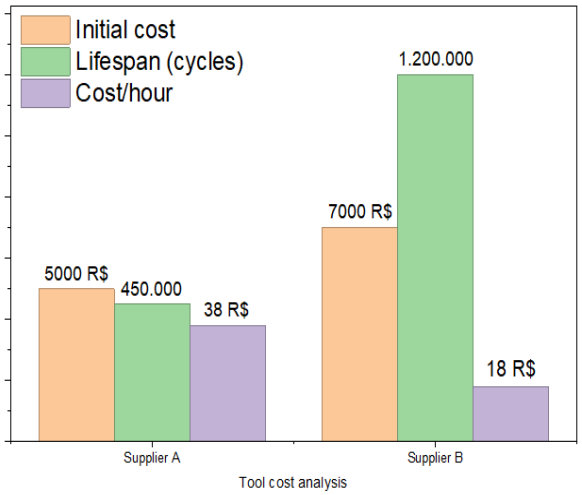

Fig. 1. *Cost analysis chart*

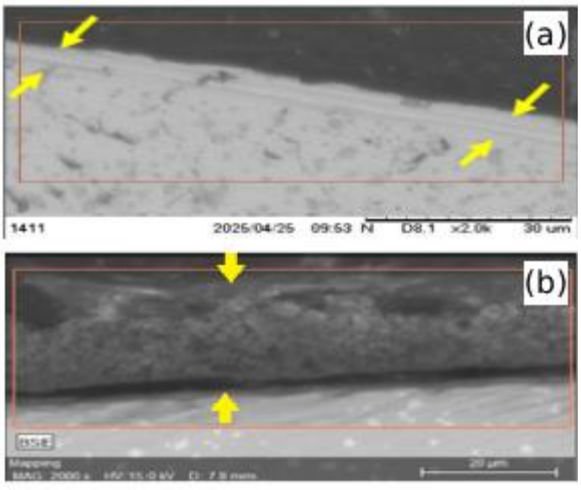

Fig. 2. *Scanning electron microscopy of PVD coatings (a) Supplier A (b) Supplier B*

4. References

[1]- S. Hogmark.; S. Jacobson. And M. Larsson., M., Wear , 246, 1–2, 20-33, (2000).
[2]- C.E. Pinedo, Encontro da Cadeia de Ferramentas, Moldes e Matrizes, 9, 99-108, (2011).

Acknowledgments

To UFSCar Sorocoba for providing the SEM/EDS analysis equipment.
*Corresponding author: jota23amaro@gmail.com

COLD PLASMA-ASSISTED MODIFICATION OF TITANIUM SURFACES FUNCTIONALIZED WITH SILVER NANOPARTICLES FOR BIOMEDICAL APPLICATIONS

Lucas Vichiato Silva[1]*, Lívia Elisabeth Vasconcellos de Siqueira Brandao Vaz[1]
[1] *Universidade Federal de Lavras (UFLA), Chemical and Materials Engineering Department, (DQM)*

1. Introduction

Titanium is widely applied in biomedical implants due to its biocompatibility, yet its surface remains prone to bacterial colonization and biofilm formation, which may compromise implant performance [1]. Cold atmospheric plasma treatment has emerged as a promising technique to enhance surface properties and enable functionalization with antibacterial agents such as silver nanoparticles (AgNPs).

2. Experimental

In this work, titanium substrates were abraded and treated under different plasma conditions, varying the distance from the torch (5, 7 and 10cm) and exposure times (15, 30 and 60s). AgNPs were subsequently deposited and naturally dried. Surface characterization was performed by SEM/EDS, FIB cross-sections and contact angle measurements.

3. Results and Discussions

Results indicated that plasma parameters strongly influenced nanoparticle morphology and distribution. Shorter distances (5cm) combined with moderate exposure (30s) promoted uniform deposition of spherical AgNPs, while longer times and intermediate distances (7cm, 60s) led to agglomeration and anisotropic arrangements. FIB analysis revealed AgNPs of 20–30 nm overlying the titanium oxide layer. Contact angle measurements confirmed enhanced surface hydrophilicity, which favors nanoparticle adhesion. These findings demonstrate that plasma treatment parameters are critical to controlling AgNPs deposition and surface energy, thus providing a tunable strategy for developing antimicrobial titanium-based biomaterials.

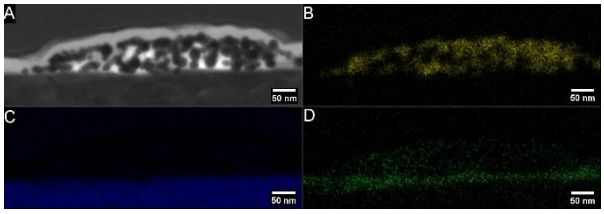

Fig. 1. *FIB/EDS micrographs of 7D60T.:(A) SEI (B) Ag map, (C) Ti map, (D) O map*

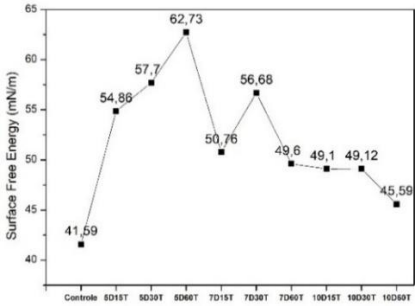

Fig. 3. *Surface energy of control and plasma treated substrates*

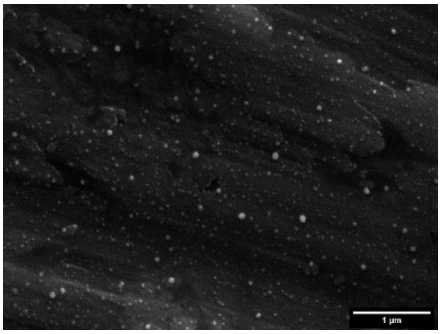

Fig. 3. *SEI of 5cm60s treated substrates*

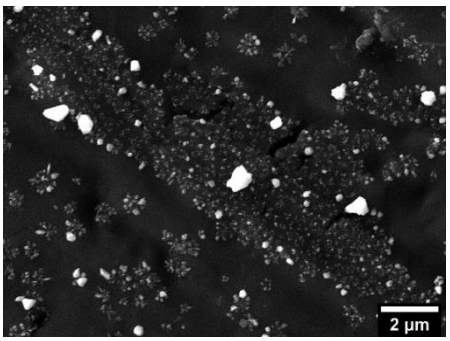

Fig. 4. *SEI of 7cm60s treated substrates*

4. References

[1] Sarraf, Masoud, et al. "A state-of-the-art review of the fabrication and characteristics of titanium and its alloys for biomedical applications." *Bio-design and Manufacturing* 5.2 (2022): 371-395.

Acknowledgments

The authors acknowledge the support from FAPEMIG and the Brazilian Nanotechnology National Laboratory (LNNano), part of CNPEM. The Electron microscopy staff is acknowledged for assistance during the experiments (20243006 and 20253259).

* Corresponding author: lucas.silva61@estudante.ufla.br

EFFECT OF NITROGEN FLOW RATE ON THE ELECTRICAL AND OPTICAL PROPERTIES OF TiN_X THIN FILMS

Josieli Honorato*, Julio César Sagás[1]
[1] *Universidade do Estado de Santa Catarina – Centro de Ciências Tecnológicas*

1. Introduction

Thin films can provide specific functional characteristics to different systems [1, 2]. Among the various materials used in thin films, titanium nitride (TiN) stands out, being studied for its electrical, optical, and mechanical properties [3].
Previous studies have shown that nitrogen concentration, temperature, and sample polarization significantly influence both the film growth and its final properties [1, 4]. A promising approach is functionally graded deposition, in which the film composition is controlled along its thickness by adjusting the flow of the reactive gas during the deposition process [5]. Based on this, the present work aims to understand how changes occur in the electrical and optical properties of TiN_x films as a function of increasing nitrogen concentration. These analyses will allow a deeper understanding of how the properties of a functionally graded film vary along its thickness

2. Experimental

The films were deposited on aluminum and silicon substrates, with and without native oxide, using the GAMS (grid-assisted magnetron sputtering) technique. Different samples were prepared by varying the nitrogen (N_2) flow gas to investigate the influence of nitrogen concentration in the film on its structural, electrical, and optical properties.

3. Results and Discussions

The structure and composition of the films change with increasing nitrogen content, initially resulting in distortions within the Ti lattice and subsequently leading to phase transitions with the formation of TiN. Regarding the optical properties, as the composition approaches stoichiometry, the films acquire a golden color with high reflectance in the longer-wavelength region of the visible spectrum, as presented in Fig. 1. Figure 2 shows that the electrical resistivity of pure titanium is on the order of $\rho \approx 4.28 \times 10^{-5}$ Ω·cm, a value consistent with that reported in the literature [6]. It increases significantly with the rise in nitrogen content, reaching a peak of approximately 1.7×10^{-4} Ω·cm for $TiN_{0.44}$ and $TiN_{0.72}$. The samples exhibit a gray coloration, typical of metals. This indicates that nitrogen is merely incorporated into the titanium structure, resulting in an increase in resistivity. However, beyond this range, further nitrogen incorporation leads to a progressive decrease in resistivity, approaching the values observed for pure titanium once again.

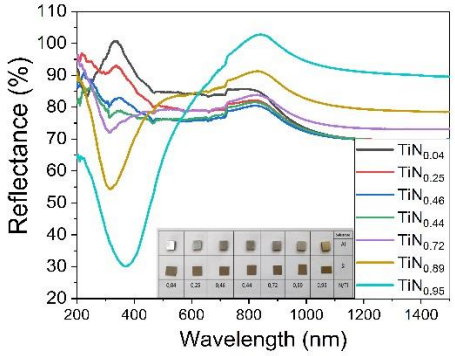

Fig. 1. *Reflectance of TiNx films*

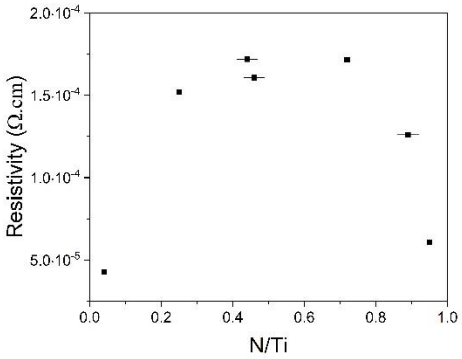

Fig. 2. *Resistivity as a function of the N/Ti ratio*

4. References

[1]- VAZ, F. et al. *Surface & Coatings Technology*, v. 191, p. 317-323, (2005)
[2]- GARG, R. et al. *Advances in Colloid and Interface Science*, v. 330, (2024)
[3]- BELIAEV, L.Y. et al. *Optical Materials*, v. 143, (2023)
[4]- HE, Z. et al. *Thin Solid Films*,v. 676, (2019)
[5]- SILVA, F. et al. *SN Applied Sciences,* v. 2, (2020)
[6]- PIERSON, H.O. *Noyes Publications*, Park Ridge. (1996)

Acknowledgments

The authors are thankful for the Multi-User Facility infrastructure from Santa Catarina State University's Technological Sciences Center, to FAPESC (grant 2024TR000258), and CNPq (grant 304053/2021-0).
*Corresponding author: josielihonorato@gmail.com

CORROSION AND CORROSION-FATIGUE BEHAVIOUR OF THE 2198-T8 ALUMINIUM ALLOY CONTAINING Nb_2O_5 THIM FILM OPTICAL PROPERTIES OF TITANIUM OXYNITRIDES THIN FILMS

Julio César Sagás[1]*, Xungang Diao[2], and Luis César Fontana[1]
[1]*Laboratory of Plasmas, Films and Surfaces, Santa Catarina State University (UDESC), Brazil*
[2]*School of Energy and Power Engineering, Beihang University, China*

1. Introduction

Titanium nitride and titanium oxides are largely studied due to their optical properties. As consequence there is a growing interest in the development of optical coatings based on titanium oxynitrides. Such films present a wide variation of optical properties according the chemical composition and crystalline structure [1,2]. In this work, we performed an exploratory study about the optical properties of titanium oxynitride thin films deposited by grid-assisted magnetron sputtering.

2. Experimental

The depositions were carried out in a grid-assisted magnetron sputtering reactor using a Ti target with 100 mm in diameter. The atmosphere was composed of ultrapure (99.999%) gases (Ar, N_2 and O_2). The plasma was generated using an Advanced Energy Pinnacle Plus power supply operating in pulsed bipolar mode with an average power of 1010 W at a frequency of 40 kHz and a reverse time of 0.4 μs. The glass substrates were kept at floating potential and room temperature. The working pressure was around 0.40 Pa and the depositions were conducted in metallic mode, resulting in an estimated thickness around 175 nm for 3,0 min of deposition. In each deposition, a Ti interlayer was grown during 15 s. The N_2 and O_2 flow rates were adjusted to change the stoichiometry of the films. The chemical composition was determined through X-ray photoelectron spectroscopy (XPS) after ion beam sputtering to remove contaminants and the relative specular reflectance was measured in a UV-Vis-NIR spectrometer.

3. Results and Discussions

Figure 1 shows the change in nitrogen and oxygen atomic concentration in the films as a function of the N_2/O_2 flow rate ratio. The increase in N_2 proportion in the working gas leads to an increase in nitrogen content and in a consequent decrease of oxygen concentration. The relative specular reflectance spectra are shown in Figure 2. We can observe that the increase in nitrogen content causes a higher reflectance in the yellow-red region of the visible spectrum. In fact, the sample $TiO_{0.42}N_{0.78}$ has a goldish color that resembles a TiN film. On the other hand, films with a higher oxygen concentration present low reflectance in the visible spectrum, with the sample $TiO_{1.71}N_{0.08}$ presenting a dark brown color. These results show that the optical properties of titanium oxynitrides films can be easily tuned through the variation of the N_2/O_2 flow rate ratio.

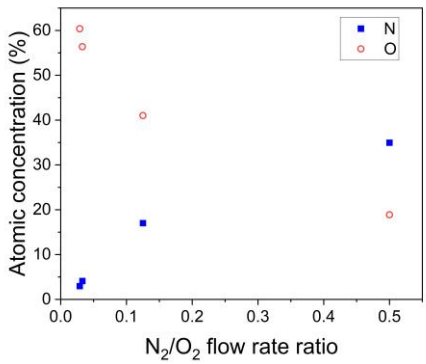

Fig. 1. *Nitrogen and oxygen concentration in the films as a function of N_2/O_2 flow rate ratio.*

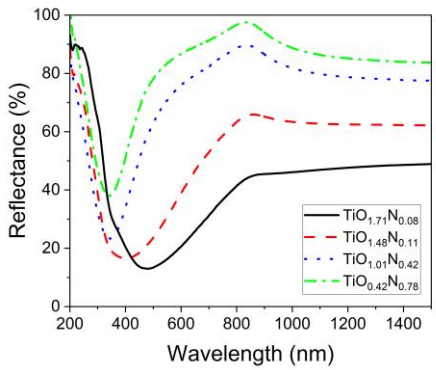

Fig. 2. *Relative specular reflectance spectrum for different titanium oxynitrides thin films..*

4. References

[1] S. Ali, R. Magnusson, O. Pshyk *et al.*, J Mater Sci, **58**, 10975–10985 (2023)
[2] N. R. Mucha, J. Som, S. Shaji *et al.* J Mater Sci, **55**, 5123–5134 (2020)

Acknowledgments

The authors are thankful for the Multi-User Facility infrastructure from Santa Catarina State University's Technological Sciences Center.
*Corresponding author: julio.sagas@udesc.br

DEVELOPMENT AND CHARACTERIZATION OF DLC FILM AND BORON-DOPED DLC FILM BY THE PECVD TECHNIQUE

Marcos Dorigão Manfrinato[1*], Leandro Almeida Silva[2], Luciana Sgarbi Rossino[1,2]
[1]*FATEC SOROCABA*
[2]*UFSCar Campus Sorocaba*

1. Introduction

Boron-doping diamond-like carbon (DLC) films provides differentiated properties such as thermal stability, greater adhesion to metal substrates, higher electrical conductivity, low coefficient of friction, and blood compatibility, which are interesting for applications in photovoltaic and solar cells, automotive parts, and medical devices. The objective of this work is the development and characterization by Raman and cyclic polarization etching of the Ti6Al4V alloy and the DLC and DLC-B (boron-doped DLC) films deposited by the PeCVD technique. The boron precursor used was trimethylborate (B(CH3O)3) on titanium alloy substrates (Ti6Al4V).

2. Experimental

The titanium alloy, Ti6Al4V, was deposited into DLC films with and without boron doping (DLC-B) by PeCVD. First, the plasma ablation process was performed using a gas mixture of 80% Ar and 20% H_2 for 1 hour at 490°C. Then, a silicon-based intermediate layer was applied using hexamethyldisiloxane (HMDSO) in a proportion of 70% HMDSO and 30% Ar, with a voltage of 500 V for 15 minutes at 300°C. Then, the DLC or DLC-B films were deposited. For the deposition of pure DLC, 90% CH_4 and 10% Ar were used, with a voltage of 500 V at 200°C for 2 hours. In the case of DLC-B, 90% CH_4 and 10% Ar were used, with a pressure of 0.050 Torr of trimethylborate at a voltage of 500 V at 200°C for 2 hours. The films were characterized by Raman and corrosion tests were performed with a 3.5% NaCl solution, initially for 30 minutes at open circuit potential and subsequently cyclic polarization with 1 mV/s.

3. Results and Discussions

Cyclic polarization corrosion showed that the DLC and DLC-B films presented better corrosion potential and pitting potential than the Ti6Al4V alloy, as illustrated in Fig. 1. The Raman spectra for DLC and DLC-B, Fig. 2, show that boron doping alters the D and G bands. The I(D)/I(G) ratio, structural disorder index, increased with boron doping, increasing the disorder of the DLC-B film. The reduction in the G band width (FWHM), Tab. 1, indicates a local reorganization of the sp^2 domains, which may be associated with greater nanometric structural homogeneity [1].

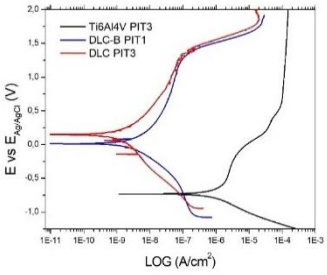

Fig. 1. *Cyclic polarization curves of Ti6Al4V, DLC and DLC-B*

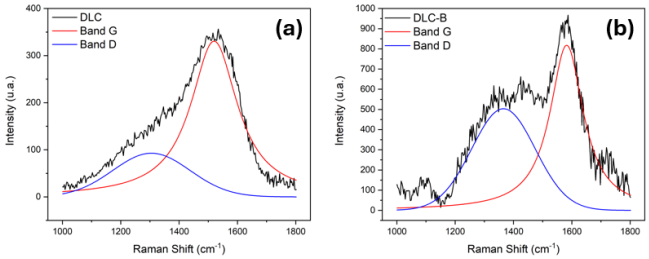

Fig. 2. *Raman spectrum for a-C:H (a) DLC and (b) DLC-B*

Tab. 1. *Spectroscopic parameters obtained from Raman analyses of DLC and DLC-B films*

	Band D	Band G	I(D)	I(G)	ID/IG	FWHM(G)
DLC	**1,305**	**1,520**	**93**	**331**	**0.28052**	**195**
DLC-B	**1,366**	**1,582**	**503**	**818**	**0.61543**	**139**

4. References

[1]- Liu, X. *et al.* Effect of silicon doping on structure and mechanical properties of diamond-like carbon films. Surface and coatings technology, v. 357, p. 1024–1030, 2019.

Acknowledgments

To the Laboratory of Plasma Technology (LaPTec) at UNESP Sorocoba for providing the potentiostat/galvanostat.
*Corresponding author: marcos.manfrinato@fatec.sp.gov.br

CORROSION RESISTANCE OF DIAMOND LIKE-CARBON COATINGS FOR PEMFC BIPOLAR PLATES

Felipe Carneiro da Silva[1,2]*, Oscar Maurício Prada Ramirez[2], Julio César Sagás[3], Luciana Sgarbi Rossino[1]
[1]*State Center of Technological Education Paula Souza, São Paulo State Technological College*
[2]*Department of Metallurgical and Materials Engineering, Universidade de São Paulo, Brazil*
[3]*Laboratory of Plasmas, Films and Surfaces, Universidade do Estado de Santa Catarina, Brazil*

1. Introduction

The decarbonization of global energy systems demands new materials for hydrogen-based devices such as proton exchange membrane fuel cells (PEMFCs). Bipolar plates (BPPs) account for ≈ 40 % of PEMFC cost and ≈ 80 % of their mass and volume, requiring both high electrical conductivity and corrosion resistance [1-2]. Stainless-steel BPPs has high mass/volume ratio, while graphite ones are brittle and expensive. Aluminium alloys represent a lightweight and low-cost alternative but suffer from poor corrosion resistance in the acidic fuel-cell environment (pH ≈ 2-4). Diamond-like carbon (DLC) coatings offer a potential solution because of their chemical stability and barrier properties [1-2]. This work investigates whether nitrogen doping of DLC films could improve their corrosion performance for aluminium-based BPPs in PEMFCs environment.

2. Experimental

DLC and N-doped DLC films were deposited on AA6061-T6 substrates by plasma-enhanced chemical vapor deposition (PECVD). An organosilicone interlayer was first applied from hexamethyldisiloxane precursor. DLC was deposited at 150 °C using CH_4/Ar (90/10 %), while N-DLC used CH_4/N_2 (70/30 %). The films were characterized by potentiostatic and potentiodynamic tests in 0.5 M H_2SO_4 + 2 ppm HF at 25 °C and 70 °C, simulating the cathodic side of the cell. Scanning electron microscopy (SEM) micrographs of the surface before and after electrochemical tests were carry to identify the possible film defects and corrosion mechanisms.

3. Results and Discussions

Both potentiodynamic and potentiostatic polarization curves (figures a-b) present similar shapes and similar cathodic slopes for all samples. The current density (i_{corr}) after 3600 s of potentiostatic polarization at +0.6 V(Ag/AgCl) reaches 2.8 µA cm^{-2} ; 145.0 µA cm^{-2} and 123.4 µA cm^{-2} at 25 °C for DLC , N-doped DLC and bare AA6061-T6 films, respectively. At 70 °C, the DLC maintained a current density below 35.7 µA cm^{-2}, while N-doped films reached ≈ 171 µA cm^{-2} (figure 1). SEM micrographs revealed homogeneous morphology for the DLC film and numerous micropores and delamination in the N-doped one (figure 2). Contact angles (≈ 78–80°) showed that both films remain hydrophilic and require further optimization for hydrophobic BPP surfaces. Despite not meeting the U.S. DOE targets ($i$corr < 1 µA cm^{-2}), this study demonstrates that undoped DLC films on aluminium offer a viable low-cost pathway for lightweight PEMFC bipolar plates, while nitrogen addition is detrimental under the tested conditions.

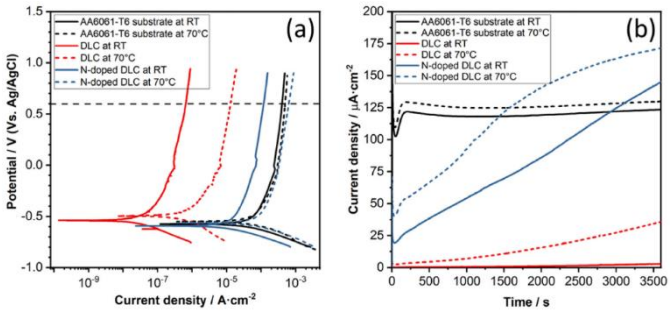

Fig 1. *(a) Potentiodynamic and (b) potentiostatic polarization curves for the AA6061-T6 substrate uncoated and coated with the DLC films at room temperature and 70 °C.*

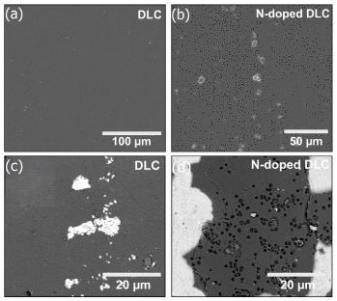

Fig 2. *SEM micrographs showing the surface of the DLC and N-doped DLC films (a-b) before and (c-d) after the electrochemical tests. The doped DLC is notably more defectiveand appears to suffer with delamination under the action of corrosive forces.[3]*

4. References

[1]- H. Dong et al., Diam. Relat. Mater. 110 (2020) 108156.
[2]- I. Alaefour et al., Int. J. Hydrog. Energy 46 (2021) 11059–11070.
[3]- F.C. Silva et al., Vacuum 241 (2025) 114574

Acknowledgments

The authors acknowledge support from CNPq (Brazil, Grant 405196/2023-7). Technical support from the Multi-User Facility of UDESC is gratefully recognized.
*Corresponding author: felipe.carneiro01@fatec.sp.gov.br

CORROSION AND CORROSION-FATIGUE BEHAVIOUR OF THE 2198-T8 ALUMINIUM ALLOY CONTAINING Nb_2O_5 THIM FILM

Uriel D. O. D. Rangel[1*], Murilo O. A. Ferreira[1], Renato M. Francoi[1], Natália B. L. Slade[2], Rogério V. Gelamo[2], Carlos A. R. Baptista[1], Haroldo C. Pinto[1], Igor Mota[3], Guilherme Y. Koga[3], Witor Wolf[1], Jéferson A. Moreto[1]
[1]*University of São Paulo - USP*
[2]*Federal University of Triângulo Mineiro – UFTM*
[3]*Federal University of São Carlos – UFSCar*

1. Introduction

High-strength aluminium alloys employed in aerospace applications require superior surface protection against pitting and corrosion-fatigue deterioration, as their native oxide layer proves insufficient in aggressive environments **[1]**. To mitigate this vulnerability, various surface treatment techniques are extensively used. Consequently, this study investigates the protective efficacy of a niobium pentoxide (Nb_2O_5)-based coating, deposited via reactive sputtering, aimed at enhancing the corrosion and fatigue resistance of the 2198-T8 aluminium alloy **[2]**.

2. Experimental

This investigation examined the efficacy of Nb_2O_5-based coatings, deposited by using the reactive sputtering, on the corrosion and corrosion-fatigue behaviour of the 2198-T8 aluminium alloy used as aircraft material. Uniform corrosion behaviour was accessed by open circuit potential (OCP), potentiodynamic polarization curves (PPc) and electrochemical impedance spectroscopy (EIS) techniques in 0.6 mol L^{-1} NaCl solution. Fatigue crack growth tests (FCGs) were conducted under controlled loading conditions in both air and saline environments. Comprehensive structural and morphological characterisations were performed using advanced microscopy and spectroscopy techniques, including AFM, SEM/EDX, Raman spectroscopy, FTIR, and EBSD.

3. Results and Discussions

Results demonstrated a significant enhancement in the corrosion and corrosion-fatigue resistance of the 2198-T8 aluminium alloy by utilising the reactive sputtering technique to produce Nb_2O_5 coatings. The observed reduction in FCGs is substantial under aggressive chloride environments, and, coupled with the improved electrochemical stability demonstrated by uniform corrosion tests, confirms therefore the protective efficacy of the Nb_2O_5 coatings. **Figure 1** displays the main results obtained in the present work.

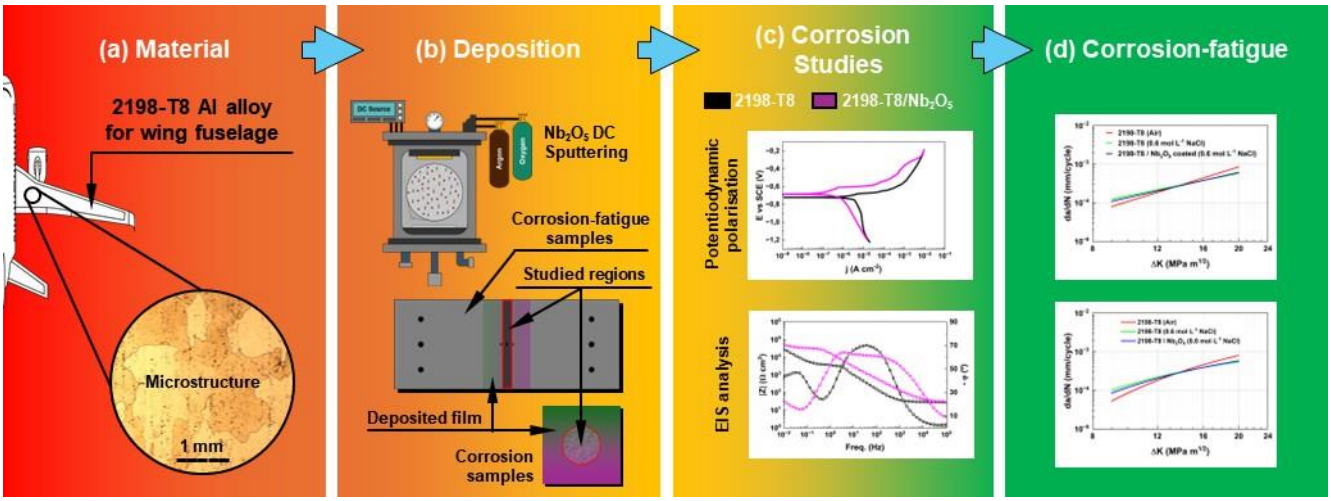

Fig 1. Summary of the main results obtained in this work. **(a)** optical image of the 2198-T8 alloy, **(b)** experimental apparatus used for deposition via PDV, **(c)** EIS spectra, PPc and FCG curves, **(d)** SEM micrographs after corrosion tests.

4. References

[1] Moreto, J.A. *et al.* Corros Sci. 84, 30-41 (2014).
[2] Rangel, U.D.O.D *et al. J. Mater. Res.* (2025).

Acknowledgements:
CNPq, FAPEMIG, CAPES and FAPESP (2024/02504-0).
*Corresponding author: urieloudinot@gmail.com

ELUCIDATING THE CORROSION BEHAVIOUR OF WE43 MAGNESIUM ALLOY WITH AND WITHOUT Nb_2O_5 COATING DURING LONG-TERM IMMERSION

Yeimer España[1]*, Murilo Oliveira Alves Ferreira[1], Rogério Valentim Gelamo[2], Witor Wolf[1], Guilherme Yuuki Koga[3], Jéferson Moreto[1]

[1]*Materials Engineering Department, São Carlos School of Engineering, University of São Paulo (USP), São Carlos, São Paulo, Brazil.*
[2]*Federal University of Triângulo Mineiro (UFTM), Uberaba, Minas Gerais, Brazil.*
[3]*Federal University of São Carlos, Department of Materials Science and Engineering, Rod. Washington Luis, km 235, CEP 13565-905 São Carlos, São Paulo, Brazil.*

1. Introduction

Magnesium (Mg)-based alloys have emerged as promising alternatives for bone implants due to their biodegradable nature upon contact with physiological fluids and enhanced compatibility with bone tissues, rendering them ideal for replacing currently used permanent metallic implants in fracture repairs and tissue healing. However, the rapid corrosion rate and challenging control of these alloys have been identified as the primary impediment to the use of this biomaterial. This work aims to propose a novel applied research approach for developing Nb_2O_5 thin films on the WE43 magnesium alloy surfaces, offering significant prospects for utilization in the biomedical field by enabling the planning, control, and localization of degradation rates in implants [1].

2. Experimental

The deposition of Nb_2O_5 coating was performed by using the reactive sputtering technique, following the same guidelines described by Moreto et al [2]. Open circuit potential (OCP), potentiodynamic polarization curves (PPc), and electrochemical impedance spectroscopy (EIS) techniques were used to assess the electrochemical behaviour of the coated and uncoated WE43 alloy in 0.01 mol L^{-1} NaCl solution. An extensive morphological analysis was performed before and after the corrosion tests via optical microscopy (OM) and scanning electron microscopy/energy-dispersive X-ray spectroscopy (SEM/EDX) techniques.

3. Results and Discussions

The application of Nb_2O_5 coating on the WE43 magnesium alloy surfaces markedly improved its electrochemical performance. The Nb_2O_5 coating resulted in a 30% reduction in the corrosion rate. The EIS results indicate that the Nb_2O_5 coating induced a positive response by enhancing the charge-transfer resistance in comparison to the base material. Moreover, the combined effect of the Nb_2O_5-based coating and the oxide layers formed on the WE43 surface after immersion results in a complex electrochemical response, significantly enhancing the service life of this alloy. This improvement represents a substantial advancement for its potential application as a biomaterial in temporary implantable devices.

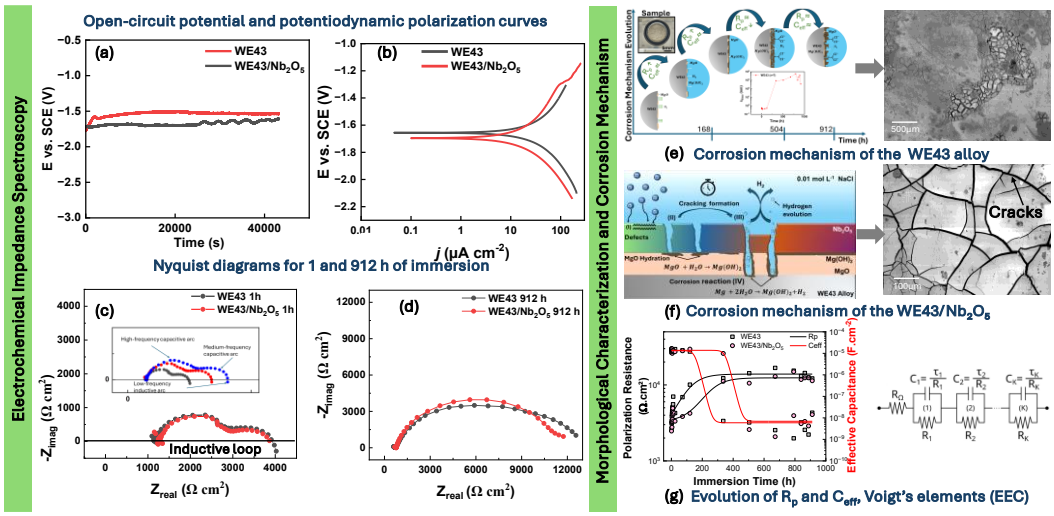

4. References

[1] M. He, L. Chen, M. Yin, *et al.*, *J. Mater. Res. Technol.*, vol. 23, pp. 4396–4419, 2023
[2] J.A. Moreto et. al. Applied Surface Science, 556(2021), 149750.

Acknowledgments
CNPq, CAPES and FAPESP (2024/02504-0).
*Corresponding author: yeimer@usp.br

ENHANCING THE CORROSION AND WEAR RESISTANCE OF 316 L SS BY USING Nb2O5 AND a-C NANOSTRUCTURED COATINGS

M.O.A. Ferreira[1]*, R.V. Gelamo[2], C.A. Fortulan[3], W. Wolf[1], H.C. Pinto[1] and Moreto J.A.[1]

[1]Materials Engineering Department, São Carlos School of Engineering, University of São Paulo (USP)
[2]Institute of Exact Sciences, Naturals and Education, Federal University of Triângulo Mineiro (UFTM)
[3]Mechanical Engineering Department, São Carlos School of Engineering, University of São Paulo (USP)

1. Introduction

Within the evolving landscape of materials for biomedical applications, 316L stainless steel (316L SS) presents itself as a cost-effective alternative to conventional titanium alloys, such as Ti-6Al-4V. However, its susceptibility to corrosion and wear in environments characterised by pH variations and aggressive ionic species—akin to those encountered in vivo—remains a significant limitation [1]. This study aims to elucidate the impact of nanostructured niobium pentoxide (Nb2O5) and amorphous carbon (a-C) coatings on the corrosion and wear behaviour of 316L SS.

2. Experimental

Coated and uncoated specimens were characterised morphologically and structurally utilising, SEM/EDX, XRD, FTIR, Raman spectroscopy, and XPS. The global corrosion behaviour was evaluated via OCP, potentiodynamic polarisation curves, and EIS. Wear performance under various environmental conditions (ambient air, sodium chloride solution, and artificial saliva) was assessed using pin-on-disc tribological tests. Subsequently, a comprehensive morphological analysis of the wear tracks was conducted to elucidate the underlying wear mechanisms.

3. Results and Discussions

The application of Nb2O5 and a-C coatings significantly improved the corrosion and wear performance of 316L SS. Both coatings reduced the corrosion current density by near 20%, while increasing Ecorr and Epitting by up to 150 mV and 250 mV (see Fig. 1), respectively, in 0.6 mol L-1 NaCl and artificial saliva solutions, indicating enhanced corrosion resistance [1]. Additionally, Nb2O5 and a-C coatings led to a consistent reduction in the coefficient of friction (CF) across all tested environments. Nb2O5 achieved around a 50% reduction in the average CF compared to the uncoated alloy. This improvement was accompanied by a notable decrease in wear volume and wear rate up to 80% for a-C and 90% for Nb2O5 within the first 300 s of testing [2]. These findings highlight the coatings' potential for improving the durability of stainless steel in aggressive service conditions.

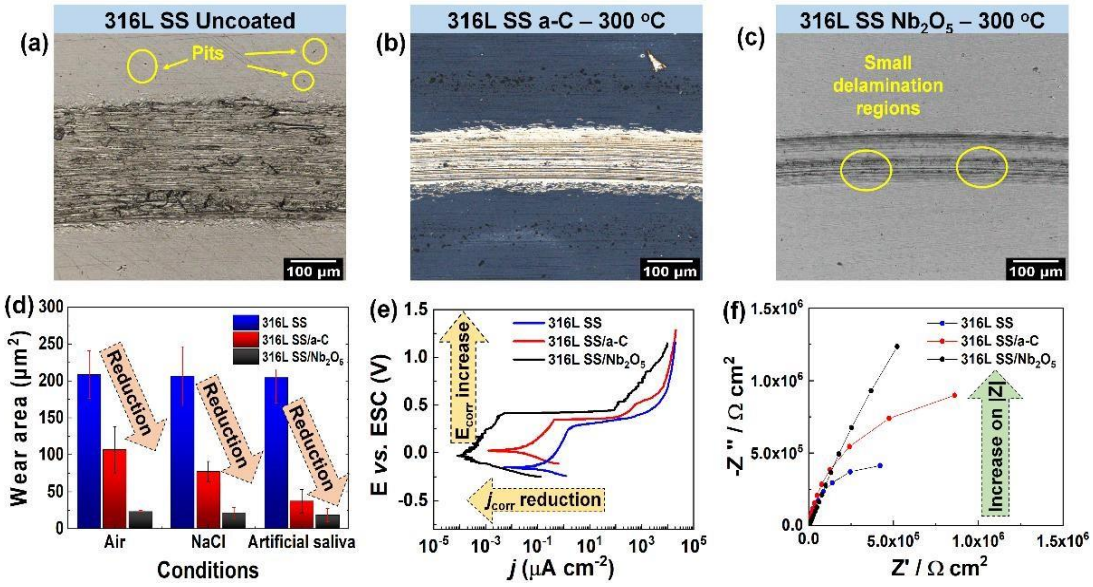

Fig. 1. *(a-c) OM analysis after the wear tests in 3.5 wt% NaCl solution, showing the presence of pits and small delamination regions, (d) wear rate as a function of the analysed environment, (e, f) Nyquist diagrams for all studied conditions.*

4. References

[1]- M.O.A. Ferreira et al. Mater. Chem. Phys., 312, (2024).

Acknowledgments

CAPES-Brazil and FAPESP (FAPESP (2024/02504-0) for the financial support.
*Corresponding author: moaferreira@usp.br

EVALUATION OF FATIGUE-CORROSION BEHAVIOUR OF THE 2524-T3 ALUMINUM ALLOY CONTAINING NANOSTRUCTURED COATINGS

K.R. Santos[1]*, M.O.A. Ferreira1, R.V. Gelamo[2], N.B.L. Slade[2], C.A.R.P. Baptista[1], H.C. Pinto[1], W. Wolf[1], J.A. Moreto[1]
[1]University of São Paulo (USP),
[2]Federal University of Triângulo Mineiro (UFTM)

1. Introduction

Aluminium alloys from the 2xxx series are extensively utilised across diverse industrial sectors owing to their high strength-to-weight ratio, corrosion resistance, and ease of fabrication. Particularly, the 2524-T3 aluminium alloy is notable for its superior resistance to fatigue crack growth (FCG) and is employed in aircraft fuselage structures [1]. Research has demonstrated that nanostructured coatings, such as Nb2O5 thin films deposited via reactive sputtering, hold considerable promise in safeguarding various substrates against localised corrosion and microwear [2]. This study explores the influence of the Nb2O5 coatings on the fatigue performance of the 2524- T3 aluminium alloy within an aggressive saline environment, with the objective of extending the material's service life, enhancing its competitiveness, and reducing associated costs.

2. Experimental

M(T)-type specimens were used, and Nb2O5 films (~ 300 nm in thick) were deposited via reactive sputtering with a niobium target (99.9% purity) under a controlled argon/oxygen atmosphere. FCG tests were performed according to ASTM E647 in air (10 Hz) and in 0.6 mol L^{-1} NaCl solution (1 Hz), with a load ratio R = 0.1. An extensive morphological analysis was performed before and after the corrosion and corrosion-fatigue tests by using optical microscopy (OM) and scanning electron microscopy/energy-dispersive x-ray spectroscopy (SEM/EDX).

3. Results and Discussions

The experimental results further confirm the exceptional properties of the Nb2O5 nanostructured coating deposited on the 2524-T3 aluminium alloy surfaces by using the reactive sputtering technique, enabling a significant reduction in FCGs of the 2524-T3 alloy. These results exhibit substantial advancements, paving the way for more efficient processes, durable materials, and smarter systems. Finally, these standards and testing principles are essential for ensuring the quality, safety, and regulatory compliance of Nb2O5 coating units from both government and professional perspectives. Figure 1 presents a schematic assembly of the experimental procedure, and the main results obtained in the present work.

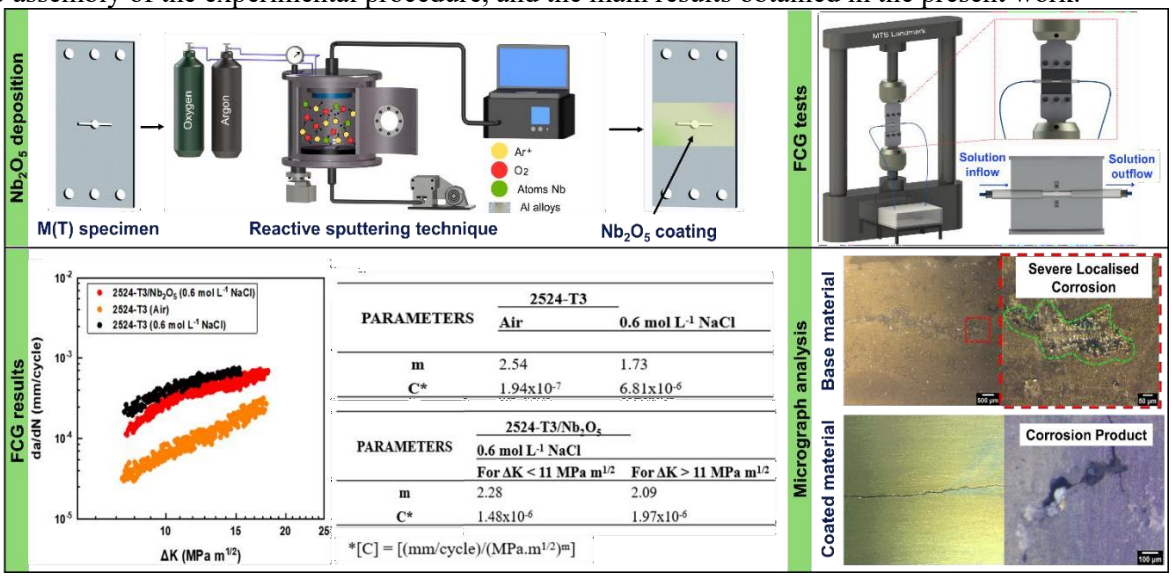

Fig. 1. *Schematic assembly of the experimental procedure, and the main results obtained in the present work.*

4. References

[1]Moreto, J.A. et al. J. Mater. Eng. Perform., 2018. doi:10.1007/s11665-018-3244-7.
[2]Ferreira, M.O.A. et al. Emergent Materials, 2024. doi:10.1007/s42247-024-00746-6.

Acknowledgments

PRPi/USP, CAPES, CNPq, FAPESP (2024/02504-0) and Dow for financial support and research scholarships.
*Corresponding author: kauesantos@usp.br

EFFECT OF LOW-LEVEL LASER THERAPY AND COLD ATMOSPHERIC PLASMA ON VIABILITY OF FIBROBLASTS AND KERATINOCYTES

Aline da Graça Sampaio[1]*, Noala Vicensoto Moreira Millhan[1], Fellype do Nascimento[2], Kostantin Goergiev Kostov[2], and Cristiane Yumi Koga-Ito[1]

[1]*Institute Of Science and Technology, São Paulo State University (Unesp), SP, Brazil.*
[2]*Guaratinguetá Faculty of Engineering, São Paulo University (UNESP), SP, Brazil.*

1. Introduction

Oral mucositis (OM) is a complex inflammatory process resulting from antineoplastic therapy toxicity that causes painful oral lesions in patients [1]. The healing of OM lesions is challenging due to the several cellular mechanisms involved and presence of diverse oral microorganisms [1]. Low-level laser therapy (LLLT) has been recommended for accelerating healing of OM [1]. However, without photosensitive agent it does not exhibit antimicrobial effect and lacks a standard parameter. Cold atmospheric plasma (CAP) has shown promising results in wound treatment, due to simultaneous tissue repairing and antimicrobial actions [2]. Also, it prevents systemic fungal infection from OM lesions [3]. In this study, fibroblasts and keratinocytes, important cells in the etiopathology of oral mucositis, were investigated for cell viability after undergoing LLLT and CAP treatments.

2. Experimental

Fibroblasts (3T3) and oral keratinocytes (NOK) were seeded, in 24-well plates, at a density of 1 x 10^5 cells/well in DMEM medium with 10% fetal bovine serum and 1% streptomycin/penicillin, in a 5% CO_2 incubator at 37 ºC until confluence of 70%. The cells were treated with LLLT (20 W and 5 J/cm³) for 10 s, at a distance of 2 mm, and with CAP generated in helium gas for 5 min, at a distance of 1.5 cm. Isolated and combined treatments were performed. The control group was not treated. The cells were incubated at 37 ºC for 24 h. Cell viability was assessed using the methyltetrazolium bromide (MTT) assay following the manufacturer's protocol. Optical density measurements were conducted at a wavelength of 570 nm. The obtained absorbance data were normalized with the untreated control group (= 100%). The tests were performed in two independent experiments (n=6/each), totaling n = 12. The cytotoxicity threshold was defined as 70% according to ISO 10993-5.

3. Results and Discussions

The final cell viabilities of 78.1% for fibroblasts (**Fig. 1**) and 73.7% for keratinocytes (**Fig. 2**) were observed after combined treatment with LLLT and He-CAP. According to ISO threshold, the results obtained are within the normative range for low toxicity and ensure safe exposure levels for the parameters used in this study. Furthermore, both isolated treatments did not show toxicity for 3T3 and NOK. Treatment with LLLT increased the cellular metabolism, mainly in fibroblasts. Previous studies have demonstrated that LLLT with near-infrared spectrum (980 nm) and He-CAP showed similar results on fibroblasts when both were applied independently [4].

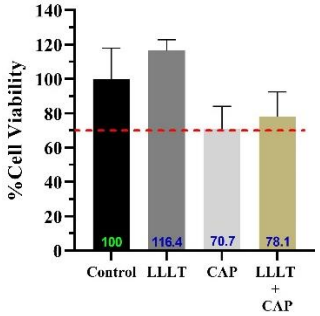

Fig. 1. *Final cell viability after exposure of fibroblasts to the treatments.*

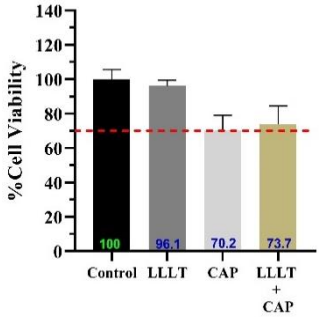

Fig. 2. *Final cell viability after exposure of keratinocytes to the treatments.*

4. References

[1]- Elad S. et al. Cancer. **126**, 4423-4431, (2020).
[2]- Von Woedtke T. In vivo. **33**(4), 1011-1026, (2019).
[3]- Sampaio A. G. et al. Int. J. Mol. Sci. **25**, 11496, (2024).
[4]- Sharif H. & Aghayan S. Immunol Gene J. **6**(2), 67-78, (2023).

Acknowledgments

The authors acknowledge National Council for Scientific and Technological Development - CNPq (grant 151911/2024) and FAPESP (2019/05856-7).

*Corresponding author: alinnsampaio@gmail.com

EXPLANATION OF TEMPERATURE DISTRIBUTION IN HELIUM STREAMS EXPANDING IN ATMOSPHERIC AIR

Fellype do Nascimento[1], Torsten Gerling[2], Bruno Honnorat[2] and Konstantin G. Kostov[1]*
[1]*Faculty of Engineering & Science – FEG, São Paulo State University – UNESP, Guaratinguetá, Brazil*
[2] *Leibniz Institute for Plasma Science & Technology – INP-Greifswald, Greifswald, Germany*

1. Introduction

In the past two decades Cold Atmospheric Pressure Plasma Jets (CAPPJs) have drown significant attention mostly because of their applications in biomedicine [1]. Nowadays, several CAPPJs designed for medical applications are commercially available. However, each medical equipment must be certified that it does not represent hazard to patients or medical staff [2]. Therefore, before it is released to the market any plasma source for medical applications should undergone an extensive characterization [3,4]. Especial attention should be given to the plasma jet gas temperature because for living tissues it cannot exceed 40°C [2]. In this work we give a brief overview of the CAPPJs development and report some results on characterization of a plasma jet system developed at UNESP for dental applications [5].

2. Experimental

The experimental setup employed in this work is presented in Fig. 1. The system operated with He, and the plasma jet was generated at the end of a 1.0-m-long flexible plastic tube, as previously reported in [6]. The gas temperature distribution was assessed by a fiber optic temperature (FOT) sensor, which practically does not perturb the plasma jet, and allows precise space-resolved measurements.

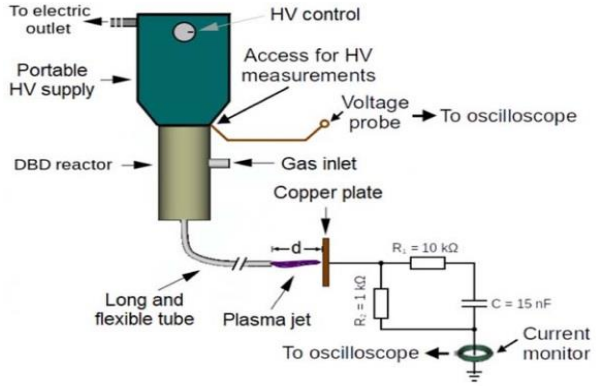

Fig. 1. *Experimental setup*

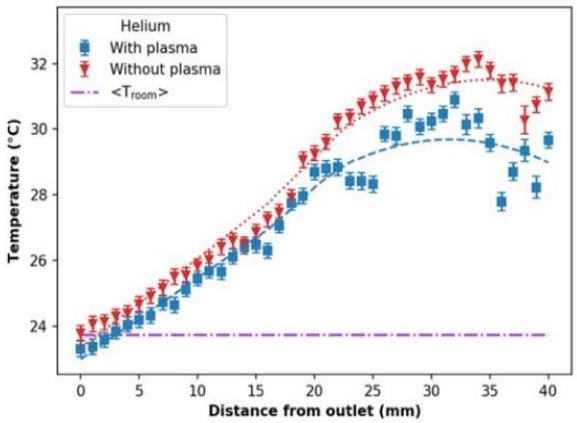

Fig. 2. *Helium stream temperature vs the distance*

3. Results and Discussions

The gas temperature of a He stream alone and with plasma excitation as a function of the distance to the target is show in Fig. 2. As can be seen the He stream heats up with the distance even in the absence of plasma. Such unexpected behavior was also observed in [4] and as demonstrated by the computer simulation in [7], can be attributed to the diffusion thermo-effect (Dufour) effect.

4. References

[1]- S. Reuter, T. von Woedtke, and K.-D. Weltmann, J. Phys. D: Appl. Phys. **51**, 233001 (2018).
[2]- DIN SPEC 91315:2014-06, General requirements for plasma sources in medicine, Beuth Verlag GmbH, 2014, https://beuth.de/en/technical-rule/din-spec-91315/203493369
[3]- A. Sobota, O. Guaitella, et al., Plasma Sources Sci. Technol., **25,** 065026 (2016).
[4]- E. Slikboer, K. Acharya, A. Sobota, E. Garcia-Caurel, and O. Guaitella, Sci. Reports, **10**, 2712 (2020).
[5]- F. do Nascimento, A. G. Sampaio, et al. IEEE, Trans. Rad. & Plasma Med. Sci. **8**, 307-322 (2024).
[6]- F. do Nascimento, T. Gerling and K. G. Kostov, Phys. Scripta **98**, 055013 (2023).
[7]- B. Honnorat, F. do Nascimento, K. G. Kostov, and T. Gerling, J. Phys. D: Appl. Phys. **58**, 281201 (2025).

Acknowledgments

We acknowledge financial support from FAPESP under grant 2019/05856-7 (research project) and 2020/09481-5 (scholarship)
*Corresponding author: konstantin.kostov@unesp.br

FUNCTIONALIZATION OF TI BY COLD PLASMA WITH SILVER NANOPARTICLES AND ADHESION ANALYSIS

Otávio Anibal Machado Silva [1], Gabriel Alves de Deus[1], Lucas Vichiato Silva[1], Lívia Elisabeth Vasconcellos de Siqueira Brandao Vaz[1, *]

[1,] *Universidade Federal de Lavras (UFLA), Chemical and Materials Engineering Department, Engineering School*

1. Introduction

Titanium is a key material in prosthetics due to its biocompatibility, but the risk of implant-associated infections persists [1]. Silver nanoparticles (AgNPs) offer antibacterial protection, and cold plasma treatment enhances their adhesion by modifying the titanium surface [2].

2. Experimental

Grade I titanium samples were sanded (Control) and plasma-treated (TP). After AgNP solution application and drying (TPA), an additional plasma treatment was applied (TPAP). Samples were characterized by AFM and SEM. AgNP adhesion was evaluated by smear tests with dry (ES) and alcohol-soaked (EA) cloths, and by dry (E) and moist (A) sterilization, followed by SEM recharacterization.

3. Results and Discussions

Plasma treatment increased titanium surface roughness and generated defects that stabilized AgNPs through thin-film formation during solvent evaporation. Plasma reapplication modified the film but did not affect AgNP morphology or distribution. In adhesion tests, abrasive rubbing (dry and with alcohol) removed most AgNPs, except in defect regions. Conversely, dry and moist sterilization showed minimal effect, indicating safe methods that preserve the integrity of the surface treatment.

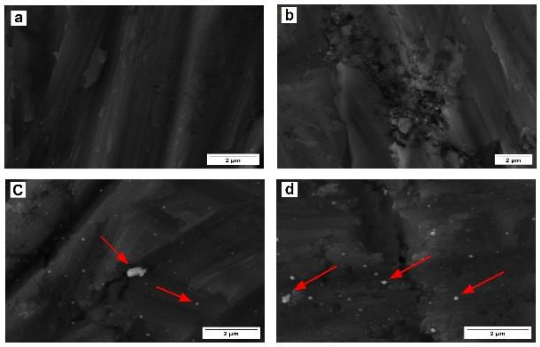

Fig. 1. *SEM micrographs of (a) Control, (b) TP, (c) TPA, (d) TPAP.*

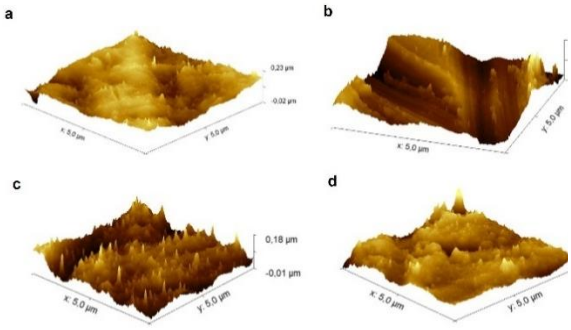

Fig. 2. *AFM images of (a) Control, (b) TP, (c) TPA, (d) TPAP.*

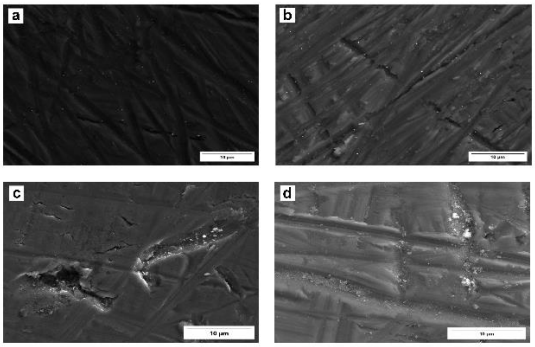

Fig. 3. *SEM micrographs of (a) TPA-ES, (b) TPAP-ES, (c) TPA-EA, (d) TPAP-EA.*

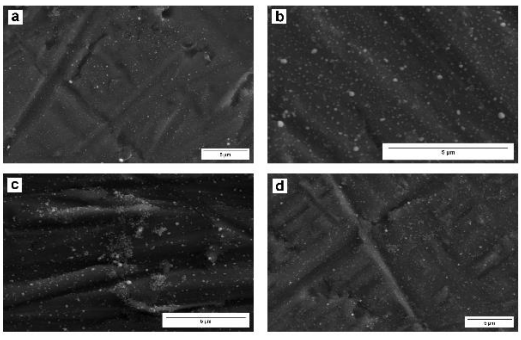

Fig. 4. *SEM micrographs of (a) TPA-E, (b) TPAP-E, (c) TPA-A, (d) TPAP-A.*

4. References

[1] H.Haugen, S.Makhtari, S.Ahmadi, B.Hussain, Materials, v. 15, n. 14, p. 5025 (2022).
[2] V.Kulieva, W.Zamora, L.Povis, Revista de la Universidad del Zulia, v. 12, n. 32 (2021).

Acknowledgments

The authors acknowledge LNNANO/CNPEM/MCTI (processes 20240177/20240208), CNPq, and UFLA for support.
*Corresponding author: livia.brandao@ufla.br

HARNESSING ATMOSPHERIC COLD PLASMA FOR EFFICIENT NITROGEN FIXATION IN FERTILIZERS

Hayanne Ywricka de Araújo Melo[12*], Jussier de Oliveira Vitoriano[123], Júlio Cesar Pereira Barbosa[123], Clodomiro Alves Júnior[123]

[1]Federal Rural University of the Semi-Arid Region (UFERSA), Brazil
[2]Department of Natural Sciences, Mathematics, and Statistics (DCME)
[3]Postgraduate Program in Materials Science and Engineering - PPGCEM

1. Introduction

Rio Grande do Norte is responsible for approximately 95% of Brazil's sea salt production. During this process, large volumes of bittern (or residual brine) are generated, an effluent rich in agriculturally valuable ions such as magnesium (Mg^{2+}) and potassium (K^+), but also containing high concentrations of chloride (Cl^-) and sodium (Na^+), which are potentially phytotoxic [1]. The selective recovery of nutrients from this brine represents a promising alternative for the production of multi-nutrient fertilizers [2].

2. Experimental

A solution was prepared by adding NaH_2PO_4 to a diluted bittern (Table 1). Then, 50 mL of this solution were stirred at 150 rpm in an Erlenmeyer flask while NaOH was added dropwise using a peristaltic pump (1 mL min^{-1} for 30 min), reaching pH 10.59 ± 0.28. The mixture was stirred for 60 min, filtered, and the precipitate dried at 100 °C until constant weight. The dried salts were then weighed in culture wells and exposed to different plasma conditions.

3.

	Concentration of the bittern (g/L)					
	Na^+	K^+	Mg^{2+}	SO_4^-	P	Cl^-
Inicial	64.50	10.12	41.81	59.61	-	186.61
After dilution and adding of NaH_2PO_4	47.09	5.06	20.91	29.81	19.97	93.31

Table 1. *Inicial concentration of the bittern and after dilution and addition of NaH_2PO_4.*

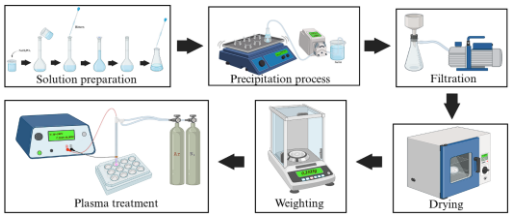

Fig. 1. *Precipitation and plasma treatment processes.*

Results and Discussions

The precipitation process produced an almost insoluble white powder, with a mass of 5.62 ± 0.75 g. Chemical analysis (Figure 2) indicated that 44.41 wt% of the precipitate corresponded to recovered ions, while the remaining 55.59 wt% was attributed mainly to water. This is consistent with the XRD patterns (Figure 3), which identified Hazenite ($KNaMg_2(PO_4)_2 \cdot 14H_2O$) as the predominant phase. Is also shown in figure 3 that NaCl is not present. Plasma increased the crystallinity of the precipitate, that was originally very amorphous.

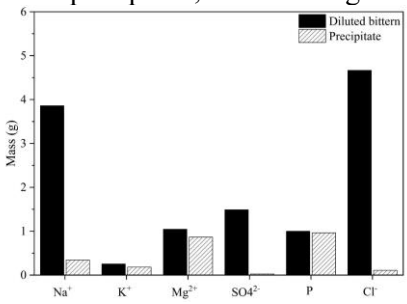

Fig. 2. *Recovery of ions in the precipitate compared to inicial amount on the solution.*

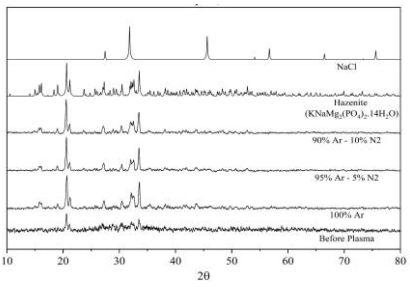

Fig. 3. *XRD pattern of the precipitate showing Hazenite as the main phase and absence of NaCl phase.*

4. References

[1]- T. Melo, L. Rocha and C. Alves Junior, IEEE Trans. Plasma Sci. PP, 1–6 (2023).
[2]- J. A. Fernandez Lozano and L. Sanvicente, Interciencia, 496-499, (2002).

Acknowledgments

This project was funded by the National Council for Scientific and Technological Development (CNPq) and National Council for the Improvement of Higher Education (CAPES).

*Corresponding author: hayanneywricka@gmail.com

IMPACT OF LOW-PRESSURE PLASMA TREATMENT TIME ON THE PHYSICOCHEMICAL PROPERTIES OF N95 RESPIRATORS

Kevin Machado Rodrigues[1], Maria Cláudia Batista[1], Elidiane Cipriano Rangel[1]
[1]*São Paulo State University (UNESP), Institute of Science and Technology (Sorocaba), Av. Três de Março, 511, 18087-180 Sorocaba, SP, Brazil*

1. Introduction

The COVID-19 pandemic has led to a significant increase in hospital waste, particularly disposable masks, creating a need for efficient and safe disinfection methods. Since plasma treatment has been demonstrated to be an effective technique for disinfection [1], this study investigates how exposure time to argon–oxygen plasma mixtures, in the presence of sodium chlorite ($NaClO_2$), affects mask fabric properties, aiming to determine the optimal treatment duration that minimizes degradation.

2. Experimental

Samples prepared from white and blue commercial N95 respirator were mounted on the upper electrode of a capacitively coupled plasma reactor. Sodium chlorite (0.8 g) was placed on the lower electrode, and the system was evacuated to the base pressure (~2.0×10^{-2} Torr). Argon and oxygen gases were then introduced to establish a working pressure of 7.0×10^{-2} Torr, and a 100 W radiofrequency excitation signal was applied to the lower electrode to promote $NaClO_2$ sputtering into the plasma. The treatment time was varied between 2 and 30 minutes. The samples were analyzed by scanning electron microscopy (SEM), contact angle measurements, and Fourier-transform infrared spectroscopy (FTIR). Wettability tests, performed using the sessile drop method, were conducted a few hours after treatment and after sample aging in air for 15 and 30 days. The plasma phase composition was characterized by optical emission spectroscopy (OES).

3. Results and Discussions

The untreated fabrics displayed smooth, tubular, and elongated fibers. After plasma exposure, no significant morphological changes were observed for treatment times up to 23 minutes (Fig. 1). The white and blue fabrics correspond to polypropylene (PP) and polyester (PE), respectively. Chlorine incorporation into the fabric structure was detected after treatment, consistently with Cl presence in plasma atmosphere (Cl, Cl_2, Cl^+) along with O, O_2, and Ar species (Fig. 2). Wettability tests revealed that PP became hydrophilic after treatment but gradually recovered its hydrophobicity after 15 to 30 days of aging in air. In contrast, PE remained superhydrophilic throughout the period. Among all tested conditions, a 16-minute exposure provided the most favorable balance, preserving the structural integrity of the fabrics and minimizing energy consumption.

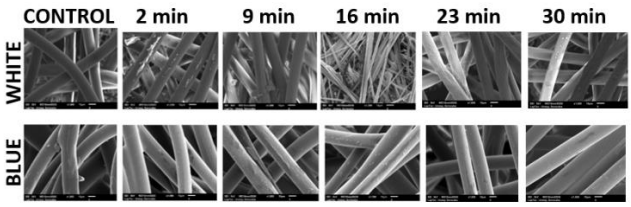

Fig. 1. *Secondary electron micrographs of the white and blue respirator fabrics following plasma treatments of varying durations, shown alongside their respective controls.*

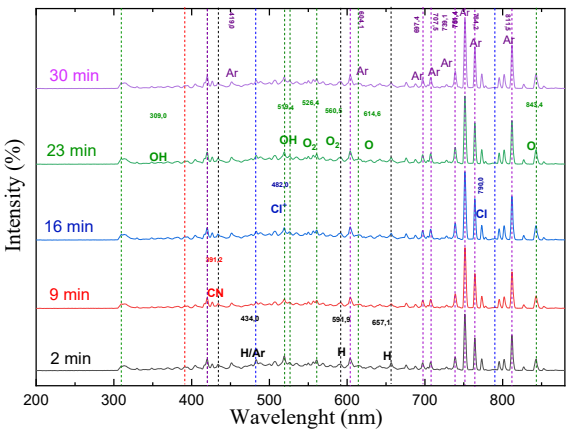

Fig. 2. *Optical emission spectra of the plasma recorded at various treatment durations.*

4. References

[1] - KALISY, N. Métodos para Inativação Microbiana em Processos Industriais. Ufsc.br, 2022.

Acknowledgments

The authors would like to thank the FAPESP (2017/21034-1), CNPq-PQ (1929/2021) and CNPq-PIBIC 2024/2025 for its financial support (process # 17954).

ROLE OF THE PLASMA EXCITATION POWER ON N95 RESPIRATORS PROPERTIES IN THE PRESENCE OF $NaClO_2$

Santos, L. G. A[1]. Batista, M. C. S. [1], Rangel, E. C.[1]
[1]Universidade Estadual Paulista (UNESP), Instituto de Ciência e Tecnologia de Sorocaba (ICTS) – Avenida Três de Março, 511 - Alto da Boa Vista - Sorocaba/SP - CEP 18087-180

1. Introduction

The COVID-19 pandemic has intensified the use and disposal of N95/PFF2 respirators, forcing the creation of sustainable sterilization methods that allow their reuse. Low-pressure plasma stands out due to its low processing temperature and controlled reactivity to interact with polymeric materials without causing significant degradation [1]. In this context, the present study aims to investigate the effect of varying excitation power in argon–oxygen plasmas, in the presence of sodium chlorite, on the physicochemical properties of N95/PFF2 respirators. The objective is to elucidate the structural and chemical changes induced by the treatment and their correlation with the plasma generation conditions.

2. Experimental

Samples of blue and white fabrics, corresponding to the outer and inner layers of N95/PFF2 respirators, were cut into 1.0 × 2.0 cm sections and treated in a low-pressure plasma system. The fabrics were mounted on the upper electrode of a capacitively coupled reactor, while 0.8 g of sodium chlorite was placed on the lower electrode. Plasma ignition was achieved by applying a 13.56 MHz radiofrequency signal to the lower electrode under an atmosphere composed of 50% O_2 and 50% Ar. The base pressure was 2.7 Pa, the working pressure 9.3 Pa, and the treatment time 600 s. The plasma excitation power was varied from 20 to 200 W, and its influence was analyzed in terms of fabric morphology (SEM), chemical structure (FTIR), elemental composition (EDS), and wettability (θ). The plasma atmosphere was monitored by optical emission spectroscopy (OES).

3. Results and Discussions

The plasma treatment affected only the surface region of the fibers, without causing damage that could compromise the material's functionality (Fig. 1). The functional groups identified in the treated fabrics indicate oxidation, evidenced by the increased intensity of the peak associated with O–H groups at 1620 cm^{-1} (Fig. 2). The white fabric, composed entirely of carbon, was identified as polypropylene (PP), whereas the blue fabric, containing 71% carbon and 29% oxygen, was identified as polyester (PE). No significant compositional changes were detected in the fabrics after plasma exposure. The PE preserved its hydrophilic character, while the PP, initially hydrophobic, became hydrophilic following plasma treatment, exhibiting a gradual recovery of hydrophobicity over time. Finally, optical emission spectroscopy (OES) confirmed the presence of reactive Cl and O species in the plasma, suggesting their involvement in the observed surface modifications.

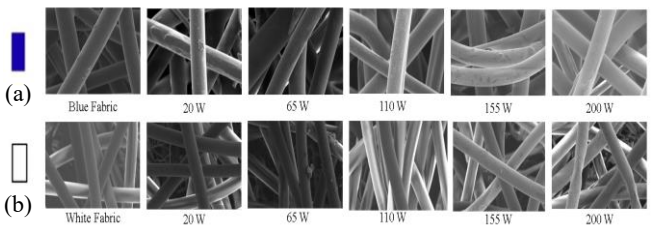

Fig. 1. *Secondary electron micrographs at 1000× magnification of (a) blue and (b) white fabric samples, untreated (control) and treated with plasma of 20; 65; 110; 155 and 200 W.*

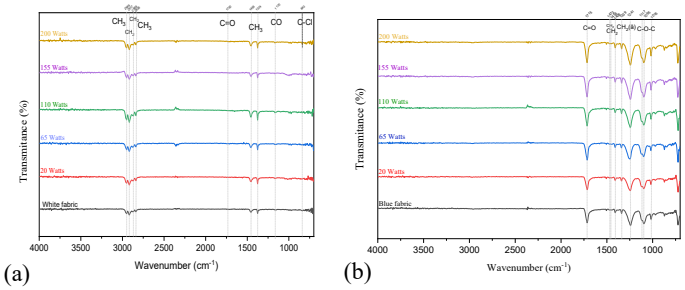

Fig. 2. *Infrared spectra of the (a) white and (b) blue fabrics exposed to plasmas with different excitation powers, along with their respective control samples.*

4. References

[1]- BENNET, D. *et al*. Evaluation of supercritical CO_2 sterilization efficacy for sanitizing personal protective equipment from the coronavirus SARS-CoV-2. **Science of The Total Environment**, v. 780, p. 146519, 2021. https://doi.org/10.1016/j.scitotenv.2021.146519

Acknowledgments

The authors would like to thank the financial support provided by FAPESP (2017/21034-1), CNPq-PQ (1929/2021), CNPq MD (#131439/2024-3) and CNPq-PIBIC 2024/2025 (#17566).

*Corresponding author: mariaclaudiasilvabatista@gmail.com

INFLUENCE OF PLASMA SPRAY PARAMETERS ON SURFACE ROUGHNESS OF THERMAL BARRIER COATINGS

Bianca Costa Rodrigues[1]*, Renata Jesuina Takahashi[1], Lucas Caetano da Silva[1], Nazir Monteiro dos Santos[2], Vera Lúcia de Óthero Brito[2], Adriano Gonçalves dos Reis[3], Danieli Aparecida Pereira Reis[1]
[1]*Universidade Federal de São Paulo (UNIFESP), Instituto de Ciência e Tecnologia, Brasil*
[2]*Instituto de Estudos Avançados (IEAv), Departamento de Ciência e Tecnologia Aeroespacial (DCTA), Brasil*
[3]*Instituto de Ciência e Tecnologia, Universidade Estadual Paulista "Júlio de Mesquita Filho", Brasil*

1. Introduction

Thermal barrier coatings (TBCs) are protective coating systems widely applied in aerospace due to their ability to protect components exposed to high temperatures [1]. These coatings are composed of three layers: an external ceramic layer (top coat); a metallic bond coat; and a thermally grown oxide (TGO) layer [2]. Considering all the deposition techniques, atmospheric plasma spraying (APS) is commonly used, and its parameters influence the resulting coating's characteristics [3]. Among these, surface roughness is critical for performance, affecting not only adhesion but also the propagation of thermal stresses and microcracks during service [4].

2. Experimental

The TBCs were produced with an 8 wt.% Yttria-Stabilized Zirconia (8YSZ) top coat and NiCrAlY bond coat, both deposited by APS on Ti-6Al-4V substrates. The top coats were applied under different process conditions. Sample TBC-1 was sprayed using a current of 700 A and 44 V, while Sample TBC-2 was sprayed using a current of 600 A and 70 V. The powder feed rate was 50 g/min. Surface roughness of the samples was measured using a profilometer (Mitutoyo SJ-210), following ISO-1997 using a Gaussian filter.

3. Results and Discussions

Surface roughness measurements are presented in Table 1 and notable differences can be observed. Sample TBC-2 presented significantly higher values of Ra, Rq, and Rz compared to Sample TBC-1. This difference can be related to the current used: 600 A for Sample TBC-2 and 700 A for Sample TBC-1. According to Martins (2023) [5], the arc current directly influences the thermal energy available for melting; therefore, lower current may lead to partially molten particles that solidify irregularly upon impact, contributing to increased roughness.

Table 1. *Surface roughness measurements*

Sample	Ra (µm)	Rq (µm)	Rz (µm)
TBC-1	4.63 ± 0.16	5.82 ± 0.11	26.34 ± 1.19
TBC-2	6.64 ± 0.57	8.53 ± 0.71	35.36 ± 2.17

In addition, literature indicates that smoother ceramic surfaces tend to accommodate thermal stresses more uniformly, reducing the likelihood of crack formation [4]. Hence, it would be expected that Sample TBC-1, with lower roughness, would exhibit fewer microcracks. These results highlight the influence of spraying current on surface roughness, reinforcing its role in performance and reliability of TBCs. Overall, the findings emphasize the importance of the spraying parameters selection to achieve the desired balance between surface characteristics, coating performance and manufacturing process optimization, ensuring both technical and cost effectiveness. Although this study focused on current, the influence of voltage on roughness deserves further investigation in future studies.

4. References

[1]- Y. Zhou et al., J. Eur. Ceram. Soc.. **44**, 3099–3111, 5, (2023).
[2]- R.J. Takahashi et al., J. Mater. Res. Technol., **19**, 4932–4938, (2022).
[3]- R. Darolia., Int. Mater. Rev., **58**(6), 315–348, (2013).
[4]- J.A. Haynes et al., Surf. Coat. Technol., **237**, 65–70, (2013).
[5]- R. F. Martins "*Estudo sobre o ataque dos silicatos fundidos (CMAS) a revestimentos para barreira térmica (TBC) depositados por aspersão térmica*", Dissertação de Mestrado em Engenharia de Materiais e Nanotecnologia, Universidade Presbiteriana Mackenzie, São Paulo, (2023).

Acknowledgments

FAPESP (Proc. 2021/02057-6), CAPES, CNPq, FINEP, IEAv - Instituto de Estudos Avançados, Alpha Metalização and Revesteel Metalização.
*Corresponding author: bianca.costa@unifesp.br

INFLUENCE OF TIME IN THE GROWTH OF ANODIC OXIDE LAYER IN A MAO-TREATED HEA TARGETED FOR BIOMEDICAL APPLICATIONS

Jhuliene E. M. Torrento[1]*, Conrado R. M. Afonso[2], Carlos R. Grandini[1], Diego R. N. Correa[1]
[1]*São Paulo State University (UNESP), Laboratory of Anelasticity and Biomaterials, Bauru, SP, Brazil*
[2]*Federal University of São Carlos (UFSCar), Department of Materials Engineering, São Carlos, SP, Brazil*

1. Introduction

High entropy alloys (HEAs) have been considered for biomedical applications due to their combination of single-crystalline structures (e.g., HCP, BCC, or FCC), low elastic modulus, and superior mechanical strength. Although the current HEAs do not fully support the complex biomechanical loads of the human body and exhibit inadequate interaction with the biological host, there are promising applications as biomaterials. Additionally, the surface of metallic biomaterials still needs to be improved to become more friendly to the biological environment of the human body [1,2]. In this context, this study aimed to functionalize the surface of a novel Bio-HEA based on non-toxic, low-cost, and non-refractory alloying elements (Ti, Zr, Mn, Al, Nb, and Fe), by micro-arc oxidation (MAO).

2. Experimental

The ingots were produced by arc melting and then subjected to homogenization heat treatment. Finally, MAO treatment was performed at 300 V and 2.5 A for 1 to 9 minutes in a Ca-, P-, and Mg-rich electrolyte. The samples after surface coating were characterized by optical, scanning electron, and transmission electron microscopy. Chemical mapping was performed by EDS, and further analyses included XRD, FTIR, XPS, confocal microscopy, and, finally, wettability and tribocorrosion measurements.

3. Results and Discussions

The MAO-treated samples exhibited a porous surface (Fig. 1) with microscale thickness and were enriched with elements from both the alloy (mainly Ti, Zr, Nb, Fe, and Mg) and the electrolyte (Ca, P, Mg, and O), present in chemical states favorable for bone regeneration and corrosion resistance (e.g., TiO_2 and ZrO_2). The oxide layer displayed amorphous and nanocrystalline structures, with a preferential concentration of bioactive ions in the outermost region. These characteristics, combining enhanced corrosion resistance with a rough and hydrophilic surface, suggest promising properties for potential biomedical applications. Furthermore, the treatment time was found to be directly proportional to both the incorporation of elements and the growth of the film, which in turn affected its porosity and thickness.

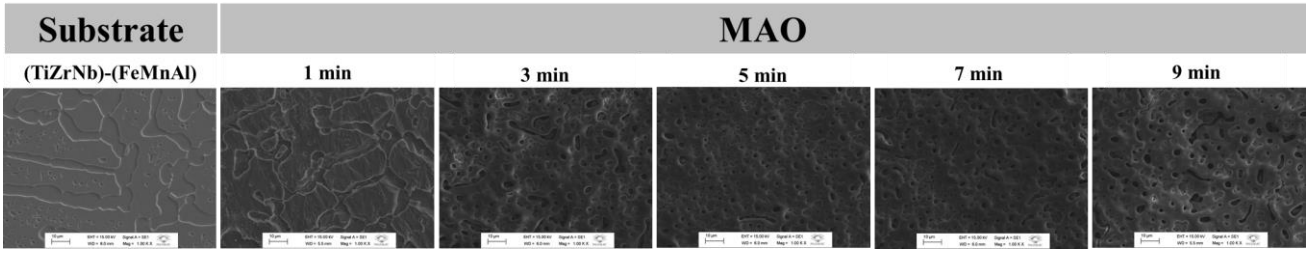

Fig. 1. *SEM micrographs of the (TiZrNb)-(FeMnAl) HEA substrate and the MAO-treated samples.*

These characteristics indicate that the functionalized Bio-HEA, particularly the sample treated with MAO for 9 minutes, exhibits surface chemistry well-suited for biomedical applications, demonstrating significant potential as a biomaterial for implants and medical devices.

4. References

[1] J.E. Torrento, et al. APL Materials, 10, 081113, (2022).
[2] J.E. Torrento, et al. Materials Characterization, 208, 113678, (2024).

Acknowledgments

Financial support: FAPESP #2023/15812-2 and #2021/13921-3.
*Corresponding author: jhuliene.torrento@unesp.br

MICROSTRUCTURE ANALYSIS OF THE Ti-40Ta ALLOY SYNTHESIZED BY LASER DEPOSITION WITH POTENTIAL USE AS BIOMATERIAL

Romualdo Emílio[1,2], Cicero Lustosa[3], Amélia Almeida[4], Odila Florêncio[1]*
[1]*Universidade Federal de São Carlos, CEP 18052-780, Sorocaba-SP, Br*
[2]*Centro Paula Souza – ETEC Fernando Prestes, CEP 18040-810, Sorocaba- SP, Br*
[3]*Mackenzie Presbyterian University, CEP 01302-907, São Paulo/SP, Br*
[4]Center of Physics and Engineering of Advanced Materials, Instituto Superior Técnico, Universidade de Lisboa, Lisboa, Pt

1. Introduction

Titanium alloys have been widely studied in the field of biomaterials because of their suitable mechanical properties, such as low elastic modulus, excellent corrosion resistance, and high biocompatibility [1]. Depending on the solidification and cooling conditions, these alloys can form with different microstructures that results in a range of mechanical properties, relevant for biomedical applications. Of particular interest are metastable phases, like the martensitic phases α' (hexagonal close-packed) and α'' (orthorhombic), and the ω phase (hexagonal). The martensitic transformation occurs due to the rapid cooling from the β-phase (body-centered cubic) and is usually characterized by the formation of a microstructure with very fine needles [2].

2. Experimental

The Ti-40Ta (wt%) alloy was synthesized by laser deposition from a mixture of Ti and Ta elemental powders using steel plates as substrate. The experiments were performed using a 1.5 kW diode laser (Laserline LDM 150-60), a powder feeder where the powder mixture is carried by a flow of argon and fed to the laser melt pool through a lateral nozzle [9] and a CN control positioning system. The alloys deposition was carried out at the Laser Laboratory of the University of Lisbon/Pt. X-ray Diffraction analysis of the Ti-40Ta alloys was performed using a Miniflex diffractometer (Rigaku), using Cu Kα radiation (λ=1.5406Å). The microstructure was analyzed by scanning electron microscopy using a Jeol JSM-6510 instrument. The structural characterization was done in the Materials Laboratory of Mackenzie Presbyterian University/Br.

3. Results and Discussion

Figure 1 presents the X-ray diffractogram of the Ti-40Ta alloy, showing that the material is predominantly formed of the α'' phase (orthorhombic) containing a small amount of the β phase (body-centered cubic), which is in good agreement with previous results [3]. The microstructure of the Ti-40Ta (Figure 2) shows a branched morphology, similar to dendrites, that corresponds to the α'' martensitic phase, while the darker regions are the untransformed β phase. Thus, a mixture of untransformed β and orthorhombic α" martensite coexists in the microstructure of the Ti-40Ta alloy, confirming the results obtained by XRD. Untransformed β-phase is stabilized at the dendrite boundaries due to segregation of Ta.

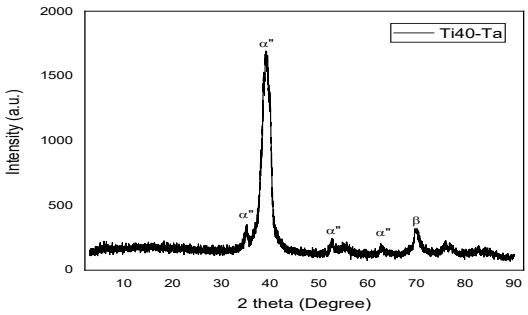

Fig. 1. *X-ray diffraction pattern of Ti-40Ta alloy.*

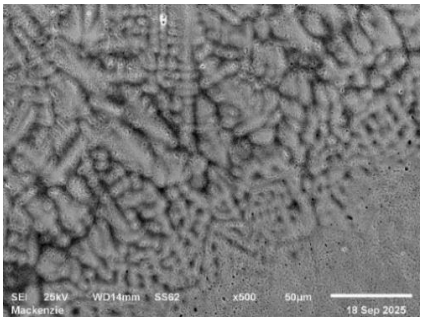

Fig. 2. *Microstructure of Ti-40Ta alloy.*

4. References

[1] M. Niinomi, J. Mech. Behav. Biomed. Mater., **1**, 30-42. (2008).
[2] G. Lutjering; J. C. Williams, Titanium. [S.l.]: Springer, (2003).
[3] M. Teixeira et al, ICALEO 2013, (CD-ROM Paper#303), 34-42 (2013).

Acknowledgments
FAPESP (2022/04825-3)/Br, FCT (CEFEMA Project UID/04540)/Pt.
*Corresponding author: odila@df.ufscar.br

ESS PROTON BEAM COMISSIONING ON DUMP AND VACUUM SYSTEM OPERATION FOR BEAM ON TARGET

Marcelo J. Ferreira[1], Adrien Besson[1], Laurence Page[1], Artur Gevorgyan[1] and Hilko Spoelstra[1]
[1]*European Spallation Source – ERIC, Accelerator Division, Vacuum Group, Lund, Sweden*

The European Spallation Source (ESS) is a multidisciplinary research infrastructure and neutron source facility based on a 2 GeV, 5 MW proton linear accelerator (LINAC). The goal of ESS is to become the brightest neutron facility, enabling groundbreaking research in various fields such as biology, environmental science, and fundamental physics. The facility includes superconducting radio-frequency (SRF) cavities in particle-free conditions [1] to accelerate a proton beam, which produces neutrons through a spallation process on a helium-cooled tungsten wheel. The facility has the capacity to host up to 42 neutron instruments.

The ESS Vacuum Group is responsible for all technical vacuum systems across the Accelerator, Target, and Neutron Scattering Instruments (NSS).

This presentation will provide an overview of the installed vacuum system for the commissioning phase of the proton accelerator and monolith target as of Q3 2025. It will cover the vacuum hardware, the vacuum control system's EPICS interface, and the early performance of the system, which includes the first beam to the tunning beam dump. Additionally, a idescription of the Target monolith vacuum system, and comments on the neutron instrument installation activities will also be included.

Fig. 1. *ESS facility site, including Accelerator, Target, experimental halls and offices building.*

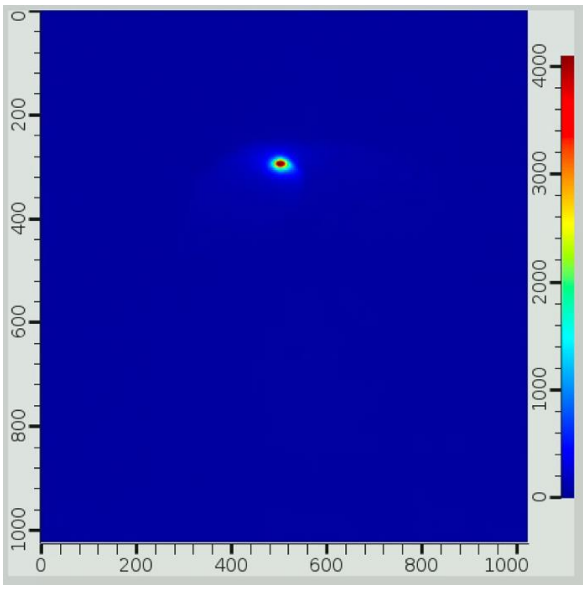

Fig. 2. *Proton beam on dump, scintillator screen [2] viewed by a camera (false-color EPICS/Area detector image system).*

References

[1] C. Jarrige, F. Ravelli, and M. Juni Ferreira, "*Developing the Particle Free Vacuum System at ESS"*, Revista Brasileira de Aplicações de Vácuo, 37(3), (2018).
[2] Erik Adli, et all, *"Progress of the ESS proton beam imaging system",* LINAC2022 proceedings, 394-1106, (2022).
*Corresponding author: marcelo.juniferreira@ess.eu

MOLECULAR BEAM SCATTERING ON OXIDIZED METAL SURFACES: DYNAMICS AND INTERACTIONS

Arved C. Dorst[1,2], Rasika E. A. Dissanayake[1,2], Daniel R. Killelea[3], Alec M. Wodtke[1,2], Tim Schäfer[1,2]*
[1]Institute of Physical Chemistry, University of Göttingen, Göttingen, Germany
[2]Max-Planck Institute for Multidisciplinary Sciences, Göttingen, Germany
[3]Department of Chemistry and Biochemistry, Loyola University Chicago, Chicago, IL, United States

Non-evaporative getter (NEG) coating is an innovative ultra-high vacuum technology originating from particle accelerators, which adds a gas adsorption function to the vacuum wall to act as a getter pump. The J-PARC vacuum group has developed this technology while exploring industrial applications.

Additionally, in the J-PARC 3GeV Synchrotron, turbo molecular pumps are employed as the main evacuation system. Currently, a new turbo molecular pump is under development, utilizing high-strength titanium alloys for rotor blades to achieve higher rotation speeds, significantly enhancing both pumping speed and compression ratio. Furthermore, additive manufacturing technologies are being applied to rotor blade production, enabling the realization of complex shapes that are challenging to achieve through traditional machining.

We combine velocity map imaging (VMI) with temperature-programmed desorption (TPD) and molecular beam surface scattering experiments to record the angular-resolved velocity distributions of recombinatively-desorbing oxygen from single crystal surfaces. We assign the velocity distributions to desorption from specific surface and sub-surface states by matching the recorded distributions to the desorption temperature.

These results provide insight into the recombinative desorption mechanisms and the availability of oxygen for surface-catalyzed reactions. We use concepts of detailed balance to analyze translational energy distributions of O_2 when shifted towards hyperthermal energies. These distributions indicate desorption from intermediate activated molecular chemisorption states [1, 2].

We build on these studies to investigate the epoxidation of styrene to styrene oxide on Ag(111), a key heterogeneous catalytic reaction in the chemical industry. Efficient conversion to styrene oxide occurs only in the presence of electrophilic oxygen on the surface [3].

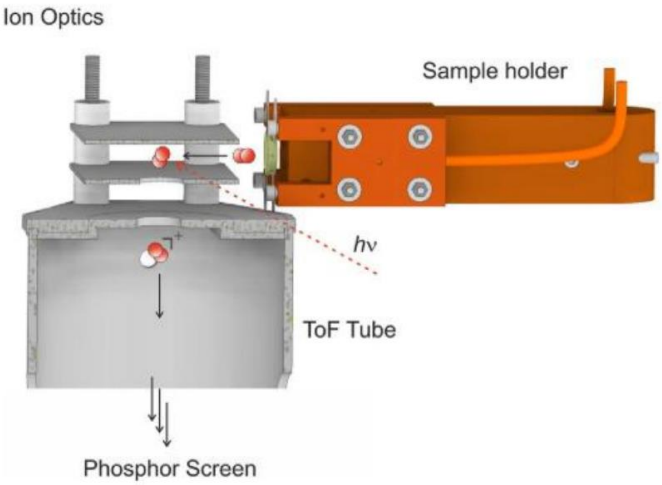

References

[1] Dorst, A. C.; Güthoff, F.; Schauermann, D.; Wodtke, A. M.; Killelea, D. R.; Schäfer, T. Velocity map images of desorbing oxygen from sub-surface states of Rh(111). Physical Chemistry Chemical Physics 2022, 24 (43), 26421-26427
[2] Dorst, A. C.; Dissanayake, R. E. A.; Schauermann, D.; Knies, S.; Wodtke, A. M.; Killelea, D. R.; Schäfer, T. Hyperthermal velocity distributions of recombinatively-desorbing oxygen from Ag(111). Frontiers in Chemistry 2023, 11,
[3] Dissanayake, R. E. A.; Dorst, A. C.; Benfreha, K.; Killelea, D. R.; Schäfer, T. Heterogeneously Catalyzed Partial Oxidation of Styrene on a Silver Surface. ChemCatChem 2024, 16 (17), e202400657

*Corresponding author: tschaef4@mpinat.mpg.de

SOCIAL IMPLEMENTATION OF VACUUM TECHNOLOGY DERIVED FROM ACCELERATORS

Junichiro Kamiya[1]*
[1]Japan Atomic Energy Agency, Japan

Non-evaporative getter (NEG) coating is an innovative ultra-high vacuum technology originating from particle accelerators, which adds a gas adsorption function to the vacuum wall to act as a getter pump. The J-PARC vacuum group has developed this technology while exploring industrial applications.
Additionally, in the J-PARC 3GeV Synchrotron, turbo molecular pumps are employed as the main evacuation system. Currently, a new turbo molecular pump is under development, utilizing high-strength titanium alloys for rotor blades to achieve higher rotation speeds, significantly enhancing both pumping speed and compression ratio. Furthermore, additive manufacturing technologies are being applied to rotor blade production, enabling the realization of complex shapes that are challenging to achieve through traditional machining.
This presentation will highlight the latest advances in the social implementation of these groundbreaking developments based on accelerator vacuum technology.

METAL–SUPPORT INTERACTION SYNERGY IN LOW-LOADED PALLADIUM CATALYSTS

Miguel D. Sánchez*
Instituto de Física del Sur (IFISUR), Departamento de Física, Universidad Nacional del Sur (UNS), CONICET, Bahía Blanca, Argentina.

Precious metals such as Pd, Pt, Ir, Rh, and Ru are well established as key components of heterogeneous catalysts, playing a crucial role in a wide range of processes, including chemical manufacturing, fuel production, environmental catalysis, photocatalysis, and electrocatalysis. A commonly cited drawback of their use is their high cost and low natural abundance, which has motivated efforts to replace them with more accessible transition metals such as Ni, Co, or Cu. However, the substitution of one catalytic metal for another cannot be justified solely based on availability or cost, as catalytic performance arises from a complex interplay of structural and physicochemical factors.

In general, catalytic activity and stability are governed by several parameters, including morphology, structure, composition, conductivity, particle size, and specific surface area. Among these, particle size and its interaction with the support are particularly decisive in determining both catalytic activity and long-term stability.

Pd-based catalysts, for instance, are widely employed in hydrogenation, oxidation, and coupling reactions. Their performance strongly depends on the ability of Pd to interact with surface oxides, which in turn is determined by the choice of support material. Reducible oxides are especially attractive in this regard. CeO_2, in particular, offers unique redox properties that can be further enhanced through the incorporation of transition metals. This interaction enriches the surface oxygen vacancies, thereby facilitating the activation of oxygen-containing molecules and improving catalytic performance.

This talk will guide you through our investigation into low-loaded Pd catalysts, with a special focus on the crucial role of reducible supports like CeO2. We have systematically studied different catalyst configurations like Pd/Al2O3, CeO2-Pd/Al2O3, and PdCeO2 solid solutions to unravel the synergy between Pd and Ce in applications like methane dry reforming [1-4] and the reverse water-gas shift reaction [5,6]. I will share our most significant findings, which were revealed by combining structural and spectroscopic techniques, to illustrate how this specific interaction dictates overall catalytic performance and stability.

References

[1]- C.E. Gigola, M.S. Moreno, I. Costilla, and M.D. Sánchez. Applied Surface Science 254, 1 (2007) 325-329.
[2]- M.D. Sánchez, M.S. Moreno, I. Costilla and C.E. Gigola. Catalysis Today 133-135 (2008) 842-845.
[3]- M.S. Moreno, F. Wang, M. Malac, T. Kasama, C.E. Gigola, I. Costilla and M.D. Sánchez. Journal of Applied Physics, 105, (2009) 083531-6.
[4]- Ignacio O. Costilla, Miguel D. Sánchez, Carlos E. Gigola. Applied Catalysis A: General 478 (2014) 38–44.
[5]- I.O. Costilla, C.E. Gigola and M.D. Sanchez. Latin American Applied Research, 2025, 55(2): 185–192.
[6]- Yésica Torres, Ignacio O. Costilla, Martín Piqueras, Carlos E. Gigola y Miguel D. Sánchez, Actas del XXII Congreso Argentino de Catálisis (2022).

*Corresponding author: msanchez@uns.edu.ar

PHOTOPHORETIC LEVITATION OF PERFORATED STRUCTURES IN NEAR-SPACE CONDITIONS

Felix Sharipov[1] and Benjamin Schafer[2]
[1]*Departamento de Física, Universidade Federal do Paraná*
[2]*Harvard University, Cambridge, MA, USA, Rarefied Technologies Inc., Albuquerque, NM, USA*

Small structures illuminated by the sun radiation could carry light equipment in near space due to the photophoretical force. The structures can be a centimeter scale in the shape of thin membranes with different temperatures on its top and bottom [1]. The variation of surface accommodation coefficients also can create the photophotetical force when a membrane is heated uniformly. In the present work, the radiometric force exerted on a thin membrane with perforations of various types are calculated by the direct simulation Monte Carlo method over wide ranges of the membrane porosity and gas rarefaction spanning free-molecular, transitional, and viscous regimes. The heat flux to surrounding gas from the membrane needed to assess its temperature is calculated too. *Ab initio* potentials are applied to model the intermolecular collisions in the frame of quantum theory of scattering [2]. The gas-surface interaction is modeled using the Cercignani-Lampis kernel considering various values of the tangential momentum and normal energy accommodation coefficients. We find that perforations increase the force several times in the viscous regime of flow but decrease the force in the free-molecular and transitional regimes. The influence of the accommodation coefficients is also studied. The effects of gas species, degree of non-equilibrium, and environment temperature are found to have relatively small effects on dimensionless quantities such that the reported results can be applied to wide ranges of these factors and, hence, to numerous practical situations.

References

[1] B.C. Schafer, J. Kim, F. Sharipov, G-S Hwang, J.J. Vlassak, D.W. Keith, Photophoretic flight of perforated structures in near-space conditions. Nature 644 362-369, (2025).
[2] F. Sharipov, Modelling of transport phenomena in gases based on quantum scattering. Physica A 508, 797-805 (2018).

Acknowledgments

F.Sh. is supported by CNPq (Brazil). B. Sch. is supported by Rarefied Technologies. The calculations were run on the FASRC cluster at Harvard University.

ZNO NANOSTRUCTURES: A VERSATILE SEMICONDUCTOR FOR NEXT-GENERATION OPTOELECTRONIC AND SENSING DEVICES

Nadia Celeste Veja

Departamento de Física, Facultad de Ciencias Exactas y Tecnología, Universidad Nacional de Tucumán (UNT), Tucumán, Argentina.
Instituto de Física del Noroeste Argentino, Consejo Nacional de Investigaciones Científicas y Técnicas (CONICET)-UNT

This presentation details our research on the synthesis and characterisation of zinc oxide (ZnO) nanostructures. It will be highlighted how diverse techniques—from vapour transport for nanowires (NWs) and nanofiber networks, to low-temperature chemical vapor deposition (LTCVD) for c-oriented thin films—enable precise control over material morphology and properties.

The possibility of surface modification of ZnO, like the sensitisation with ruthenium(II) complexes that optimise its optoelectronic properties, is discussed. An extensive characterisation, including SEM, HRTEM, and XRD, will be presented to confirm the successful controlled growth and robust sensitiser anchoring, which is crucial for efficient charge transfer.

Finally, the remarkable versatility of these nanostructures is demonstrated across multiple fields, with their superior performance in solar cells (DSSCs and OSCs), high sensitivity in UV light sensors and gas sensors, and promising potential in energy storage applications, such as lithium-ion batteries. These findings collectively position ZnO as a fundamental and highly adaptable material for the development of next-generation devices.

THE INTERPLAY OF ELECTRONIC STRUCTURE, MORPHOLOGY AND CHARGE TRANSFER DYNAMICS OF SEMICONDUCTORS WITH APPLICATION IN ORGANIC SOLAR CELLS

Maria Luiza Rocco[1]*
[1]*Institute of Chemistry, Federal University of Rio de Janeiro, 21941-909, Rio de Janeiro, RJ, Brazil*

1. Introduction

Energy production is a global concern. An alternative to energy production is to use solar energy, which is a renewable, clean and abundant source. In recent years, there has been a great advance in the research for the use of molecular solids in optoelectronic devices, which have clear advantages over inorganic devices, such as low production cost, sustainable character, easy processability and the possibility to produce lighter and more flexible devices. One of the major challenges in this area is the development of organic semiconductors with high charge mobility and environmentally stables. Therefore, information related to the electronic structure, ordering and molecular orientation as well as charge transfer dynamics in these materials become highly necessary to understand the conduction mechanism and, therefore, to assist in future applications. In this way, spectroscopic techniques with the use of synchrotron light were employed for the study of new organic semiconductors, in order to broaden our understanding of the relation between the electronic, structural and morphological properties of these materials and the response of the device, aiming at thus contributing to the area of Organic Electronics.

2. Experimental

Near edge X-ray absorption fine structure (NEXAFS) spectra were measured at the Brazilian Synchrotron Light Source (LNLS). NEXAFS spectra were collected in the total electron yield mode (electron current at the sample) simultaneously with a photon flux monitor (Au grid). The final data was normalized by this flux spectrum to correct for fluctuations in beam intensity. The energy calibration at the double crystal Si(111) monochromator was performed by taking the well-known value for the L_{III} transition ($2p_{3/2} \rightarrow 4d$) of metallic molybdenum. Polarization dependence was evaluated by measuring NEXAFS spectra at different incoming X-rays incident angles. Resonant Auger spectra (RAS) were also measured in the same ultrahigh vacuum chamber with a base pressure of 10^{-8} mbar using a hemispherical electron energy analyzer. The take-off direction of Auger electrons was 45º and a pass energy of 20 eV was used during the experiment. No beam damage effects were observed throughout the measurements as monitored by photoabsorption and photoemission spectra.

3. Results and Discussions

NEXAFS and RAS using the core-hole clock (CHC) approach were applied in the investigation of molecular orientation and ultrafast electron dynamics in the low femtosecond regime for thiophene based-polymers following S K-edge photoexcitation. Remarkable changes developed in the sulfur $KL_{2,3}L_{2,3}$ Auger decay spectra by tuning the photon energy along the sulfur 1s absorption edge, depending on the nature of the intermediate core excited states. It was possible to disentangle transitions to π* and σ* states not resolved by photoabsorption. Competition between core hole decay and delocalization of the photoexcited electron was monitored and the branching ratio of spectator and normal Auger channels derived. Electron delocalization times in the femtosecond domain were calculated for poly(thiophene) with a value of less than 10 fs on resonance. Results for more complex thiophene-based polymers processed through halogenated and non-halogenated solvents and blended with fullerene/non-fullerene acceptors as well as studies on an ITO-free electrode were also performed, demonstrating the importance of NEXAFS and the CHC approach to probe molecular ordering and femtosecond electron delocalization dynamics in polymeric thin films for organic photovoltaics.

4. References

[1]- C. P. C. Ferreira et al., RSC Advances, **14**, 9051-9061, (2024).
[2]- W. A. Misael et al., Journal of Physical Chemistry C, **126**, 10807-10817, (2022).

Acknowledgments

Research partially supported by LNLS – National Synchrotron Light Laboratory, Brazil. The author would like to acknowledge CNPq and FAPERJ for financial support.
*Corresponding author: luiza@iq.ufrj.br

OBTAINING TWO-DIMENSIONAL MATERIALS FOR SENSOR APPLICATIONS

Marcelo Eduardo Huguenin Maia da Costa[1]*
[1]*Departamento de Física, PUC-Rio*

1. Introduction

There is a growing need for chemical sensors capable of detecting increasingly smaller quantities of substances, especially when dealing with toxic elements such as methylmercury, or when aiming to produce selective sensors for trace amounts of materials. Sensors can operate based on different mechanisms, but a crucial factor is the interaction between the toxin—or the target element—and the sensor itself.

In this context, two-dimensional materials present enormous potential due to the fact that all atoms forming the layer are exposed to the surrounding environment. When this layer is exposed to the medium to be sensed, any interaction between surfaces—such as the adsorption of a molecule on the material's surface—can lead to measurable responses through the modification of certain properties, such as resistivity, photoluminescence, or others.

A key aspect in producing these sensors lies in the selection and synthesis of the two-dimensional material, which is not always a simple or straightforward process. Several choices must be made, beginning with the type of material, which is closely linked to the sensor's operating principle, the target analyte, production costs, and other factors.

In this work, we discuss several methods for obtaining materials such as transition metal dichalcogenides (MoS_2, WS_2, etc.), graphene, oxidized and reduced graphene, as well as their doping and surface decoration. We address physical and chemical exfoliation methods, and chemical vapor deposition (CVD) growth processes, emphasizing the different characteristics that arise depending on the synthesis method employed.

Acknowledgments

I would like to thank the funding agencies CNPq, CAPES, and FAPERJ for their financial support.

*Corresponding author: maiacosta@vdg.fis.puc-rio.br

SPUTTERING ON LIQUIDS FOR THE PRODUCTION OF MULTIMETALLIC NANOPARTICLES

E. Rangel[1], T. Passeti[2], L. Almeida[3], R. P. Ribeiro[1], A. Sauldubois[4], P. Andreazza[5], A-L. Thomann[6], E. Robert[6], A. Caillard[6]

[1]*São Paulo State University (UNESP), Institute of Science and Technology (Sorocaba), Av. Três de Março, 511, 18087-180 Sorocaba, SP, Brazil*

[2]*Municipal University of São Caetano do Sul, R. Santo Antônio, 50, 09521-160, São Caetano do Sul, SP, Brazil*

[3] *Polytechnic School, University of São Paulo - USP, São Paulo, SP, Brazil*

[4]*MACLE-CVL, UAR CNRS, 1B Rue de la Ferollerie, 45071 - Órleans Cedex 2, France*

5 ICMN, Université d'Orléans, CNRS, UMR7374, 1b rue de la Férollerie, F-45071 Orléans, France

[6]*GREMI, Université d'Orléans, CNRS, UMR 7344, 14 rue d'Issoudun, BP6744, 45067 Orléans cedex 2, France*

1. Introduction

The synthesis of metallic nanoparticles (NPs) has garnered significant interest from researchers as it enables the fabrication of nanocomposite materials with unique properties [1]. Metallic NPs allow for the creation of new sensors, optoelectronic devices, catalysts, as well as medical treatments and diagnostics. In this study multi-metallic NPs were synthesized in colloidal suspension via sputtering of noble metal targets into various liquid matrixes, a method known as SoL. It was specifically investigated the effect of the supporting fluid on the physicochemical properties and antimicrobial properties of the NPs.

2. Experimental

The nanoparticles (NPs) were synthesized using a magnetron sputtering system via the Sputtering onto Liquids method, employing PtAu and Pt targets. The liquid matrix was placed in a Petri dish positioned on the lower electrode in front of the target. Argon was introduced at a pressure of 1.0 Pa, and plasma was generated by applying DC power (100 W) to the magnetron electrode containing the target. Each deposition process was carried out for 5 minutes per target. The influence of the liquid matrix, specifically glycerol, [BMI][BF_4], and polyethylene glycol (PEG), on the properties of the resulting NPs was evaluated. The structural and morphological characteristics of the NPs were analyzed by Small-Angle X-ray Scattering (SAXS) and Transmission Electron Microscopy (TEM). The deposition rate of the metallic species was determined by depositing a solid film on a silicon substrate and measuring its thickness using a profilometer. The bactericidal effect of the colloidal suspensions was assessed by *in vitro* microbiological tests against *Staphylococcus aureus* and *Escherichia coli*.

3. Results and Discussions

Visual inspection revealed a noticeable darkening of the liquid matrix after the dual sputtering process (Fig. 1). The deposition rate of the metallic species was approximately 80 nm/min (Fig. 2), resulting in nanoparticles with an average diameter of about 2.0 nm. In some cases, agglomeration and precipitation of the nanoparticles were observed, affecting the overall stability of the suspensions. Nanoparticles collected on polymeric substrates were detected in metallic or positively charged states, with evidence of alloy formation between Pt and Au. The colloidal suspensions exhibited either bactericidal or bacteriostatic effects, depending on the liquid matrix employed and the bacterial strain tested.

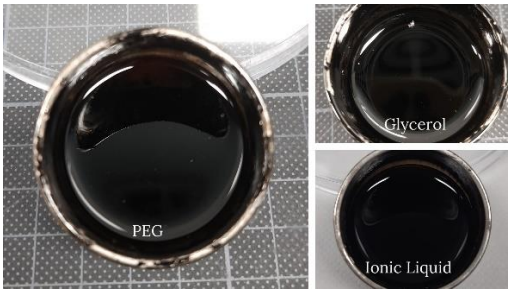

Fig. 1. *Photographic images of colloidal suspensions produced in PEG, glycerol and ionic liquid.*

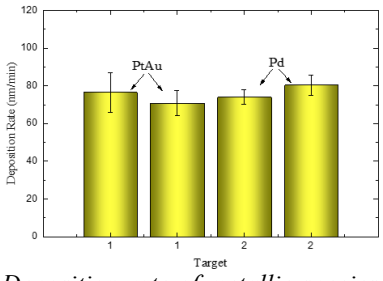

Fig. 2. *Deposition rate of metallic species using the two different targets: PtAu and Pd.*

4. References

[1] A. Sergievskaya, A. Chauvin, S. Konstantinidis, Beilstein Journal of Nanotechnology, **13**, 10 (2022).

Acknowledgments

This research was funded by the Brazilian agency CAPES, grant number 88887-977646/2024-00 and by the French national research agency (InnOxicat ANR-20-CE05-0010 project).

*Corresponding author: elidiane.rangel@unesp.br

WOUND REPAIR USING ELECTROSPUN PVA-CA DRESSINGS AND COLD PLASMA IN VIVO

Jonalba Mendes Pereira , Emilia Angela Lo Schiavo Arisawa,*Lucia Vieira
Instituto de Pesquisa e Desenvolvimento, Universidade do Vale do Paraiba, Avenida Shishima Hifumi, 2911,Urbanova, São Jose dos Campos 12244-000, SP, Brazil;

1. Introduction.

Wound healing remains a major clinical challenge, particularly in cases where infection, poor vascularization, or chronic inflammation delay tissue repair[1]. Recent advances in biomaterials and plasma medicine have opened new avenues for accelerating the healing process through the combination of biocompatible dressings and non-thermal plasma (NTP) treatments. Polyvinyl alcohol (PVA), a synthetic polymer with excellent film-forming and hydrophilic properties, has been widely used in wound dressings, while citric acid (CA) serves as a natural crosslinker that enhances mechanical stability and biocompatibility[2]. The development of electrospun PVA-CA dressings, when combined with NTP exposure, offers a promising synergistic approach to stimulate cell proliferation, angiogenesis, and collagen synthesis[2],[3]. This study investigates the in vivo wound healing potential of electrospun PVA-CA dressings used alone and in conjunction with cold plasma, providing valuable insights into their therapeutic efficacy and mechanism of action.

2. Experimental.

Polyvinyl Alcohol (PVA)-based dressings combined with Citric Acid (CA), referred to as PVA-CA, were applied with and without Non-Thermal Plasma (NTP) in the treatment of wound healing in animal models. For the study, 36 male Wistar rats were used, each with three cutaneous wounds, distributed into six experimental groups: Control (C), PVA-CA, PVA-CA+Ag, NTP alone, PVA-CA+NTP, and PVA-CA+Ag+NTP. Wound healing progression was monitored on postoperative days 3, 7, and 14 through macroscopic and histological analyses.

3. Results and Discussions

The results showed that all treatments were superior to the Control group. However, the association of NTP with the electrospun PVA-CA dressing yielded the best outcomes, with a significant reduction in wound size ($p<0.05$) and increased collagen deposition. Histological analysis also revealed greater angiogenesis and epithelialization in areas treated with this combination. Thus, the integration of NTP with electrospun PVA-CA dressings proved to be an effective and practical strategy to enhance wound healing, emerging as a promising protocol for both acute and chronic wounds.

[1]- Deng, S. (2025). Adoption of polyvinyl alcohol electrospinning materials for skin wound healing [Systematic review]. Journal of Materials Science: Materials in Medicine. https://doi.org/10.1007/s10856-025-06945-9
[2]- Pereira, J. M., Arisawa, E. A. L. S., Filho, A. L. M. M., Figueredo-Silva, J., Alves, N., da Silveira, C. H., & Vieira, L. (2025). Bioabsorbable poly(vinyl alcohol)–citric acid dressings: Wound healing studies in an experimental in vivo model. European Burn Journal, 6(2), 18. https://doi.org/10.3390/ebj6020018
[3]- Zhou, J., Sun, Z., Wang, X., Wang, S., Jiang, W., Tang, D., & Xiao, F. (2025). Low-temperature cold plasma promotes wound healing by inhibiting skin inflammation and improving the skin microbiome. Frontiers in Bioengineering and Biotechnology, 13, 1511259. https://doi.org/10.3389/fbioe.2025.1511259

Acknowledgments. We would like to thank CAPES, CNPq, and Fapesp for financial support.
*Corresponding author: lucia.vieira@univap.br

PALLADIUM NANOFOAMS APPLIED TO HYDROGEN STORAGE

Alisson Steffli Thill[1], Virginia Perez-Dieste[2], and Fabiano Bernardi[1]*

[1]*Laboratório de Física de Nanoestruturas, Instituto de Física, Universidade Federal do Rio Grande do Sul*
[2]*ALBA Synchrotron Light Source, Cerdanyola del Vall`es, Barcelona, 08290, Spain*

1. Introduction

Hydrogen has attracted an enormous scientific interest recently mainly due to the possibility of using it as a renewable and sustainable fuel. However, aiming to confirm the expectations, the development of more efficient ways of hydrogen storage is still required [1,2]. In the literature, it is possible to find several studies utilizing different materials to store hydrogen with chemical bonds or interaction forces. In particular, metallic and oxide nanostructures are investigated to improve the efficiency of carbon materials on hydrogen adsorption [3]. In a previous work of our group [4], it was demonstrated the possibility to synthesize NiO nanofoams highly promising for hydrogen storage applications, considering their great performance on mild conditions (room temperature and ambient pressure) compared to literature results. In part, this great performance is explained by the existence of the quasi-molecular bonding regime for the hydrogen adsorption process in NiO nanofoams. The quasi-molecular bonding of hydrogen with solid materials is the key factor for reaching the ultimate goal for hydrogen storage applications [5]. In the present work, the nanofoams synthesis method was extended aiming to obtain Pd nanofoams. By considering the high hydrogen affinity of Pd and the promising hydrogen adsorption results obtained by NiO nanofoams, the development of Pd nanofoams has great conditions to display an even higher hydrogen storage performance.

2. Experimental

The Pd nanofoams were synthesized following the method described in the previous work [4] using the five different phases of the phytantriol/water system as template. Therefore, five different Pd nanofoams samples were obtained. The synthesized Pd nanofoams were characterized by means of Scanning Electron Microscopy (SEM), Transmission Electron Microscopy (TEM), X-ray Diffraction (XRD), Small-Angle X-ray Scattering (SAXS) and Ambient Pressure X-ray Photoelectron Spectroscopy (AP-XPS). The AP-XPS was measured before and during hydrogen exposure aiming to determine which sample presents the higher interaction with hydrogen. Hydrogen adsorption measurements were also performed in order to obtain the hydrogen adsorption performance of all samples. Furthermore, Density functional theory (DFT) calculations were performed to determine the binding energy of hydrogen molecules in Pd structures.

3. Results and Discussions

For all samples, SEM and TEM images shown that the synthesis resulted in Pd nanofoams composed of interconnected nanoparticles with diameters in the tens of nanometers range, forming channels with diameters around 50-100 nm. However, it should be noted that the samples synthesized also contained isolated nanoparticles with diameters in the range of 4 nm. As shown by XRD, the nanofoams presented tunable amount of metallic Pd and PdO fractions. In all cases the surface is almost fully oxidized to PdO, as obtained from AP-XPS before hydrogen exposure. However, as the samples were exposure to hydrogen, they rapidly reduced. From the analysis of the AP-XPS data recorded during hydrogen exposure, it was possible to determine that the hydrogen interaction and formation of a Pd-H bond is dependent on the sample. These results can be correlated with theoretical calculations and morphology properties of the samples in order to explain their hydrogen adsorption performance.

4. References

[1]- J. O. Abe, et al., International journal of hydrogen energy, 44(29), 15072-15086, (2019).
[2]- P. A. Le, et al., RSC advances, 13(40), 28262-28287, (2023).
[3]- D. S. Pyle, et al., International Journal of Hydrogen Energy, 41(42), 19098-19113, (2016).
[4]- A. S. Thill, et al., Materials Advances, 4(2), 476-480, (2023).
[5]- P Jena, The Journal of Physical Chemistry Letters, 2(3), 206-211, (2011).

Acknowledgments
CNPq, CAPES, FAPERGS, ALBA, CNANO-UFRGS, CMM BR-Sul, CM-UFMG.
*Corresponding author: bernardi@if.ufrgs.br

UNRAVELING THE CREEP BEHAVIOR: A MECHANICAL ASSESSMENT OF ADVANCED THERMAL BARRIER COATINGS FOR AEROSPACE APPLICATIONS

Danieli Aparecida Pereira Reis[1]
[1]*Laboratório de Comportamento Mecânico de Metais (LCMM), Universidade Federal de São Paulo (UNIFESP), Instituto de Ciência e Tecnologia, São José dos Campos, São Paulo, Brasil*

1. Introduction

Thermal barrier coatings (TBCs) are a critical technology in the development of aero-engine turbines. Their advancement enables higher operating temperatures and greater thermal efficiency. TBCs have been widely used for protecting turbine blades. A typical TBC system consists of four layers: the ceramic top coat (TC), the thermally grown oxide (TGO), the bond coat (BC), and the substrate [1]. The outer ceramic layer serves as a thermal insulator, and its primary function is to protect the substrate from high temperatures [2-4]. The application of a TBC is a common and effective method for protecting turbine blades, in addition to improving their creep resistance [5].

2. Experimental

The TBCs were produced using an 8 wt.% Yttria-Stabilized Zirconia (8YSZ) top coat and a NiCrAlY bond coat. Both layers were deposited via Atmospheric Plasma Spray (APS) onto Ti-6Al-4V substrates. The top coats were applied under different process conditions. Creep tests were conducted on each specimen to analyze the effects of various TBC deposition and surface treatment conditions. Microstructural characterization and fractographic analysis were performed using optical microscopy, scanning electron microscopy, and transmission electron microscopy.

3. Results and Discussions

The creep behavior of Ti-6Al-4V coated with a thermal barrier coating (TBC) applied by a commercial air plasma spray (APS) process demonstrates that the coated alloy has greater protection against oxidation and higher creep resistance than specimens that are uncoated or only have a bond coat.

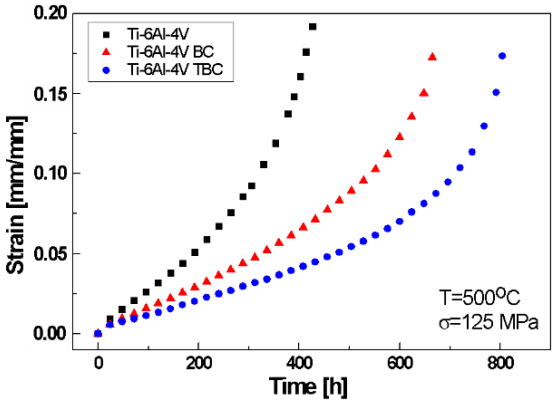

Fig. 1. Ti-6Al-4V alloy creep curves with BC and TBC at 125 MPa. (a) 500 °C

4. References

[1]- C. G. Levi, Current Opinion in Solid State and Materials Science, **8**(1), 77–91, (2004).
[2]- R. J. Takahashi et al., Journal of Materials Research and Technology, **19**(c), 4932–4938, (2022).
[3]- D. A. P. Reis, et al., Materials Science and Engineering A, **399**(1–2), 276–280, (2005).
[4]- D. A. P. Reis, et al., Materials Science and Engineering A, **486**(1–2), 421–426 (2008).
[5]- L. Yuan, et al., "Review on Creep Phenomenon and Its Model in Aircraft Engines", Hindawi Limited. (2023).

Acknowledgments

FAPESP (Proc. 2021/02057-6), CAPES, CNPq and FINEP.
*Corresponding author: danieli.reis@unifesp.br

PLASMA ELECTROLYTIC OXIDATION APPLIED TO THE DEVELOPMENT OF ALUMINUM/COMPOSITE HYBRID JOINTS

Rafael Resende Lucas[1]*, Rita de Cássia Mendonça Sales-Contini[2], Francisco José Gomes da Silva[3], Edson Cocchieri Botelho[1], Rogério Pinto Mota[1]

[1]*São Paulo State University (UNESP), School of Engineering and Sciences, São Paulo, Brazil*
[2]*Technologycal College, São José dos Campos Professor Jessen Vidal Centro Paula Souza, Av Cesare Mansueto Giulio Lattes, 1350 Distrito Eugênio de Melo, São José dos Campos 12247-014, SP, Brazil*
[1]*CIDEM, ISEP, Polytechnic of Porto, Rua Dr. António Bernardino de Almeida, 4249-015 Porto, Portugal*

1. Introduction

Academia and industry have been pursuing energy efficiency, sustainability, and the circular economy. In this context, fiber-reinforced thermoplastics (FRTP) stand out for their low density, which reduces fuel consumption in vehicles, high specific strength, excellent corrosion resistance, and high recycling potential. The application of FRTP in critical structures is limited by interfacial challenges, while conventional joining methods, such as mechanical fastening and adhesive bonding, present structural and efficiency constraints [1]. Plasma Electrolytic Oxidation (PEO) can enhance the interfacial adhesion between dissimilar materials, thereby improving the performance of hybrid joints. This is achieved through the development of ceramic coatings with micropores, which facilitate the mechanical anchoring process [2].

2. Experimental

In this study, 2024 aluminum and glass fiber-reinforced polyetherimide (PEI/GF) substrates were used to produce hybrid interfaces. Aluminum samples were treated by PEO using a sodium tetraborate (3 g/L) and potassium hydroxide (1,5 g/L) solution, promoting good oxide coating adhesion without excessive growth. Spot-type ultrasonic welding (SPOT) was performed with a Mecasonic machine, applying controlled pressure and time, with the sonotrode vibration parallel to the samples, suitable for metals.

3. Results and Discussions

Shear tests of AA2024/PEI-glass fiber joints showed that PEO treatment did not improve shear strength, with a reduction from 5.36 MPa to 4.19 MPa (≈21.8%) compared to the control group. None of the samples met the minimum industry requirements (7.1 kN). Although the creation of micro- and macrostructures is known to enhance adhesion between dissimilar materials, these mechanisms can introduce instability in the results. Compared to the literature, the values obtained are still promising, indicating the feasibility of the ultrasonic welding process even without optimization, allowing for comparative analysis with other studies. In the untreated sample, fracture was predominantly adhesive (≈55%), with thin-layer cohesive failure accounting for the remaining ≈45%, and small regions of fiber pull-out in the aluminum were insignificant. In the PEO-treated sample, a new fracture mechanism—fiber rupture (≈41%)—emerged, along with equally distributed cohesive and adhesive failures (≈29.5% each), indicating that the surface treatment significantly altered the fracture mode, promoting stress transfer into the composite, although not homogeneously.

	Control	PEO
Maximum Loading (N)	3350.60	2616.30
Lap Shear Strength (MPa)	5.36	4.19
Standard Error	0.83	0.80

Table. 1. *Maximum load and mechanical resistance of dissimilar joints*

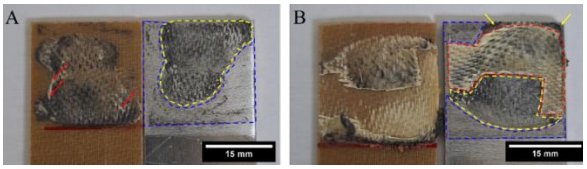

Fig. 2. *Surfaces of the samples after the LSS test. (A) Control sample. (B) PEO-treated sample.*

4. References

[1]- F. Lambiase, *et al.* Materials, **14**(8), 1890, (2021)
[2]- R. Lucas, *et al*. Applied Sciences, **14**(17), 7972, (2024).

Acknowledgments

The authors would like to thank the Coordination for the Improvement of Higher Education Personnel (CAPES) for the financial support provided under grant number 88881.933644/2024-1, and São Paulo State Research Support Foundation (FAPESP) for the scholarship, under the process number 2023/07918-5.
*Corresponding author: rr.lucas@unesp.br

RELATIONSHIP OF WO_3 STRUCTURAL PHASE ON OZONE GAS SENSING PERFORMANCE BASED ON SURFACE CHARACTERIZATION

Enzo L. Breancini[1]*, Rafael T. L. Oliveira[1], João V. N. de Palma[1], and Luís F. da Silva[1]
[1]*LM2N, Federal University of São Carlos, São Carlos, SP, Brazil*

1. Introduction

Semiconducting Metal Oxides (SMOX) are crucial for monitoring toxic pollutants, such as ozone (O_3), thereby protecting public health and the environment. Nanostructured tungsten trioxide (WO_3), exhibits polymorphic characteristics and it has been extensively employed in resistive gas sensors for detecting both toxic and non-toxic species across diverse structural phases. Also, photostimulation offers a promising strategy to enable the operation of gas sensors at mild temperatures. Herein, we conducted a controlled synthesis of WO_3 nanostructures with distinct crystalline phases via hydrothermal method, investigating their properties and their performance as an ultraviolet light-assisted O_3 gas sensor operating at room temperature [1,2].

2. Experimental

WO_3 structures with different crystalline phases, were synthesized via hydrothermal route. The microstructure of the samples was investigated by X-ray Diffraction (XRD) and Scanning Electron Microscopy (SEM). The surface chemical analysis was performed by X-ray Photoelectron Spectroscopy (XPS) under ultra-high vacuum (UHV) conditions, with a base pressure of 10−9 mbar. For the gas sensing tests, films were deposited by drop casting onto SiO_2/Si/Pt using a dynamic sensing workbench. The gas-sensing tests were performed evaluating O_3 at different concentrations. All measurements were collected at room temperature under continuous UV illumination.

3. Results and Discussions (bold face Times New Roman 11 pt)

X-ray diffraction analysis confirmed the successful formation of hexagonal, and orthorhombic WO_3 phases obtained using distinct synthesis parameters. XPS results confirmed the presence of W, O, and C in all samples, with tungsten in the W^{6+} oxidation state. Also, it was observed a slight difference between O 1s high resolution spectra of the samples. Regarding gas sensing evaluation, across a broad ozone concentration range (10–300 ppb), both phases exhibited measurable sensor responses. Variations in sensing behavior were dependent on crystalline structure, with the orthorrombic phase demonstrating superior sensitivity compared to hexagonal phase.

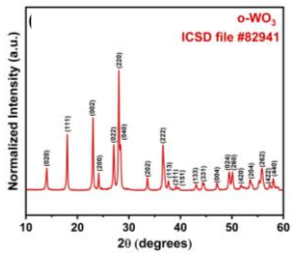

Fig. 1. *XRD pattern of orthorrombic WO_3.*

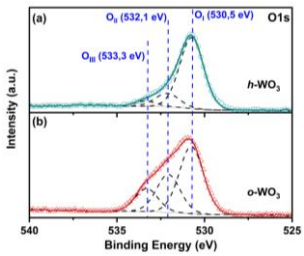

Fig. 2. *XPS spectra of (a) hexagonal and (b) orthorrombic WO_3.*

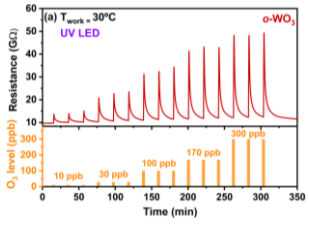

Fig. 3. *Sensing performance of orthorrombic WO_3 to O_3 gas.*

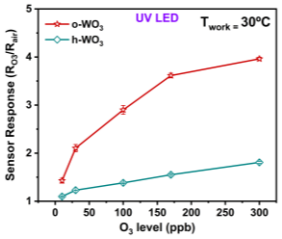

Fig. 4. *Sensor response as a function of O_3 concentration for WO_3 samples.*

4. References

[1]- X. Li, L. Fu, et al., Heliyon 10, 6, e27740, (2024).
[2]- A. Staerz, S. Somacescu, et al., ACS Sensors 5, 1624, (2020).

Acknowledgments

The authors acknowledge financial support from FAPESP (Grant 2024/13181-8), CAPES (Grant No.: 88887.982097/2024-00 and 88881.125796/2025-01) and CNPq.
*Corresponding author: enzobreancine@gmail.com

STRUCTURAL ANALYSIS OF THE INTERFACE IN THE GROWTH OF IRON ON β-Ga_2O_3(100)

Yosef S. A. Medeiros[1*], Alexandre Pancotti[1], Abner de Siervo[2], Pedro A. P. Nascente[3], Tyson Back[4]
[1]*Federal University of Jataí, Institute of Exact and Technological Sciences, Jataí, GO, Brazil*
[2]*State University of Campinas, "Gleb Wataghin" Institute of Physics, Campinas, SP, Brazil*
[3]*Federal University of São Carlos, Department of Materials Engineering, São Carlos, SP, Brazil*
[4]*United States Air Force, Air Force Research Laboratory, Dayton, OH, USA*

1. Introduction

Gallium oxide (β-Ga_2O_3) is a wide-bandgap semiconductor that has attracted great interest for high-power electronics applications due to its exceptional chemical and thermal stability [1]. This study investigates the growth of iron (Fe) nanoparticles on the (100) surface of β-Ga_2O_3, which is a natural cleavage plane of the crystal and one of the most used orientations for epitaxial growth [2]. Understanding the Fe/β-Ga_2O_3 interface is fundamental for device development, as the structure of the metal-semiconductor interface can dictate the electronic properties of the system. This work focuses on the atomic-level structural characterization of the interface formed between Fe nanoparticles and the β-Ga_2O_3(100) substrate.

2. Experimental

Fe nanoparticles were deposited by Physical Vapor Deposition (PVD) under ultra-high vacuum (UHV) conditions onto the clean and ordered surface of the β-Ga_2O_3(100) substrate. The characterization of the structure, chemical composition, and oxidation states was performed *in situ* by a suite of surface analysis techniques, including low-energy electron diffraction (LEED), X-ray photoelectron Spectroscopy (XPS), and X-ray photoelectron diffraction (XPD). Quantitative structural determination was obtained by comparing the experimental XPD patterns with theoretical multiple scattering simulations using the reliability factor (R-factor) [3].

3. Results and Discussions

The analysis of the clean β-Ga_2O_3(100) surface by XPD revealed the coexistence of two surface terminations, with the gallium-rich B termination being the most stable, composing approximately 72% of the analyzed area. After deposition and thermal annealing, XPS analyses of the Fe 2p level indicated the coexistence of metallic iron (Fe^0) and oxidized species (Fe^{2+}), suggesting a reactive interaction at the interface. The (1×1) LEED pattern of the substrate surface remained unchanged after deposition, which suggests that the Fe atoms coalesced, forming islands or nanoparticles. To investigate the nature of the reactive interface, a model was proposed in which Fe atoms substitute Ga atoms in the first layer of the substrate. XPD simulations using the Average T-Matrix Approximation (ATA) [4] were performed to test this hypothesis. The results demonstrate that the best agreement between the experimental Fe 2p XPD pattern and the theoretical one was achieved when considering a 52% substitution of Ga atoms by Fe in the outermost layer of the substrate. This result elucidates the origin of the oxidized iron species detected by XPS and confirms the formation of an interface with atomic diffusion.

4. References

[1]- S. J. Pearton *et al.*, Appl. Phys. Rev., **5**, 011301, (2018).
[2]- R. Schewski *et al.*, APL Mater., **7**, 022515, (2019).
[3]- L. Henrique *et al.*, J. Phys. Chem. C 127, 8795-8802 (2023).
[4]- E. A. Soares *et al.*, Surf. Sci., **497**, 205-213, (2002).

Acknowledgments

The authors acknowledge financial support from the USA Air Force Office of Scientific Research (AFOSR) under grants #FA9550-21-1-0440, #FA9550-20-1-0164, and #WOS 182060, and from the Conselho Nacional de Desenvolvimento Científico e Tecnológico (CNPq) under grants #310774/2020-9 and #303082/2021-6.
*Corresponding author: yosef.abreu@ufj.edu.br

STUDY OF THE CORROSION RESISTANCE OF PLASMA-NITRIDED AISI 304 STEEL BY ASPN

Pedro Augusto de Brito Inácio[1*], Luciana Sgarbi Rossino[1,2], Marcos Dorigão Manfrinato[1]
[1]*FATEC SOROCABA*
[2]*UFSCAR Campus Sorocaba*

1. Introduction

To increase resistance to fatigue, corrosion, and wear, thermochemical treatments are used, among which plasma nitriding stands out for its ease of use, low application temperature, and absence of residues after treatment [1]. In this work, plasma nitriding of AISI 304 austenitic stainless steel was performed using a cathode cage to eliminate the edge effect. Cyclic polarization corrosion tests were performed using 3.5% NaCl to determine the corrosion and pitting potential.

2. Experimental

In this work, Ø25.4x13 mm bars of AISI 304 austenitic stainless steel were used. The samples were subjected to solution heat treatment at 1050 °C for 45 min and quenched in water. The surfaces of the specimens were sanded according to ASTM E3-2017 standard and subsequently polished with 0.5 µm alumina. Before nitriding, the specimens were subjected to sputtering at 300 °C for 1 hour with a gas mixture of 80% vol. argon and 20% vol. hydrogen, with a working pressure of 2 Torr. After sputtering, nitriding was carried out at 400 °C for 6 hours with a gas mixture of 80% vol. nitrogen and 20% vol. hydrogen at 3.2 Torr. Metallographic characterization of the layer thickness and open circuit potential tests was performed for 30 minutes at 1 mv/s and subsequent corrosion test by cyclic polarization with 3.5% NaCl solution.

3. Results and Discussions

The plasma nitriding treatment with a cathodic cage eliminated the edge effect on the surface, and the nitrided layer was uniform across the surface and had a thickness of 8 ± 0.4 µm. The open circuit potential (Fig. 1) remained stable after 30 minutes, and the untreated sample had a higher potential than the nitrided sample with the cathodic cage. Observing the polarization and OCP curves (Fig. 2), it is noted that the corrosion and pitting potentials for the nitrided samples were lower than those for the untreated sample. The pitting potentials for the untreated and nitrided specimens were 0.48 ± 0.04 V and -0.05 ± 0.03 V, respectively. The corrosion potentials were -0.47 ± 0.02 V for the untreated sample and -0.57 ± 0.07 V for the nitrided sample. When analyzing the metallography of the nitrided layer, dark spots are observed in the layer that are probably CrN together with the expanded austenite layer (S phase) that reduces corrosion resistance, resulting in lower corrosion and pitting potential [1, 2].

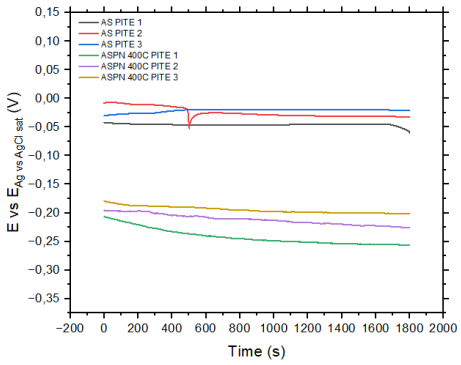

Fig. 1. *Open circuit potential (OCP) of as-received and ASPN samples.*

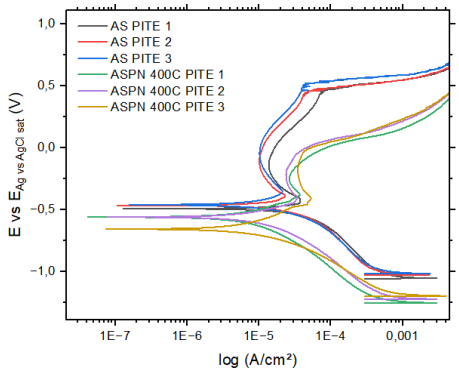

Fig. 2. *Cyclic polarization curves of as-received and ASPN samples*

4. References

[1]- M. D. Manfrinato, Uni. Fed. de São Carlos, Brazil, (2023).
[2]- CRUZ, D. et al, Rev. Br. de Aplic. de Vac., 37, 3, 102-113, (2018).

Acknowledgments

To the Laboratory of Plasma Technology (LaPTec) at UNESP Sorocaba for providing the potentiostat/galvanostat.
*Corresponding author: pedro.inacio2@fatec.sp.gov.br

STUDY OF THE USE OF ARTIFICIAL INTELLIGENCE TO DETERMINE GRAIN SIZE IN ACCORDANCE WITH ASTM E112 STANDARD

Waldemar Bonventi Júnior[1*], Pedro Augusto de Brito Inácio[1], Marcos Dorigão Manfrinato[1],
[1]*FATEC Sorocaba*

1. Introduction

The Metallographic analysis to determine the grain size of steels is typically manual and time-consuming. ASTM E112 standard indicates three methods for grain size evaluation: comparative evaluation by frames, grain counting methods, and the interception method [1]. In this work, two artificial intelligence algorithms were developed to automate grain size measurement using the planimetric and intercept methods [2] for hot-forged and normalized SAE 1040 steel.

2. Experimental

The metallographic preparation of the hot-forged and normalized SAE 1040 steel samples was performed according to ASTM E3-2017, followed by coating with 0.5 µm alumina and etching with 3% Nital to reveal the microstructure. The images were taken at 100X magnification for subsequent application of AI algorithms to determine the grain size. The resolution of the collected images was 0.5045 µm/pixel. Two algorithms were executed to segment the grain boundaries: 1) segmentation and 2) morphological watershed. For each method, five metallographic images from different regions were used to measure grain size. The latter proved to be more stable for etched grains, with the following parameters: contrast equalization (CLAHE), Gaussian smoothing σ=1.2 (light), and thresholding (Otsu) by distance (h=0.30) to avoid excessive grain fusion. Post-filter: minimum area of 4.0 µm² and circularity ≥ 0.02. N_A (mm²) was obtained for use in the planimetric method. Then, lines were generated in random directions to apply the intercept method and obtain G (µm).

3. Results and Discussions

Artificial intelligence (AI) software for measuring grain size is fast. Fig. 1 shows the segmentation method and Fig. 2 the random line method used by the software. Fig. 3 shows the grain size distribution obtained by the algorithm using the planar and intercept techniques, and the output values of the analysis are presented in Table 1 (variation <0.5). The intercept algorithm yielded a grain size of 7.48 ± 0.08, while the planimetric method algorithm yielded a grain size of 7.11 ± 0.07; both results are more consistent with the watershed algorithm.

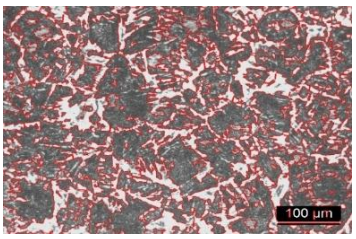

Fig. 1. *Microscopy with segmented grains*

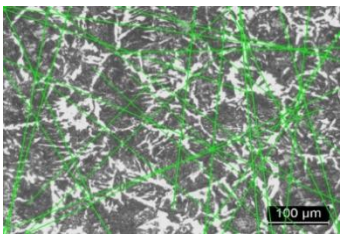

Fig. 2. *Random lines for intercept method*

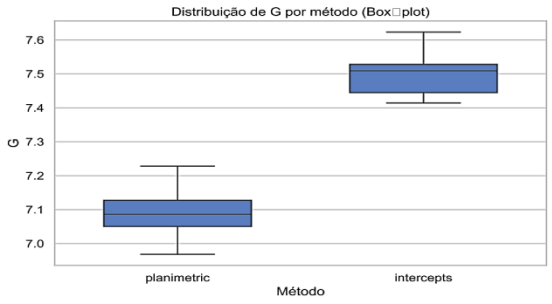

Fig. 3. *Comparison between planimetric and intercept methods*

sample	method	N_A (mm²)	$\bar{\ell}$ (µm)	G	n_{100}
image.png	planim	1027		7.1	66
image.png	intercep		24.5	7.4	85
image01.png	planim	1053		7.1	68
image01.png	intercep		23.6	7.5	92
image02.png	planim	970		7.0	63
image02.png	intercep		24.2	7.4	87
image03.png	planim	1161		7.2	75
image03.png	intercep		23.7	7.5	91
image04.png	planim	1083		7.1	70
image04.png	intercep		22.8	7.6	99

Tab. 1. *Comparison between planimetric and intercept methods*

4. References

[1] ASTM E112 – Standard Test Methods for Determining Average Grain Size. (2010)
[2] NIST. Grain Size Analysis Tools (GSAT). https://github.com/usnistgov/grain-size-analysis-tools. (2025).

Acknowledgments
FATEC of Sorocaba for the use of the metallography laboratory

*Corresponding author: waldemar.junior@fatec.sp.gov.br

SURFACE CHARACTERIZATION OF TI-NB-ZR ALLOY COATINGS

Ana L. C. Garcia[1], Valmor R. Mastelaro[2], Pedro A. P. Nascente[1*]
[1]*Federal University of Sao Carlos, Department of Materials Engineering, 13565-905, Sao Carlos, SP, Brazil.*
[2]*University of Sao Paulo, Sao Carlos Institute of Physics, 13560-590, Sao Carlos, SP, Brazil.*

1. Introduction

The medical grade stainless steel (SS) type AISI 316L (ASTM F138-19) is the most used metallic material in the production of biomedical implant devices; however, it presents two disadvantages. The cytotoxicity caused by the release of Cr and Ni ions, and an elastic modulus that is much higher than human bone, which can cause. Failure. Titanium and its alloys, especially those having β (bcc) phase have showed to be better biomaterials than AISI 316L SS for manufacturing implants. Among the β-Ti alloys, the Ti-Nb-Zr ternary system has been one of the most investigated biomedical materials, since Ti, Nb, and Zr are non-toxic and non-allergenic elements that have total solubility among themselves, and present excellent biocompatibility [1]. A major disadvantage of Ti-Nb-Zr alloys compared to SS is the cost. An economical option would be to coat an implant with a Ti-Nb-Zr with adequate composition to enhance the material biocompatibility [2]. Combinatorial strategies allow for simultaneous production of many alloys, and magnetron sputtering is suitable for producing ternary alloy coatings with various compositions.

2. Experimental

Ti, Nb, and Zr target were positioned in a triangular configuration below a Si(100) wafer, and a composition gradient was formed over the substrate by magnetron co-sputtering. Energy dispersive spectroscopy (EDS), X-ray diffraction (XRD), atomic force microscopy (AFM), and X-ray photoelectron spectroscopy (XPS) were used to assess the physicochemical, structural, and morphological characteristics for the samples: (a) near the Ti target, (b) near the Nb target, (c) in the wafer center, (d) near the Zr target, and (e) opposite the Ti target.

3. Results and Discussions

EDS analysis yielded the following compositions (in at. %): (a) $Ti_{49}Nb_{13}Zr_{38}$, (b) $Ti_{22}Nb_{58}Zr_{20}$, (c) $Ti_{43}Nb_{42}Zr_{15}$, (d) $Ti_{67}Nb_{21}Zr_{12}$, and (e) $Ti_{36}Nb_{59}Zr_5$. XRD diffractograms indicated mainly the presence of the β phase, with a minor contribution of the α (hcp) phase. The mean grain sizes measured by AFM were: 72.3, 51.7, 83.1, 74.5, and 84.2 nm for the five coatings. For the same sequence, the roughness values were: 2.0, 1.2, 0.6, 1.3, and 0.9 nm. For comparison, the roughness of the Si(100) substrate was 0.1 nm. XPS results indicated that the alloy coating surfaces were oxidized, and also a surface enrichment of both Ti and Zr concomitant with a surface depletion of Nb on the oxide surface layers.

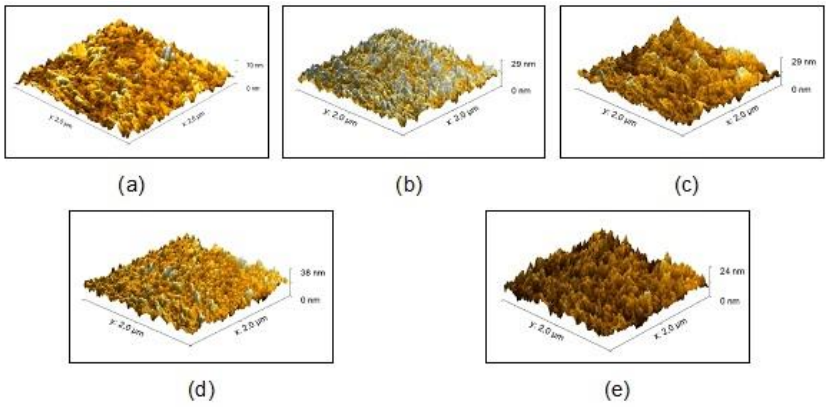

Fig. 1. *AFM images for the (a) $Ti_{49}Nb_{13}Zr_{38}$, (b) $Ti_{22}Nb_{58}Zr_{20}$, (c) $Ti_{43}Nb_{42}Zr_{15}$, (d) $Ti_{67}Nb_{21}Zr_{12}$, and (e) $Ti_{36}Nb_{59}Zr_5$. X alloy coatings deposited on Si (100).*

4. References

[1]- E. D. Gonzalez *et al*., Mater. Today Commun., **32**, 104069 (2022).
[2]- E. D. Gonzalez *et al*., Thin Solid Films, **721**,138565, (2021).

Acknowledgments

The authors would like to thank Conrado R. M. Afonso, Angelo L. Gobbi, Lucas L. D. Lemos, Ricardo Boldrini, Sidney C. Z. Costa, and Bruno B. Aquino for their assistance. This work was supported by FAPESP, CNPq, and CAPES.
*Corresponding author: nascente@ufscar.br

THE FIRST 2,5 CARAT POLISHED DIAMOND PRODUCED IN BRAZIL VIA MPACVD METHOD

José Vieira da Silva Neto[1]*, Javier Sierra Gómez[1], Vladimir Jesus Trava-Airoldi[2], Evaldo José Corat[2]
[1]*TCarbon Diamond Ind LTDA, São José dos Campos, São Paulo, Brazil*
[2]*National Institute for Space Research, São José dos Campos, São Paulo, Brazil*

1. Introduction

Diamond has captivated generations of scientists for centuries, from Lavoisier's 1772 early combustion experiments to Tennant's 1797 demonstration that it is pure carbon[1]. This fascination led to early laboratory attempts in the 19th and 20th centuries, culminating in HPHT synthesis by GE in 1954 and the later development of CVD methods by pioneers like Eversole, Angus, and Deryagin. The discovery of atomic hydrogen's critical role enabled metastable diamond growth at low pressure[2]. Today, MPACVD technology produces high-purity crystals, and Brazil joins this legacy as TCarbon Diamond, applying vacuum technology and plasma science in their full potential, unveils the first 2.5 ct polished diamond grown in the country.

2. Experimental

The crystal was homoepitaxially grown on a commercially available 10 × 10 × 0.3 mm³ seed substrate (Jiangxi Solen Tenth) through three consecutive growth steps, each lasting approximately 168 hours. Growth conditions were maintained at 950 °C and 120 Torr, using a gas mixture of 10% CH_4 in H_2 (CH_4 purity 99.995% and H_2 purity 99.9999%), which was consistently applied in all steps without the addition of other gases. Between each growth step, the diamond block was laser-cut to remove polycrystalline material using an IPG Photonics ITGD Marker 30 W, H, f163 laser system with a wavelength of 1064 nm, supplied by CVD Vale. The crystal quality was assessed by photoluminescence spectroscopy using a Horiba Labram HR Evolution system, at 514 nm excitation wavelength at room temperature.

3. Results and Discussions

Figure 1 shows a digital photograph of the CVD diamond crystal after it was cut and polished into a round brilliant shape. Although the stone was not submitted to a reputable grading laboratory, its color was visually estimated to fall within the G to I range (near-colorless), with a clarity grade of approximately VS. Figure 2 presents the photoluminescence spectra of the crystal after each growth step. In all stages, the characteristic diamond-related peak appears around 552 nm, and the emissions associated with nitrogen-vacancy (NV) centers are observed at 575 nm (NV^0) and 638 nm (NV^-), respectively. Additionally, a subtle shoulder around 742 nm becomes noticeable in layers 2 and 3, corresponding to the GR1 center, which is related to neutral vacancies. This increase is typically associated with a higher concentration of vacancies caused by the propagation of dislocations as the crystal thickens.

Fig. 1. *TCarbon Diamond 2,5 ct round brilliant CVD diamond.*

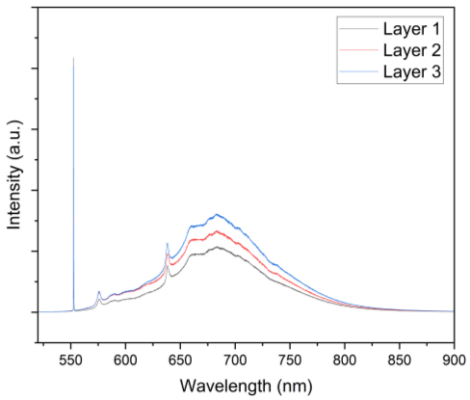

Fig. 2. *Photoluminescence spectra for each consecutive grown layer of the diamond crystal.*

4. References

[1] J.E. Butler, and A.N. Katrusha, "Synthesis of Diamonds and Their Identification," in *Diamond: Genesis, Mineralogy and Geochemistry*, (De Gruyter, 2023), pp. 689–754.
[2] J.C. Angus, "Diamond synthesis by chemical vapor deposition: The early years," Diam Relat Mater **49**, 77–86 (2014).

Acknowledgments
FAPESP and Finep.
*Corresponding author: jvneto.ifsp@gmail.com

UV-ENHANCED NO_2 GAS SENSING BASED ON SURFACE CHARACTERIZATION OF ZN-DOPED SnO_2 NANOPARTICLES

João V. Almas[1]*, Sandrine Bernardini[2], Ariadne C. Catto[1,3] and Luís F. da Silva[1]
[1]*LM2N, Department of Physics, Federal University of São Carlos, São Carlos, SP, Brazil*
[2]*Aix-Marseille Université, CNRS, IM2NP, Marseille, France*
[3]*NACA, Institute of Physics of São Carlos, University of São Paulo, São Carlos, SP, Brazil*

1. Introduction

The monitoring of toxic pollutants, such as nitrogen dioxide (NO_2), is crucial for public health and environmental protection. SnO_2 is a widely used as a semiconductor material for resistive gas sensors, however, its application often requires high operating temperatures. Photo-stimulation emerges as an alternative to enable room temperature operation, while Zn doping proves to be an effective strategy to modulate its properties. Herein, we investigate the effect of zinc doping on the characteristics of SnO_2 nanoparticles and their performance as a ultraviolet light assisted NO_2 gas sensor [1,2].

2. Experimental

Pure and Zn-doped SnO_2 nanoparticles with different nominal concentrations (0.4, 1.9, and 5.0 at. %, respectively SZ04, SZ19 and SZ50), were synthesized via a microwave-assisted route. The morphology of the samples was investigated by Transmission Electron Microscopy (TEM), operated under high-vacuum conditions (approx. 10^{-7} mbar). The surface chemical analysis was performed by X-ray Photoelectron Spectroscopy (XPS) under ultra-high vacuum (UHV) conditions, with a base pressure of 10^{-9} mbar. For the gas sensing tests, films were deposited by spin-coating onto SiO_2/Si/Pt using a dynamic sensing workbench. The gas-sensing tests were performed evaluating the following analytes: NO_2, O_3, CO_2, CO, and NH_3. All measurements were collected at room temperature under continuous UV illumination.

3. Results and Discussions

TEM analyses revealed that the nanoparticles have a quasi-spherical morphology and that doping with 5.0 at. % Zn promoted a significant reduction in particle size compared to the pure SnO_2 sample. XPS results confirmed the presence of Sn, O, and Zn in the doped samples, with the elements in the Sn^{4+} and Zn^{2+} oxidation states. It was observed that the increase in dopant concentration raised the (Zn+Sn)/O atomic ratio on the surface, indicating a more oxygen-deficient structure. Electrical measurements showed that all samples were sensitive to all NO_2 levels, presenting total recovery after each exposure cycle. Notably, the sensor with 5.0 at. % Zn (SZ50) exhibited a response 5 times higher than that of the pure SnO_2 sensor when exposed to 500 ppb of NO_2.

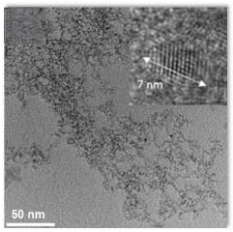

Fig. 1. *TEM micrograph of the 5.0 at.% Zn-doped SnO_2 (SZ50) nanoparticles, with an single particle.*

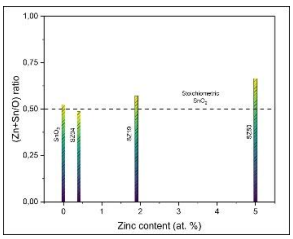

Fig. 2. *The (Zn+Sn)/O atomic ratio on the sample as a function of zinc content, determined by XPS.*

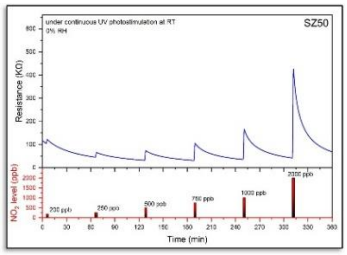

Fig. 3. *Sensing performance of the SZ50 to NO_2 gas.*

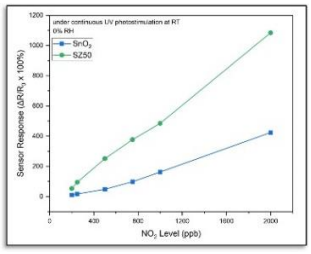

Fig. 4. *Sensor response as a function of NO_2 concentration for the pure and SZ50 samples.*

4. References

[1] - Jabłczyńska, K. et al. Nanoscale Advances 6, 1259–1268 (2024).
[2] - Casals, O. et al. ACS Sensors 4, 822–826 (2019).

Acknowledgments
The authors acknowledge financial support from FAPESP (Grant 2025/07284-1) and CNPq.
*Corresponding author: jvalmas04@gmail.com

IN-FIELD SPATIAL CHARACTERIZATION OF THE PARROT SEQUOIA MULTISPECTRAL CAMERA'S NARROWBAND SENSORS

Salles, T. da S.[1]*, Damião, A. J[1,2], Castro, R. M. de[2,3]
[1]*Instituto Tecnológico de Aeronáutica (ITA), São José dos Campos-SP*
[2]*Instituto de Estudos Avançados (IEAv), São José dos Campos-SP*
[3]*Universidade de Taubaté (UNITAU), Taubaté-SP*

1. Introduction

Remote sensing cameras are widely employed in a diverse range of imaging applications, spanning from precision agriculture to intelligence activities. Consequently, understanding the spatial characteristics of the sensors utilized, such as spatial resolution and Ground Sampling Distance (GSD) as a function of flight height, is essential for their effective operational deployment [1].

2. Experimental

The spatial characteristics of four narrowband sensors (Green: 530-550 nm, Red: 640-680 nm, Red Edge: 730-740 nm, and NIR: 770-810 nm) of the Parrot Sequoia multispectral camera were determined. The camera was positioned at NADIR, imaging a black and white painted concrete target featuring four transition edges, as shown in Fig. 1. The vertical distance to the target was 590 mm, and it was 9º relative to the camera's vertical pixel lines. Eleven rectangular Regions of Interest (ROIs), shown in Fig. 1, measuring 50 x 30 pixels horizontally (or 30 x 50 pixels vertically), were selected. These ROIs were then processed using a Matlab® routine via the SFRMAT5 plugin, applying the Slanted Edge method [2]. The spatial resolution for each sensor, defined by MTF5, MTF10, and MTF50, was calculated as the arithmetic mean of the eleven identified ROIs per sensor. The Sampling Efficiency for each sensor was also determined, expressed as a percentage, representing the ratio between the MTF10 (in cy/px) and the half-sampling frequency (Nyquist frequency) [3].

3. Results and Discussions

A 4 mm focal length was used for the narrowband sensors, yielding a GSD of 0.57 mm/px at a flight height of 590 mm. Using the formula: $GSD = p \cdot H / F \cdot \cos\theta$ [1], the pixel pitch (p) was estimated at 3.88 µm. This estimated pitch is close to the 3.75 µm identified by [4], with a difference of -3.35%. The calculated spatial resolutions for MTF5, MTF10, and MTF50 were, respectively: for the Green sensor, 0.57 mm, 0.90 mm, and 1.64 mm; for the Red sensor, 0.57 mm, 0.81 mm, and 2.05 mm; for the Red Edge sensor, 0.57 mm, 0.78 mm, and 1.97 mm; and for the NIR sensor, 0.57 mm, 0.89 mm, and 2.16 mm. Fig. 2 presents the MTF curves for the narrowband sensors. Sampling efficiency for the Green sensor was 64.76%, for Red 71.63%, for Red Edge 75.68%, and for NIR 65.69%.

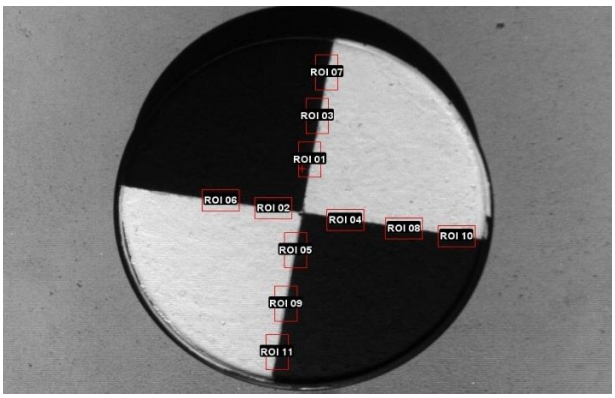

Fig. 1. Checkered target and the defined ROIs for MTF5, MTF10, and MTF50 calculation.

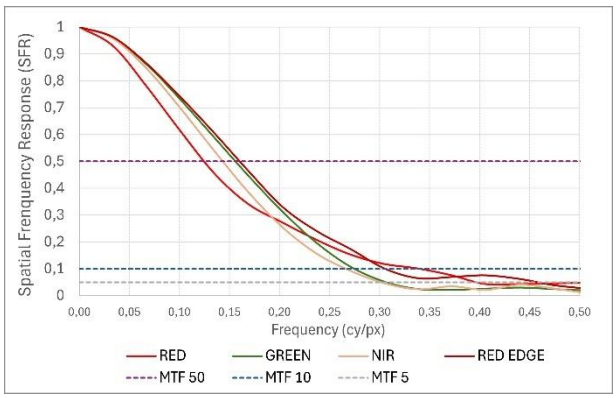

Fig. 2. SRF of the Parrot Sequoia's narrowband sensors for H = 590 mm.

4. References

[1]- S. Kabir; L. Leigh; D. Helder. Remote Sens, **12**, 4029, (2020).
[2]- International Organization for Standardization. ISO 12233:2024 (2024).
[3]- P. Burns, Burns Digital Imaging. http://burnsdigitalimaging.com/software/sfrmat/iso12233-sfrmat5/ (2023).
[4]- M. Franzini *et al.*, Applied Sciences, **9**, 5314, (2019).

Acknowledgments
The author thanks the Projeto de Processamento de Imagens em Tempo Real (PITER) and Laboratório de Radiometria e Caracterização de Sensores Eletro-ópticos (LaRaC) at Instituto de Estudo Avançados (IEAv) for providing facilities, the Parrot Sequoia camera, and the target used for this research.
*Corresponding author: salles@ita.br

EFFECT OF ABLATION TESTING ON THE MICROSTRUTURE INTEGRITY OF THERMAL BARRIER COATINGS ON Ti-6Al-4V ALLOY SUBSTRATE

Agatha C. Corrêa[1*], Roberson J. Silva[1], Nazir M. dos Santos[1]
[1]*Instituto de Estudos Avançados (IEAv)*

1. Introduction

Thermal Barrier Coatings (TBCs) protect metallic substrates from severe thermal loads typical of aerospace and energy applications [1]. A conventional system comprises a ceramic top coat (TC) for thermal insulation and a metallic bond coat (BC) for adhesion and oxidation resistance. Under high heat fluxes and rapid transients, these coatings undergo complex degradation driven by thermal stresses and oxidation. Ablation testing is used to simulate such extreme conditions and assess the resulting microstructural damage, providing insight into oxidation, cracking, and interfacial stability.
This study investigates the microstructural evolution of an air plasma–sprayed (APS) YSZ/NiCrAlY coating on a Ti-6Al-4V substrate after exposure to a plasma heat flux of 1.0 MW/m² for 10–50 s. Optical microscopy was employed to identify the main degradation mechanisms affecting coating integrity.

2. Experimental

Ablation tests were performed to evaluate the thermal resistance and degradation behavior of the TBC system. The experiments were conducted at the Plasma and Process Laboratory (LPP) of the Aeronautics Institute of Technology (ITA). The samples were exposed to a high-enthalpy plasma jet generated by a DC plasma torch operating at atmospheric pressure [2]. Each sample was subjected to a controlled heat flux of 1.0 MW/m² for exposure times of 10, 30, and 50 s. Cross-sections of the coatings were analyzed before and after the tests using optical microscopy to evaluate microstructural changes.

3. Results and Discussions

Before ablation testing, the coating showed a typical APS microstructure with overlapping lamellae, interlamellar porosity, and localized oxidation in the bond coat (Figure 1). This structure provides good adhesion and low thermal conductivity but also introduces uneven pore distribution and microcracks [3]. After exposure to a heat flux of 1.0 MW/m², progressive degradation occurred. The sample exposed for 10 s displayed a continuous thermally grown oxide (TGO) layer at the TC/BC interface [4]. With longer exposures (30 and 50s), oxidation and porosity increased, accompanied by interfacial cracking and partial melting of the titanium substrate. The TGO became discontinuous, indicating disruption from thermal stresses and oxidation in the metallic layers (BC and Ti-6Al-4V).
These findings show that ablation testing promotes progressive damage in the TBC, primarily driven by oxidation, crack propagation, and thermal expansion mismatch. Adjusting bond coat composition and exposure parameters is essential to enhance coating durability under extreme conditions.

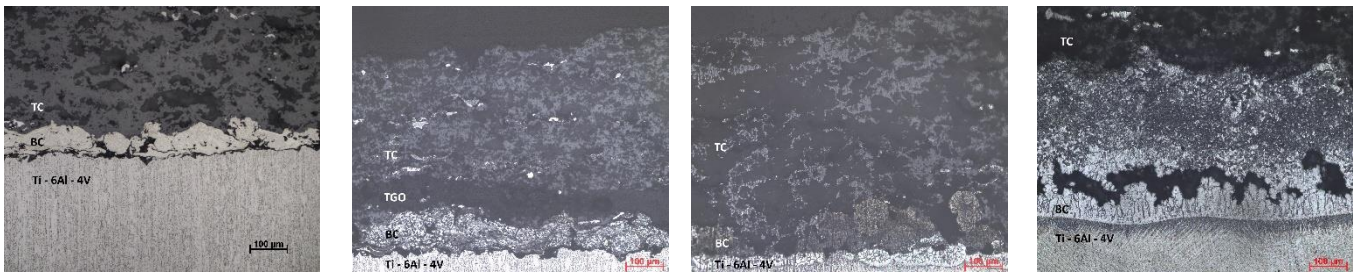

(a) (b) (c) (d)

Figure 1. *Optical micrographs of the TBC: (a) before ablation testing, and after ablation testing at a heat flux of 1.0 MW/m² for exposure times of (b) 10 s, (c) 30 s, and (d) 50 s.*

4. References

[1] Oliveira, J. P.; Duarte, J. F. **Cerâmica**. (2013). DOI: https://doi.org/10.1590/S0366-69132013000100023.
[2] Silva, R.J., et al. **Int J Thermophys 40**, 88 (2019). https://doi.org/10.1007/s10765-019-2555-8
[3] VanEvery, K., et al. **J Therm Spray Tech 20**, 817–828 (2011). https://doi.org/10.1007/s11666-011-9632-2
[4] A. Sezavar et al. **J. Eur. Ceram. Soc.** (2025) https://doi.org/10.1016/j.jeurceramsoc.2025.117274

Acknowledgments

CNPq (Proc. 157898/2025-3) and COMAER - Ed. CAPA IEAV- PropHiper (Proc. 67720.009933/2024-93).
*Corresponding author: agathacoelho.correa@gmail.com

POTASSIUM INTERCALATION IN PRUSSIAN BLUE THIN FILMS FOR SUSTAINABLE BATTERY APPLICATIONS

André Avelino Pasa*
Programa de Pós-Graduação em Física, Universidade Federal de Santa Catarina, Florianópolis, SC, Brazil

1. Introduction

Potassium Prussian Blue (KPB), with the chemical formula $KFe[Fe(CN)_6]$, is a promising cathode material for potassium-ion batteries (PIBs) due to its high performance, safety, environmental compatibility, elemental abundance, and relatively simple, low-cost synthesis [1,2]. Its cubic open framework enables the reversible storage of potassium ions, making it a strong candidate as an alternative to lithium-ion batteries. The insertion and extraction of potassium ions occur via the redox reaction $KFe^{3+}[Fe(CN)_6] + K^+ + 1e \rightleftharpoons K_2Fe^{2+}[Fe(CN)_6]$, where the reduced form is referred to as Potassium Prussian White (KPW).

2. Experimental and Theory

In this study, potassium-ion intercalation was investigated using both experimental and theoretical approaches. Prussian Blue thin films were electrodeposited onto graphite electrodes from an electrolyte containing $K_3Fe(CN)_6$ and $FeCl_3$. The reversible storage of potassium ions—via intercalation and deintercalation—was characterized using the Potentiostatic Intermittent Titration Technique (PITT). The site occupancy of monovalent potassium ions (K^+) within the crystal structure was analyzed using density functional theory (DFT)[3].

3. Results and Discussions

Starting with the theoretical results, DFT calculations were performed by initially inserting K^+ ions into the cubic structure of KPB at the Wyckoff positions 8c, 24d, 32f, and 32f′. The insertion of K^+ at the 8c site preserved the original cubic symmetry upon structural relaxation. In contrast, placing the ion at the 24d site led to a distortion into an orthorhombic structure, while insertion at the 32f and 32f′ sites resulted in a rhombohedral symmetry. Among these, the 32f site—located near the nitrogen atoms bonded to Fe^{3+}—was found to be the most energetically favorable interstitial site for K^+. A similar procedure was applied to the cubic structure of KPW. Upon relaxation, K^+ insertion at the 32f and 32f′ sites also led to a rhombohedral distortion, closely resembling the relaxed 8c configuration, which retained its cubic symmetry. The optimized crystal structures of KPB and KPW with K^+ initially placed at the 32f site are shown in Figures 1a and 1b, respectively.
Experimentally, PITT measurements were performed on crystalline, compact thin films with a thickness of approximately 2000 nm, electrodeposited at +0.30 V vs. SCE. From the current responses to a sequence of applied potential pulses, the diffusion coefficient (D) of potassium ions was extracted, as shown in Figure 2. A diffusion coefficient of approximately $D \approx 10^{-12}$ cm²/s was obtained near the redox potential of Fe ions ($Fe^{3+} + 1e^- \rightleftharpoons Fe^{2+}$) at around +0.2 V vs. SCE. This result is significant, indicating that K^+ intercalation primarily occurs near the redox potential. The intercalation mechanism and its correlation with the redox potential will be discussed in detail during the presentation.

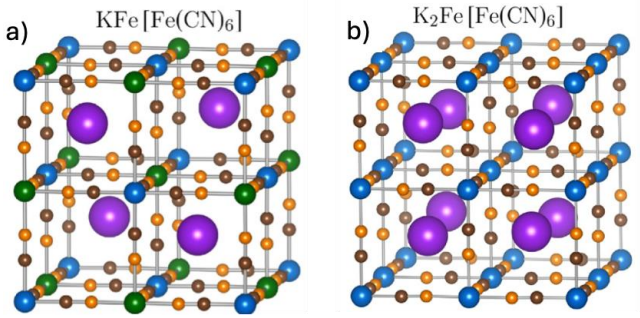

Fig. 1. *Optimized crystal structures of a) KPB and b) KPW with K initially at the 32f*

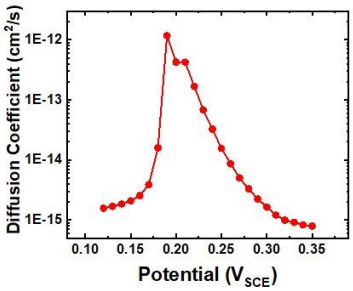

Fig. 2. *Diffusion coefficient of K^+ in thin films of Potassium Prussian Blue.*

4. References

[1]- R. Wu, B. Ren, X. Wang, J. Lin, X. Li, J. Zheng, and H. Y. Yang, Adv. Funct. Mater., **35**, 2418018, (2025).
[2]- Z. Hu, B. Zhang, H. Zhang, and Y. Ma, Batteries and Supercaps, **8**, e202400448, (2025).
[3]- M. V. C. Issler, C. Vicente, I. S. Brandt, B.F. Baggio, R. Faccio, M. A. Tumelero, and A. A. Pasa, Phys. Chem. Chem. Phys., **27**, 15204-15212, (2025).

Acknowledgments

The author acknowledges the financial support from CNPQ, CAPES, and FINEP.
*Corresponding author: andre.pasa@ufsc.br

SURFACE MODIFICATION OF AZ31 MAGNESIUM ALLOY BY PLASMA ELECTROLYTIC OXIDATION

Henrique Engelhardt[1], Juliana Layber Mota Engelhardt[1], Rafael Resende Lucas[1], André Luiz Reis Rangel[1], Rogério Pinto Mota[1]

[1]*São Paulo State University (UNESP), School of Engineering and Sciences, São Paulo, Brazil*

2 Fluminense Federal Institute of Education, Science and Technology (IFF), Campos dos Goytacazes, Brazil.

1. Introduction

The AZ31 magnesium alloy has emerged as a promising biomaterial due to its biocompatibility, biodegradability, and favorable mechanical properties — essential characteristics for medical applications such as implants. However, its low corrosion resistance, resulting from high reactivity with water and moisture, limits its performance in physiological environments. To overcome this limitation, recent studies have explored surface modification techniques, particularly plasma electrolytic oxidation (PEO), which has shown great potential for improving corrosion resistance and controlling biodegradation, thereby enhancing the suitability of the AZ31 alloy for biomedical applications [1,3].

2. Experimental

In this study, surface modification of a commercial AZ31 magnesium alloy was carried out using the plasma electrolytic oxidation (PEO) process. The samples were treated with calcium glycerophosphate as the electrolyte at a concentration of 0.07 g/L. The applied voltage was varied at three levels: 260 V, 320 V, and 440 V, for a duration of three minutes. Characterization of the treated samples was performed by Fourier-transform infrared spectroscopy (FT-IR), in the scanning range of 4000 to 650 cm^{-1}, with 32 scans and a spectral resolution of 4 cm^{-1}.

3. Results and Discussions

The results indicate the formation of a porous oxide film exhibiting superhydrophilic behavior. Superhydrophilic surfaces enhance the adhesion of biological fluids, promoting biomineralization and cell adhesion — key processes for implant osseointegration. The FT-IR analysis revealed an inclined band near the wavelength of 1000 cm^{-1}, associated with the formation of an oxide film, and a curvature around 4000 cm^{-1}, attributed to hydroxyl groups (-OH), indicating a reactive surface composed of magnesium oxide that favors the material's biocompatibility. Therefore, the PEO treatment proves to be an effective approach for developing magnesium alloys with improved performance in medical applications, particularly for biodegradable implants [2].

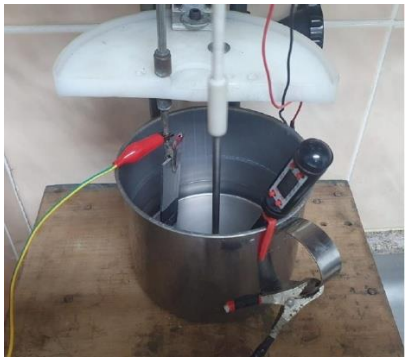

Fig. 1. *Experimental setup used for the plasma electrolytic oxidation (PEO) treatment of the AZ31 magnesium alloy.*

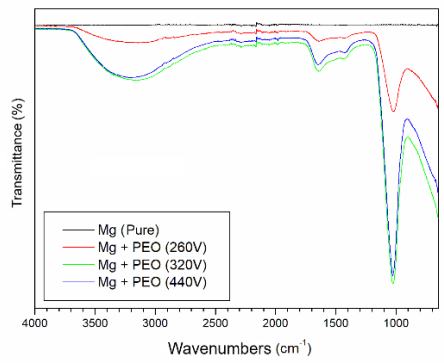

Fig. 2. *FT-IR spectrum of the AZ31 alloy, indicating the presence of groups related to the surface oxide.*

4. References

[1] - D. KAJÁNEK, *et al*. Koroze a ochrana materiálu, **63**(2), 65-71, (2019)
[2] - G. VALENCIA; R. PILEGGI. Cerâmica, **64**, 197-206, (2018)
[3] - M. NOCCHETTI, *et al.* Journal of Functional Biomaterials, **16**(1), 22, (2025).

Acknowledgments

The authors thank UNESP-FEG and the Graduate Program in Engineering for their support and the opportunity to participate in academic conferences.

*Corresponding author: h.engelhardt@unesp.br

STUDY OF LOW-PRESSURE CF_4 AND SF_6 PLASMAS IN A CAPACITIVELY COUPLED PLASMA USING SPECTROMETRY

Thaís Macedo Vieira*[1], Marcelo Pego Gomes[1], Rodrigo Sávio Pessoa and Argemiro Soares da Silva Sobrinho[1]
[1]*Instituto Tecnológico de Aeronáutica (ITA), São José dos Campos, SP, Brazil*

1. Introduction

Fluorine-based plasmas generated from SF_6 and CF_4 gases are used in microelectronics and nanotechnology for material etching processes, such as reactive-ion etching of silicon. In these plasmas, fluorine atoms react with silicon to form volatile SiF_4, as a result of gas dissociation and the production of highly reactive radicals[1,2]. This work aims to investigate the dissociation mechanisms and reactive species formation in low-pressure CF_4 and SF_6 plasmas using actinometry and mass spectrometry diagnostics in a capacitively coupled plasma (CCP) reactor.

2. Experimental

The experiments were carried out in a RIE-CCP reactor [2]. CF_4 and SF_6 discharges were maintained at 10-2 Torr with RF powers of 10, 50, 100, 200, and 300 W. The gas flow rates were 10 sccm for CF_4 and 20 sccm for SF_6. Optical emission spectroscopy and actinometry [2] were used to estimate the relative atomic fluorine density, using Argon as the reference gas with concentrations of 2.5% for CF_4 and 1% for SF_6 plasmas. The optical fiber was positioned at a fixed distance of (22.65 ± 0.05) mm from the reactor window, and each spectrum was acquired with an integration time of 100 ms during 2 minutes. Experiments were performed with and without a silicon substrate placed on the powered electrode, with an exposed area of 94.1 cm^2. A mass spectrometry (MS) was used to record the time evolution of the main species in the gas phase, enabling the identification of dissociation fragments and volatile etching products.

3. Results and Discussions

Fig. 1 shows the atomic fluorine density (n_F) at 703.7 nm obtained by actinometry in CF_4 and SF_6 plasmas without the silicon substrate. The n_F increases with RF power for both gases, indicating stronger gas dissociation with energy input. SF_6 plasmas produced higher n_F than CF_4, consistent with the larger fluorine content per molecule and lower dissociation energy. However, Fig. 2 shows the partial pressure evolution of the main species detected by MS. The CF_3^+ specie decreases, while CF_2^+ and F_2^+ increase, revealing the progressive dissociation of CF_4 and recombination of F atoms. The rise of SiF_3^+ confirms the formation of volatile SiF_4 as a product of chemical etching. These results demonstrate efficient CF_4 dissociation and active silicon etching under low-pressure CCP operation.

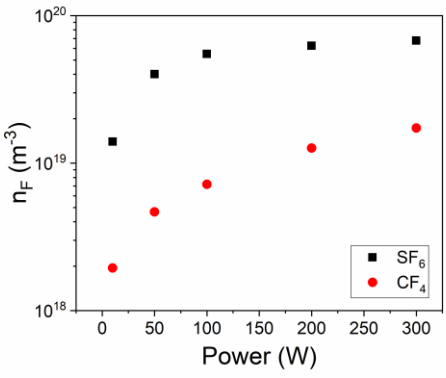

Fig. 1. *Relative atomic fluorine density vs. RF power for CF_4 (red) and SF_6 plasmas (black).*

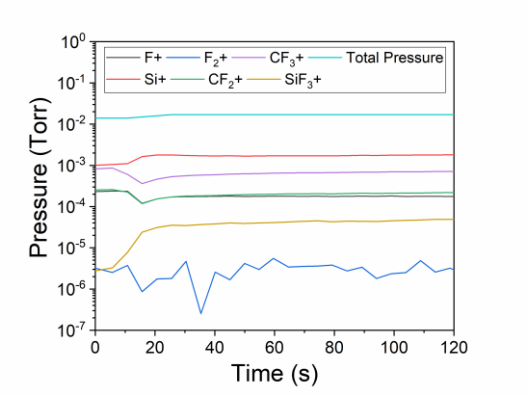

Fig. 2. *Partial pressure evolution of CF_4 fragments and SiF_4 during CF_4 plasma at 200 W.*

The study is still in progress, and future work will include the development of a global (0D) model for comparison with the experimental diagnostics.

4. References

[1]- C. Cardinaud, *Comptes Rendus Chimie*, 21, 723–739, (2018).
[2]- R. S. Pessoa, PhD Thesis, Instituto Tecnológico de Aeronáutica, São José dos Campos, SP, (2009).

Acknowledgments

Thaís M. Vieira thank to Coordenação de Aperfeiçoamento de Pessoal de Nível Superior (CAPES) for doctorate grant (Finance Code 001).
*Corresponding author: vieira.thaism@gmail.com

LOW-VACUUM GLOW DISCHARGE FOR THE INNOVATION IN BIOMATERIALS AND IMPLANTS FOR HEALTH, FOOD AND AGRICULTURE

Diego Mantovani[1], Pascale Chevallier[1], Carlo Paternoster[1], Francesco Copes[1], Andranik Sarkissian[1]
[1]*Laboratory for Biomaterials and Bioengineering (LBB-ULaval), Laval University, Quebec, Canada & LBB-BioPark, Toledo, Brazil;* [2]*Plasmionique, Varennes, Canada*

Over the last 50 years, biomaterials, prostheses and implants saved and prolonged the life of millions of humans around the globe. The main clinical complications for current biomaterials and artificial organs still reside in an interfacial mismatch between the synthetic surface and the natural living tissue surrounding it. This is particularly true on implants for organs and tissue replacement, as well as for materials considered for driving organs and tissue regeneration (1).
Today, additive manufacturing, nanotechnology, nanomaterials and surface modifications provide new insight to bring effective advances to the current problem of clinical complications and even allow us to envisage strategies for organ shortage (2). Advanced technologies from materials science (3-5), merged with new biological paths towards the development of functional solutions for clinical applications (6,7), open new doors for conferring properties to metallic biomaterials that a decade ago were unthinkable. In this talk, the potential of merging 1) novel processes from surface science allowing grafting of biologically active molecules, with 2) advanced processes for metals showing extreme properties and controlled composition to provide engineering solutions to clinical challenged will be depicted.
Focus will be on low-vacuum glow discharge surface modifications might or might not fulfill the expectations for personalized medicine, on how nanostructures might or might not answer to the demand of metals-by-design implants, and how surface modifications might or might not confer what is required for the metal to interface and integrate the surrounding tissue and cells. The intrinsic goal of this talk is to present an extremely personal look at how the next generation of biodegradable and not-biodegradable metals can impact clinics and surgery, and how the resulting unique properties allowed biomedical functional applications to progress, from their introduction to the promising future that materials may or may not continue to hold for improving the quality of the life of millions worldwide.

References

[1] S Diaz-Rodriguez, et al. Coronary stent CD31-mimetic coating favours endothelialization and reduces local inflammation and neointimal development in vivo. European Heart Journal, 2021.
[2] SH Um, et al. Biomedical Device Surface Treatment by Laser-Driven Hydroxyapatite Penetration-Synthesis Technique for Gapless PEEK-to-Bone Integration. Advanced Healthcare Materials, 2024.
[3] A Cherqaoui, et al. Degradation behavior of austenite, ferrite, and martensite present in biodegradable Fe-based alloys in three protein-rich pseudo-physiological solutions. Bioactive Materials, 2024.
[4] S Loffredo, et al. Effect of silver in thermal treatments of Fe-Mn-C degradable metals: Implications for stent processing. Bioactive Materials, 2022.
[5] CC Bortolan, et al. Development of Ti-Mo-Fe alloys combining different plastic deformation mechanisms for improved strength-ductility trade-off and high work hardening rate. Journal of Alloys and Compounds, 2022.
[6] LM De Andrade, et al. Electropolishing Fe-based biodegradable metals for vascular applications: impact on surface properties, corrosion and cell viability, RSC Applied Interfaces, 2025.
[7] CC Bortolan, et al. Plasma-immersion ion implantation surface oxidation on a cobalt-chromium alloy for biomedical applications, Biointerphases, 2020.

Acknowledgments

The authors would like to support the NSERC-Canada, FRQ and Quebec Ministry of Economy and Innovation and Prima, the Canadian Foundation for Innovation for continuous support since 2000. Moreover, punctual funding from FAPESP-Brazil, CNPq and Capes-Brazil, as well Horizon-Europe are also acknowledged.
*Corresponding author: diego.mantovani@gmn.ulaval.ca

PRESSURE METROLOGICAL SETUP

Caroline Mendes da Silva[1], Francisco Tadeu Degasperi[2]
[1] [2] Faculdade de Tecnologia de São Paulo - FATEC-SP – CEETEPS São Paulo - SP

1. Introduction

Pressure metrology is crucial in science and industry, particularly in vacuum systems where precision is vital for process control and equipment optimization. This research aims to build a vacuum pressure measurement bench using various gauges, mercury column, Vacustat™, capacitive diaphragm, and Bourdon, covering a range from 1300 to 0.04 mbar for accurate laboratory and industrial measurements.

2. Experimental

The pressure measurement system was developed to ensure accurate readings through calibration with known standards, allowing comparison with measured values [1]. It applies Boyle–Mariotte's and Stevin's laws to relate pressure with gas volume, height, and fluid density, enabling precise calibration under varying conditions.

$$p1.V1 = p2.V2 \quad (1)$$

$$p = \rho g h \quad (2)$$

The analyses were conducted at the Vacuum Technology Laboratory (LTV/FATEC-SP), where the experimental setup is currently being assembled. To ensure reliability, different gauges were used: **Mercury Column:** Primary standard, operating from 103 mbar to 1 mbar. **Vacustat™:** Used for medium vacuum, covering the pressure range from 4 mbar to 4 × 10^{-2} mbar. **Bourdon Gauge:** Suitable for pressures above atmospheric, ranging from 0.6 bar to 700 bar. **Capacitive Diaphragm Gauge:** Covers from partial to ultra-high vacuum, operating from 10^{-6} mbar to 1000 mbar. The combination of these instruments ensures accurate measurements across a wide pressure range.

3. Results and Discussions

The metrological pressure setup was built with an aluminum structure for strength and 3D-printed supports for flexibility and customization. In the next phase, gauges will be installed and leak tests by pressure drop will be conducted to identify leaks and ensure system integrity and safety [2]. The leakage rate (Equation 3) is determined by multiplying pressure by the rate of volume change over time, representing the system throughput.

$$Q = \frac{\Delta p \; x \; V}{\Delta t} \quad (3)$$

Fig. 1. Experimental setup.

Fig. 2 . Vacustat™ gauges.

4. References

[1]- JOUSTEN, Karl.Handbook of Vacuum Technology. 2ª ed.Weinheim:Wiley-VCH, 2008.1050 p.
[2]- EDWARDS, Detecção de vazamento sob vácuo Edwards, Edwards.

*Corresponding author: *caroline.silva120@fatec.sp.gov.br*

PRESSURE FIELD IN A CONICAL TUBULAR HIGH AND ULTRA-HIGH VACUUM SYSTEM AS A FUNCTION OF PUMPING SPEED

Samuel da Silva Lima[1]* and Francisco Tadeu Degasperi[2]
[1, 2] *Faculdade de Tecnologia de São Paulo*

1. Introduction

Conical tubular high-vacuum systems are widely used in science and technology and must be properly designed to avoid rework and resource waste. This study aims to analyze the behavior of the pressure field as a function of the variation in pumping speed [1].

2. Experimental

To obtain the pressure field curves, an analytical modeling of a conical tubular system with a high-vacuum pump at the left end was carried out, based on an adaptation of the diffusion equation for vacuum environments (Equation 1). The solution of this equation provides the expression for the system's pressure field, presented in Equation 2.

$$c(x)\frac{\partial^2 p(x)}{\partial x^2}+\frac{dc(x)}{dx}\cdot\frac{\partial p(x)}{\partial x}=-q(x) \quad (1)$$

$$p(x)=\frac{\beta}{4\alpha a}\left(C1\ -\ \frac{b^2}{a}\right)\frac{1}{(ax\ +\ b)^2}-\frac{\beta}{2\alpha a^2}ln(ax+b)\ +\ C2 \quad (2)$$

Where $a\ =\left(\frac{D_M-D_m}{2L}\right)$, $b=\frac{D_m}{2}$, $\alpha=\frac{2\pi}{3}\left(\frac{8RT}{\pi M}\right)^{\frac{1}{2}}$ and $\beta\ =q_0\ 2\ \pi\ \sqrt{1+\ a^2}$. To determine the constants C1 and C2, the following boundary conditions are applied:

$$c(0)\left|\frac{dp(x)}{dx}\right|_{x=0}=+S_0p(0) \quad \text{and} \quad \left|\frac{dp(x)}{dx}\right|_{x=L}=0$$

The system characteristics are: length: 400 cm; diameters: 6 and 3 cm; outgassing rate: $5\text{x}10^{-9}$ mbar.l.s^{-1}.cm^{-2}; temperature: 293,15 K.

3. Results and Discussions

To obtain the results, the effective pumping speed S0, equal to the orifice conductance, was calculated. Then, speeds lower than, close to, and higher than S0 were considered. The resulting pressure fields are shown in Figure 2.

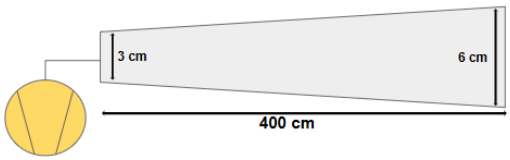

Fig. 1. *Conical tubular high-vacuum system*

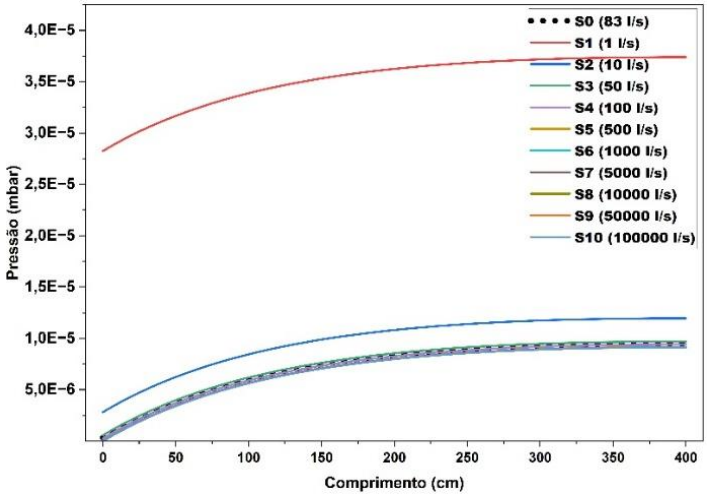

Fig. 2. *Pressure fields varying with pumping speed*

The results indicate that if the pumping speed is lower than the orifice conductance, the maximum pressure depends on it; whereas if it is higher, the pressure is limited by the conductance. Therefore, the pump design must take the system's geometry into account to avoid unnecessary expenses.

4. References

[1]- Degasperi, F. T., & Ricotta, R. M. (2023). High and Ultra-high Vacuum Pressure Profile and Its Gradient of the Conic Tube. **Brazilian Journal of Physics**, 53(2), 44.

Acknowledgments
To CNPq for the scientific initiation scholarship.
* Corresponding author: samuellima0919@gmail.com

WATER DESALINATION WITH VACUUM AND HEAT, EXPERIMENTAL ARRANGEMENT AND MODELLING

Angelus Marcio de Paula Silva*, Kennyon Andrade de Brito, Daniel de Almeida Franco, Robert Ramon de Souza Oliveira, Francisco Tadeu Degasperi
Faculdade de Tecnologia de São Paulo - FATEC-SP - CEETEPS- São Paulo- SP -Brasil

1. Introduction

Water is one of the most important resources for all living beings of the planet.Unfortunately 97,5% of the water on the planet is saline water. Around the world some countries already uses desalination techniques, in the Middle East is where it is most used, they can produce ~12 million m^3 of water per day, here in Brazil we actually do not use the Desalination in large scale, because we do have fresh water basins although in the Northeast region, there is a lack of water, the reason for that is the semi-arid climate, and dessert regions. This study has the objective to create an arrangement to be used in the Northeast Region of Brazil.

2. Experimental

For the experimental arrangement, we use a pressure pan, as vacuum chamber, involved by a thermal blanket. To energize the blanket, we are taking advantage of the sun of the semi-arid climate by using a photovoltaic board to electrically feed it. The distillation will be done in rough vacuum (10^3mbar – 1mbar), as the pressure goes down, the boiling water temperature will get low along with it, to exemplify it, in São Paulo state, at the Sea level, the boiling temperature is 100 °C (373,15 K), in capital city the boiling temperature is 97°C (370,15 K), with that we are going to use less energy to boil the water. To make the vacuum we use an oscillating piston pump, it is a free oil pump (or dry pump), since we are using a dry pump we need to protect the bomb, preventing that the water vapor reaches the pump, to do it we made a PVC (Polyvinyl Chloride) pipe with silica gel balls to absorb the water vapor. To condensate the water, we will use a water pump, the water (in ambient temperature) flows through the condenser transferring its temperature to the vapor making it condense.

3. Results and Discussions

The arrangement is almost complete, we received a photovoltaic board, and it is being installed on the Hydraulic Lab from FATEC São Paulo. The water sample, that will be desalinated, is from RMBS (Metropolitan Region of Baixada Santista), that is stored cooling to maintain your characteristics. When this project is completed, it might help with studies of how to develop low costs desalination systems for small communities, and that can be operated by common citizens.

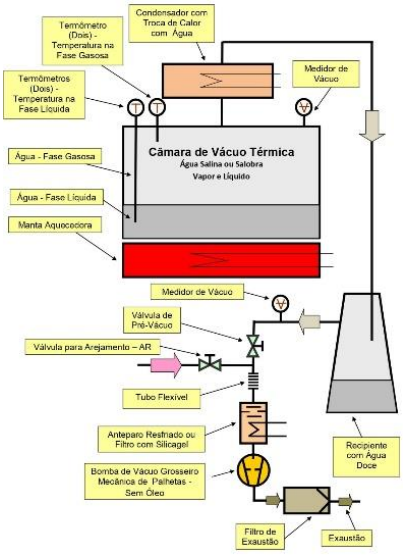

Fig. 1. *Experimental arrangementdiagram*

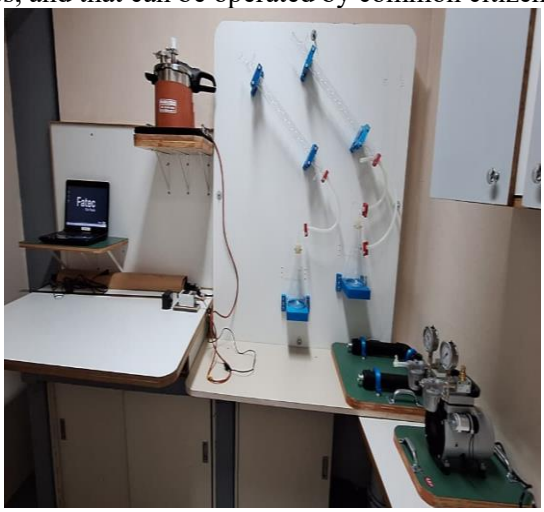

Fig. 2. *Experimental arrangement*

4. References

[1]-DA SILVEIRA, Ana Paula Pereira et al. Dessalinização de águas. Oficina de Textos, 2015.

Acknowledgments

To D.V.P Brasil Bombas de Vácuo for thevacuum pump. To Abrinstal for the photovoltaic board.
To CNPq for the Pibic scholarship.
*Corresponding author: angelusmarcio@gmail.com

PLASMA-ACTIVATED LIQUIDS: GENERATION, CHARACTERIZATION AND APPLICATIONS IN BIOMEDICINE AND MATERIALS SCIENCE

Rodrigo S. Pessoa[1]*, Nilton F. Azevedo Neto[1], Felipe S. Miranda[1,2], Isabela Horta[1], and Cristiane Koga-Ito[2]
[1] *Laboratório de Plasmas e Processos (LPP), Instituto Tecnológico de Aeronáutica (ITA), São José dos Campos, Brazil*
[2]*Instituto de Ciência e Tecnologia, Universidade Estadual Paulista (UNESP), São José dos Campos, Brazil*

1. Introduction

Plasma-activated liquids (PALs), such as plasma-activated water (PAW) and saline (PAS), have emerged as promising chemical systems for biomedical, agricultural, and materials applications. Their reactivity is governed by the formation of reactive oxygen and nitrogen species (RONS), including H_2O_2, NO_2^-, NO_3^-, and O_3, generated by non-thermal plasma discharges interacting with liquids. Understanding how plasma parameters influence the chemical composition and stability of PALs is essential for developing controlled formulations for selective oxidative treatments and advanced functional materials.

2. Experimental

PALs were generated using different plasma configurations: dielectric barrier discharge (DBD), gliding arc plasma jet (GAPJ), and surface wave discharge (SWD, "surfatron") systems operating at atmospheric pressure. The plasma–liquid interaction was studied using various gases (Ar, air, and Ar/air mixtures). Optical emission spectroscopy, UV–Vis absorption, Raman and FTIR spectroscopies, along with pH, conductivity, and ORP measurements, were employed to characterize the physicochemical properties of the activated liquids. In parallel, biological and technological evaluations were performed, including tests on microbial and fungal inactivation, biocompatibility, and surface modification of materials.

3. Results and Discussions

The results demonstrate that plasma configuration and gas composition strongly affects RONS balance and liquid properties. DBD–GAPJ systems favor the simultaneous production of NOx and H_2O_2, while SWD reactors provide electrode-less activation, preventing contamination and yielding chemically pure PAW. UV–Vis and DFT analyses enabled molecular-level interpretation of RONS absorption bands, revealing protonation-dependent spectral shifts. Raman/SERS characterization improved the detection sensitivity of nitrates and peroxides at milligram-per-liter levels.

Biological assays showed significant antibacterial and antifungal activities of PALs, with selective effects on *Candida albicans* biofilms and melanoma cells, while maintaining high mammalian cell viability. Furthermore, PALs proved stable after refrigerating or frozen storage and effective in surface cleaning and film deposition processes such as PAW-assisted atomic layer deposition (PAW-ALD). These findings highlight PALs as versatile plasma-derived media, bridging plasma physics, chemistry, and applied biomedicine.

4. References

[1] N.F. Azevedo Neto *et al.*, *Eur. Phys. J. D* **79**, 126 (2025).
[2] F.S. Miranda *et al.*, *Physica Scripta* **100**, 075623 (2025).
[3] L.G. Lima *et al.*, *J. Phys. D: Appl. Phys.* (2025).
[4] S.S. dos Santos *et al.*, *ACS Appl. Sci. Eng.* (2025).
[5] N.F. Azevedo Neto *et al.*, *Vibrational Spectroscopy* **136**, 103765 (2024).

Acknowledgments

The authors acknowledge financial support from FAPESP (2019/05856-7, 2022/11544-0) and CNPq (PQ-309863/2021-9).
*Corresponding author: rspessoa@ita.br

GLIDING ARC PLASMA AS A GREEN TECHNOLOGY FOR CELL DISRUPTION AND FATTY ACID EXTRACTION FROM RHODOTORULA TORULOIDES

Thainá Barbosa de Lima Cordeiro*, Ana Bárbara Azevedo Gomes Goulart, José Geraldo da Cruz Pradella, Virginia Klausner de Oliveira, Lucia Vieira
University of the Paraíba Valley

1. Introduction

The search for sustainable and efficient methods for microbial lipid recovery has intensified due to the increasing demand for biofuels and high-value compounds. Oleaginous yeasts such as *Rhodotorula toruloides* (*R. toruloides)* are particularly notable for their high capacity to accumulate intracellular fatty acids. However, cell wall disruption remains a major technological bottleneck, often requiring toxic solvents or high-energy mechanical methods [1-3].
In this context, non-thermal gliding arc plasma emerges as an innovative and environmentally friendly approach, capable of promoting cell disruption through reactive species, ultraviolet radiation, and strong electric fields, without the need for aggressive chemical reagents [1,4]. Although promising, this technique is still not fully established for microbial lysis, making it essential to evaluate its efficiency in releasing intracellular lipids.

2. Experimental

The samples were treated using a non-thermal gliding arc plasma reactor powered by a 60 Hz alternating current (AC) source. 50 mL of the *R. toruloides* cell suspension were placed in a glass beaker positioned 10 mm below the reactor. **Rupture.**The system was operated with continuous flows of 4 $L \cdot min^{-1}$ compressed air and 6 $L \cdot min^{-1}$ argon for a total exposure time of 5 minutes [5]. **Cell Separation.** After treatment, samples were centrifuged and the supernatant discarded, and the cell pellets were subjected to lipid extraction and transesterification to be used at Gas Chromatography-Flame Ionization Detection analysis(GC-FID). **Briefly Transesterification.** samples were sequentially reacted with methanolic KOH and H_2SO_4, heated at 85 °C, extracted with hexane/water, and centrifuged [6]. **GC-FID**. was performed using standard conditions: Clarus 580/Elite-5 column for chemically treated samples and Clarus 600/SP-2560 column for plasma-treated samples. Methyl esters were identified and quantified by comparison with the Supelco 37 FAME standard mixture.

3. Results and Discussions

Treatment with sliding arc plasma promoted partial cell wall rupture, facilitating the release of lipids into the medium. GC-FID analysis confirmed the presence of major fatty acids, predominantly oleic acid (C18:1) and palmitic acid (C16:0), characteristic of *R. toruloides*. These results demonstrate that sliding arc plasma is a promising green technology for cell pretreatment and lipid extraction, with potential applications in biotechnology and industrial processes. The study also opens opportunities for optimizing plasma parameters and investigating the physicochemical mechanisms underlying cell lysis.

4. References

[1]- S. Liang, Y. Zhang, L. Lyu, S. Wang, Z. Zhao, Secretory expression of β-1,3-glucomannanase in the oleaginous yeast *Rhodosporidium toruloides* for improved lipid extraction, Bioresources and Bioprocessing, 10, (2023).
[2]- M. Zainuddin, C. Fai, A. Ariff, L. Rios-Solis, M. Halim, Current pretreatment/cell disruption and extraction methods used to improve intracellular lipid recovery from oleaginous yeasts, Microorganisms, 9, (2021).
[3]- C. Dias, B. Nobre, J. Santos, T. Da Silva, A. Reis, Direct lipid and carotenoid extraction from Rhodosporidium toruloides broth culture after high pressure homogenization cell disruption: strategies, methodologies, and yields, Biochemical Engineering Journal, (2022).
[4]- R. Thirumdas, C. Sarangapani, U. Annapure, Cold plasma: a novel non-thermal technology for food processing, Food Biophysics, 10, 1–11, (2015).
[5]- A. C. O. C. Doria et al., Application of post-discharge region of atmospheric pressure argon and air plasma jet in the contamination control of Candida albicans biofilms, Research on Biomedical Engineering, 31(4), 358–362, (2015).
[6]- J. Mendham et al., Vogel Análise Química Quantitativa, 6th ed., LTC, 488 p, (2002).

Acknowledgments

We would like to thank CAPES (Scholarship No. 88887.992108/2024-00) and CNPq (Project No. 407946/2022-5), Brazil, for financial support.
*Corresponding author: thainablcordeiro@gmail.com

FRICTION TESTS OF WC - Co VACUUM SINTERED WITH DIFFERENT SLUDGE CONTENTS

Fábio Miranda[1], Luan Matheus Chagas[2]*, Suzilene Real Janasi[1], Julia Marinzeck de Alcantara Abdala[2], Lúcia Vieira[2], Fernando Santos Ortega[2]

[1] *BRATS – Indústria e Comercio de Produtos Metálicos Especiais Ltda*

[2]*Universidade do Vale do Paraíba, Instituto de Pesquisa e Desenvolvimento, IP&D. Av. Shishima Hifumi, 2911. São José dos Campos – SP.*

1. Introduction

The study of friction encompasses the analysis of various mechanisms that govern the resistance to relative motion between contacting surfaces. Tribology, as an interdisciplinary field, combines principles of mechanics, materials science, and surface chemistry to understand and optimize these interactions [1,2]. The coefficient of friction (COF) is a critical parameter that reflects the performance of materials subjected to sliding contact, influencing wear behavior and service life. Tungsten carbide–cobalt (WC–Co) composites are extensively used in cutting and wear-resistant applications due to their superior hardness and toughness. However, the limited availability and high cost of tungsten and cobalt, together with supply-chain and environmental constraints, have driven growing interest in recycling worn tools and grinding sludge from WC–Co production. The incorporation of grinding sludge and the associated processing conditions may affect the tribological behavior and in-service performance of WC–Co alloys. This study investigates the influence of varying sludge contents (0%, 50%, and 100%) in WC–Co composites produced by vacuum sintering, focusing on their friction and wear behavior.

2. Experimental

WC–Co composites were produced with sludge contents of 0%, 50%, and 100%. The powders were compacted by uniaxial pressing and vacuum-sintered to avoid cobalt oxidation. Tribological tests were performed using a Bruker-CETR tribometer in a linear reciprocating configuration. Each sample was tested under a normal load of 50 N and a sliding speed of 10 mm/s, over a stroke length of 10 mm for a total duration of 166 minutes. All tests were conducted in duplicate to ensure reproducibility. During testing, the friction force and wear mass loss were continuously recorded. After testing, the mass of each sample was measured to quantify wear, and the coefficient of friction (COF) was calculated as the ratio of the tangential friction force to the applied normal load.

3. Results and Discussions

The results of mass loss and COF measurements for the samples with different sludge contents are summarized as follows: For the 0% sludge sample (2A-0%), the material exhibited the highest mass loss, indicating reduced wear resistance compared to samples with higher sludge content. The average coefficient of friction remained relatively constant, showing no significant deviation from the other samples. In the 50% sludge sample (2B-50%), the wear rate decreased, demonstrating that moderate sludge content contributes to a denser microstructure and improved cohesion between the WC particles and the Co binder. The COF maintained similar values to those of the 0% sample, confirming that the sludge content had limited influence on frictional behavior under the tested conditions. The 100% sludge sample (2C-100%) exhibited the lowest mass loss, suggesting enhanced wear resistance. The COF remained similar to the other compositions, reinforcing that the main effect of increasing sludge content was the reduction in wear rather than frictional resistance. These findings indicate that the vacuum sintering process promotes the formation of a stable tribolayer, which, together with strain hardening of the Co matrix, contributes to wear resistance. The results align with the literature, which reports that tribological performance in WC–Co composites depends primarily on the microstructural integrity and mechanical stability of the binder phase, rather than on variations in the friction coefficient [1,2].

3.Conclusions

In summary, while the COF of the composites was similar across all compositions, the wear resistance improved significantly with increasing sludge content, emphasizing the beneficial effect of sludge addition on the mechanical performance of vacuum-sintered WC–Co materials.

4. References

[1]- Iakovakis, E. Avcu, E. **Wear.** 486–487,1-12, (2021)
[2]- Usmani et al., **Tribology Transactions**, 40, 470-478 (1998).

Acknowledgments We would like to thank CAPES, and CNPq (Project No. 407946/2022-5, 441780/2024-5, 350440/2025-5 and 350485/2025-9), FAPESP (Processes 2019/08927-2 e 2022/06201-7), Brazil, for financial support.

COMPARATIVE ANALYSIS OF DIELECTRIC BARRIER DISCHARGE (DBD) AND SURFATRON PLASMAS FOR WATER ACTIVATION AND ANTIMICROBIAL EFFICIENCY FOR NEBULIZED PAW

Marina Clara Ribeiro dos Santos[1]*, Eduardo Ferreira Martins[1], Michaela Shiotani Marcondes[1], Felipe Santos de Almeida[2], Anelise Osorio Cesar Doria[2], Rodrigo Sávio Pessoa[1]

[1] *Plasma and Process Laboratory, Aeronautics Institute of Technology (ITA), 12228-900, São José dos Campos (SP), Brazil*

[2] *Research and Development Institute (IP&D), University of Paíba Valley (UNIVAP), 12244-000, São José dos Campos (SP), Brazil*

1. Introduction

The use of non-thermal atmospheric pressure plasma to generate Plasma-Activated Water (PAW) represents a significant advancement in non-chemical disinfection and material science, including applications in medicine, dentistry, and nanotechnology [1, 2]. The cold plasma process, when interacting with water, alters its physicochemical properties, leading to the formation of Reactive Oxygen and Nitrogen Species (RONS, e.g., H_2O_2, NO_2^-, and NO_3^-). Previous work demonstrated that different sources yield distinct PAW chemistries and antimicrobial efficacy [2]. This study compares PAW generated by a Dielectric Barrier Discharge (DBD) system and a Surfatron (Surface Wave Sustained Discharge) to understand the difference in RONS production and subsequent antimicrobial efficacy. This comparative analysis is crucial for optimizing plasma technology for specific biomedical applications.

2. Experimental

PAW samples were generated using two distinct atmospheric plasma sources: a Dielectric Barrier Discharge (DBD) reactor and a Surfatron reactor. Deionized (DI) water (40 mL) was exposed to plasma for 40 minutes in both systems. The DBD reactor operated using compressed air, while the Surfatron was fed with Argon gas, maintaining similar power inputs (e.g., 70 W for Surfatron) and controlled reflected power. The physical-chemical properties of the activated water were immediately characterized. Measurements included pH, Electrical Conductivity (EC), and the concentration of key RONS, such as Hydrogen Peroxide (H_2O_2), Nitrite (NO_2^-), and Nitrate (NO_3^-), using specific reagents and UV-Vis spectroscopy. The DBD plasma was characterized using Optical Emission Spectroscopy (OES) to identify the main species generated, essential for correlation with the measured liquid properties. For biological assays, the PAW from both systems was nebulized directly onto biofilms of medically relevant microorganisms, including *Escherichia coli* (*E. coli*) and *Staphylococcus aureus* (*S. aureus*). Post-treatment, Colony Forming Units (CFU) counting was performed to evaluate the inactivation rate for each plasma source.

3. Results and Discussions

Preliminary characterization data for the Surfatron PAW shows high concentrations of H_2O_2 (e.g., >30 mg/L), a potent oxidizing agent, with a moderate pH (e.g., 3.62). In contrast, it is hypothesized that the air-fed DBD plasma will favor the production of Nitrogen RONS (NO_2^- and NO_3^-) from the air, resulting in PAW with higher acidity (pH≈3.0) and significantly increased electrical conductivity [2]. The OES analysis of the DBD plasma is expected to confirm the presence of high-energy nitrogen species and hydroxyl radicals (OH), which are precursors to these species in the liquid. The differences in RONS profiles are projected to be reflected in the biological assays. The Surfatron PAW, due to its high H_2O_2 content, is expected to show total microbial inhibition for the tested bacteria, aligning with previous findings [4]. The DBD PAW, being more acid and less rich in peroxides, is expected to show reduced or no significant antimicrobial efficacy under the tested nebulization conditions. This difference highlights that while both systems activate water, the Surfatron's chemistry is more suitable for strong microbial inactivation through direct oxidative stress from peroxides.

4. References

[1]- Pessoa, R. S. et al., Appl. Surf. Sci. 422, 73-84 (2017).
[3]- Chiappim, W. et al., Plasma Processes and Polymers, v. 18, n. 11, (2021).

Acknowledgments

To the Fundação de Amparo à Pesquisa do Estado de São Paulo (Process: 2023/10438-5), the Programa Nacional de Pesquisa Científica of the Conselho Nacional de Desenvolvimento Científico e Tecnológico (Process 166041/2024-6) and the Conselho Nacional de Desenvolvimento Científico e Tecnológico (Process: 178682/2025-0).

*Corresponding author: marinaclara@ita.br

HIGH-ENTROPY ALLOYS FOR MEDICAL DEVICES: MICROSTRUCTURE, ELECTROCHEMISTRY, TRIBOCORROSION AND CYTOCOMPATIBILITY.

Carlos Eduardo Manreza[1], Diego Rafael Nespeque Correa[2], Mariana Luna Lourenço[3], Edriely de Oliveira Saraiva[4], Carlos Roberto Grandini[5].
[1]*UNESP, School of Sciences, Campus Bauru, Laboratory of Anelasticity and Biomaterials, Bauru, SP, Brazil*
[2]*UNESP, Institute of Biosciences, Botucatu, Department of Chemistry and Biochemistry, Bauru, SP, Brazil*

1. Introduction

High-entropy alloys (HEAs) combine five or more principal elements, forming single-phase FCC or BCC solids that unite strength, passivity, and biocompatibility (synergy), which are key properties for medical devices [1, 2]. This work investigates four equiatomic HEAs (CoCrFeMnNi, FeCoCrMnNi, TiNbTaZrMo, and TaNbHfZrTi) to correlate their microstructure, hardness, electrochemical stability, tribocorrosion, and cellular response in simulated physiological media.

2. Experimental

The alloys were arc-melted **under high vacuum** (pump-down < 10^{-4} mbar, Ar back-fill) and subsequently heat-treated **under vacuum** to minimize segregation and improve homogeneity. Microstructure was examined **under high-vacuum** SEM (SE/BSE) and EDS, while OM and XRD confirmed FCC/BCC phases. Vickers microhardness (300 gf, 15 s) characterized mechanical response. Electrochemical behavior in PBS (37 °C) was studied by OCP, PDP, and EIS (10^{6}–10^{-1} Hz, 10 mV, Rs–CPE–Rp). Tribocorrosion was evaluated using a pin-on-disk setup with Al_2O_3 counterbody, monitoring COF(t) and OCP(t) during sliding, with post-test wear by profilometry and SEM. MTT (24/72 h) and Crystal Violet (24 h) assessed viability and adhesion relative to Ti–6Al–4V.

3. Results and Discussions

The high-vacuum melting route ensured clean and reproducible surfaces, enabling reliable passive-film formation. SEM-BSE revealed homogeneous FCC grains in Fe-containing alloys and dendritic BCC contrast in Ti-based HEAs, consistent with hardness values (≈143–468 HV). TiNbTaZrMo and TaNbHfZrTi combined mechanical durability, electrochemical stability, and cytocompatibility, while CoCrFeMnNi and FeCoCrMnNi performed better under wear-dominated, low-corrosion conditions, suitable for external devices or as coating substrates. From arc-melting to high-vacuum SEM, the vacuum route was crucial for robust structure property correlations. These results highlight the potential of HEA design as a route for next-generation biomedical devices.

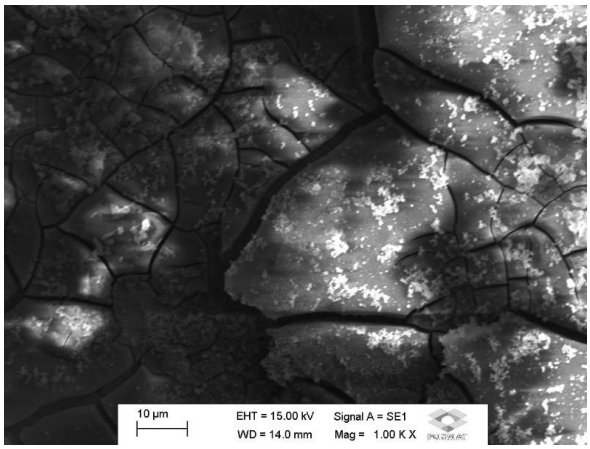

Fig. 1. *High-vacuum SEM-BSE microstructure*

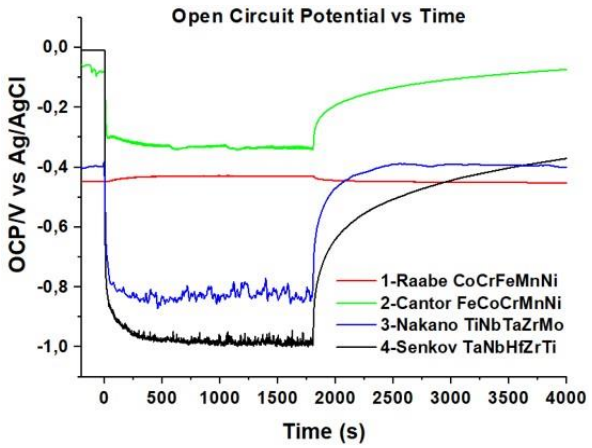

Fig. 2. *OCP curves of the four HEAs*

4. References

[1]- HUA, N. *et al.* Mechanical/corrosion/wear of biomedical Ti–Zr–Nb–Ta–Mo HEA, **J. Alloys Compd.** 861 (2021) 157712.
[2]- SANTOS, G.C. *et al.* Tribocorrosion of Ti-Zr-Mo alloys in Hanks' solution, **Materials** 16 (2023) 3741.

Acknowledgments:
CNPq (PIBIC), UNESP, Universal CNPq, and the Laboratory of Anelasticity and Biomaterials for technical and theoretical support.
Corresponding author: carlos.manreza@unesp.br

USE OF NON-THERMAL PLASMA FOR ELIMINATION OF PARACETAMOL IN EFFLUENTS

Igor dos S. Faria[1], *Heloisa Maria P. de Almeida[1], Nilson C. da Cruz [2], Silvia P. Irazusta[1,3]
[1]Faculdade de Tecnologia de Sorocaba (FATEC)
[2]Instituto de Ciência e Tecnologia (UNESP) - Campus Sorocaba
[3]*PPG - Mestrado Profissional em Gestão e Tecnologia em Sistemas Produtivos, CEETEPS*

1. Introduction

Emerging contaminants, such as paracetamol, have been found in rivers, lakes and even drinking water, posing environmental and human health risks. Conventional water treatment systems cannot completely remove these compounds. In this context, the use of non-thermal plasma appears as a promising alternative, capable of degrading the drug through the action of oxidizing radicals, promoting a more efficient and sustainable treatment. [1].

2. Experimental

In the analyses performed with distilled water, paracetamol solutions were prepared at different concentrations: 0.5; 1; 1.5; 2; 5; 15; and 25 µg/mL. The treatment was conducted using two types of non-thermal plasma: the kINPen plasma jet, operating with argon gas at a flow rate of 5 L/min, applied for 15 minutes to 100 mL of sample, maintaining a distance of 25 mm between the jet and the solution surface; and the dielectric barrier discharge (DBD) plasma, using compressed air as the operating gas, also for 15 minutes of exposure. After treatment, the samples were analyzed by UV-Vis spectrophotometry at 243 nm to determine the variation in paracetamol concentration and calculate the removal efficiency for each method, as shown in Tables 1 and 2.

3. Results and Discussions

In the experiments, two non-thermal plasma methods were applied: kINPen plasma jet and dielectric barrier discharge (DBD) plasma. The kINPen acts on the sample surface, while the DBD operates submerged, providing greater contact between the plasma and the solution, which favors paracetamol degradation. According to Table 1, the kINPen treatment in distilled water showed variable efficiency depending on the concentration: at the lowest concentrations (0.5 µg/mL), removal reached 63%, but decreased to only 3% at 2 µg/mL, demonstrating that increasing concentration reduces process efficiency. Table 2, referring to the DBD plasma in distilled water, revealed more impressive results, with removal of up to 60% of paracetamol. This difference is attributed to the fact that DBD allows for greater homogenization of the plasma in the liquid medium, intensifying the generation of reactive oxygen species (such as hydroxyl radicals and ozone), which promote oxidation and breakdown of the drug molecule. Thus, the results indicate that DBD plasma is more efficient than kINPen in degrading paracetamol in water, especially at lower concentrations, confirming the potential of this technology for the treatment of water contaminated with pharmaceuticals.

Referência (µg/mL)	Amostra não tratada (µg/mL)	Amostra tratada (µg/mL)	% concentração (µg/mL)	% de extração
0,5	0,5134	0,189	0,3244	63
1	0,8724	0,7528	0,1197	14
1,5	1,4126	1,3465	0,0661	5
2	2,1843	2,1134	0,0709	3

***Fig 1**. Treatment with kINPen in distilled water, UV-Vis analysis of 0.5-2 ug/mL*

Referência (µg/mL)	Amostra não tratada (µg/mL)	Amostra tratada (µg/mL)	% concentração (µg/mL)	% de extração
1	1,7905	0,7118	1,0787	60
5	5,4629	3,148	2,3149	42
15	13,9165	10,5212	3,3953	24
25	23,8708	17,9196	5,9512	25

***Fig 2**. DBD treatment in distilled water, UV-Vis analysis of 1-25 ug/mL*

4. References

[1] WU, S.; ZHANG, L.; CHEN, J. *Paracetamol in the environment and its degradation by microorganisms.* Applied Microbiology and Biotechnology, v. 96, n. 4, p. 875–884, 2012.

Acknowledgments

We thank CNPq for the scientific initiation scholarship.
*Corresponding author: heloisa23mari@gmail.com

ANTIMICROBIAL ACTIVITY OF MULTI-WALLED CARBON NANOTUBES (MWCNTs) PRODUCED BY PECVD

Hilda Geovana Alves Pinto[1]*, Larissa Solano De Almeida[2], Luciana Sgarbi Rossino[1], Silvia Pierre Irazusta[1,3]
[1]Faculdade de Tecnologia de Sorocaba (FATEC)
[2]Universidade Federal de São Carlos (UFSCar) - Campus Sorocaba
[3]*Mestrado Profissional em Gestão e Tecnologia em Sistemas Produtivos, CEETEPS*

1. Introduction

Microbial resistance caused by the improper use of antibiotics and antifungals represents a global threat to public health, requiring new antimicrobial approaches. Nanomaterials, due to their unique physicochemical and mechanical properties, have shown promise in combating microorganisms. Among them, carbon nanotubes stand out for their antimicrobial action based on mechanical interaction with cell membranes. Studies indicate that multi-walled carbon nanotubes (MWCNTs) can effectively damage fungi. Thus, this work aims to evaluate the antimicrobial activity of MWCNTs produced by PECVD in the microbiological control of surfaces [1].

2. Experimental

The multi-walled carbon nanotubes (MWCNTs) will be synthesized using the PECVD technique at the LabTES laboratory of FATEC Sorocaba. Microbial suspensions will be prepared from standardized fungal cultures of *Fusarium spp.* according to the MacFarland scale. Serial dilutions and exposure of the samples to the nanomaterial will be performed, with a control tube for comparison. The inhibition zone assay will be applied to evaluate antimicrobial activity at different concentrations (10–50 mg/L). Finally, the inhibition halos will indicate the effectiveness of the MWCNTs against fungi.

3. Results and Discussions

The present study demonstrated that a concentration of 50 mg/L of multi-walled carbon nanotubes exhibited effective antifungal activity. The colony count on the plates, after 48 hours of incubation with CNTs, showed significant inhibition at the 50 mg/L concentration. Consistent with other findings in the literature [2], Fusarium spp. was inhibited, but at a tenfold lower concentration.

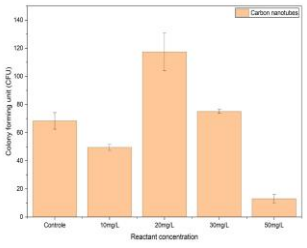

Fig. 1. *Colony forming unity.*

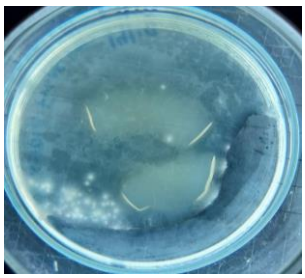

Fig. 2. *Control plate.*

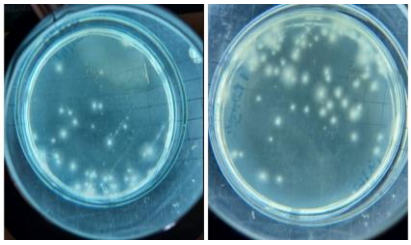

Fig. 3. *A. concentration of 10mg/L and B. concentration of 20mg/L.*

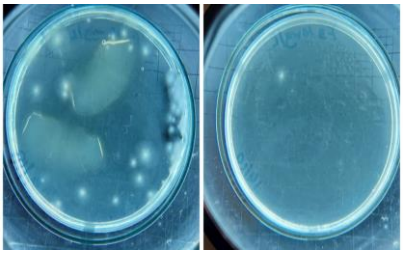

Fig. 4. *A. concentration of 30mg/L and B. concentration of 50mg/L.*

4. References

[1] ALMEIDA, Larissa Solano de**.** Produção e Caracterização de Nanoestruturas de Carbono por PECVD. Dissertação (Mestrado em Ciência dos Materiais) – Universidade Federal de São Carlos, campus Sorocaba, Sorocaba, 2021.
[2] MANZOOR, Sadia, *et al.* Journal of Integrative Agriculture, v. 25, n, 4, 2025

Acknowledgments
We thank CNPq for the scientific initiation scholarship.
*Corresponding author: hildasgeoalves@gmail.com

PLASMA-ASSISTED OPTIMIZATION OF PDMS SURFACE FUNCTIONALIZATION FOR DURABLE CHITOSAN-BASED BIOFUNCTIONAL COATINGS

Francisco Alfaro[1]*, Cecilia Zorzi Bueno[1], Helton José Wiggers[1] and Diego Mantovani[2]
[1]*Laboratory for Biomaterials and Bioengineering (LBB-BPK), Biopark Education, Toledo, PR, Brazil;*
[2]*Laboratory for Biomaterials and Bioengineering (LBB-ULaval), Laval University, Quebec, Canada*

1. Introduction

Surface functionalization of polydimethylsiloxane (PDMS) is essential to enhance coating adhesion, hydrophilicity, and biocompatibility in biomedical applications. Plasma treatment provides a clean and controllable approach to introduce polar surface groups, improving wettability and coating stability. Previous studies reported significant reductions in water contact angle (WCA) through oxygen or oxygen/argon plasmas [1,2], reinforcing the relevance of this work.

2. Experimental

PDMS substrates were cleaned with water and ethanol, followed by oxidation in piranha solution (H_2SO_4/H_2O_2 = 3:2 v/v, 10 min) or plasma activation, which was performed in an inductively coupled RF reactor (Flarion, Plasmionique Inc., Canada) using Ar, O_2, and Ar/O_2 mixtures (>99.999%), varying flow (8–45 sccm), pressure (8–233 mTorr), power (30–150 W), and time (1–17 min). Wettability was evaluated by sessile-drop measurements (OCA 11, DataPhysics), and statistical and clustering analyses correlated plasma parameters with WCA. After activation, substrates were coated with a polydopamine interlayer (2 mg/mL, 24 h) and a chitosan-based film containing tannic acid, $FeSO_4$, and moxifloxacin, then dried at 37–40 °C.

3. Results and Discussions

Systematic variation of plasma parameters revealed optimal conditions for enhancing PDMS hydrophilicity and coating adhesion. As shown in Fig. 1, Ar/O_2 plasmas at high power and short exposure times produced the lowest WCA values (≈ 40–43°), indicating optimal surface activation. Cluster 1, identified by k-means analysis, exhibited the best wettability, supported by correlation results showing a negative relationship between plasma power and WCA, and highlighting the adverse effect of excessive treatment time due to hydrophobic recovery. Increasing Ar content raised WCA, whereas O_2-rich plasmas promoted effective oxidation. The visual comparison in Fig. 2 further demonstrates the improved coating uniformity and adhesion achieved after plasma activation, confirming this approach as a clean, tunable, and efficient method for producing durable chitosan-based biofunctional coatings on PDMS.

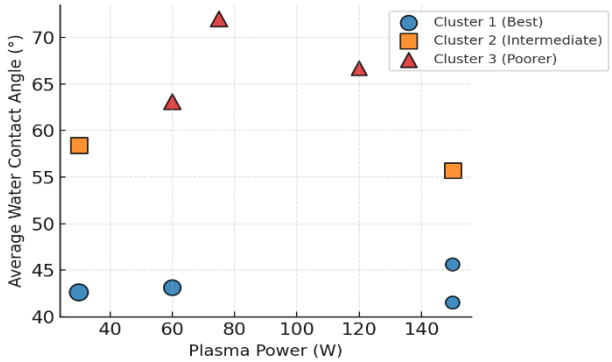

Fig. 1 – Effect of plasma power and time on surface wettability. *Average WCA decreased with higher plasma power and shorter exposure; marker size indicates treatment time, and colors show k-means clusters: Cluster 1 (blue) – best, Cluster 2 (orange) – intermediate, Cluster 3 (red) – poorer wettability.*

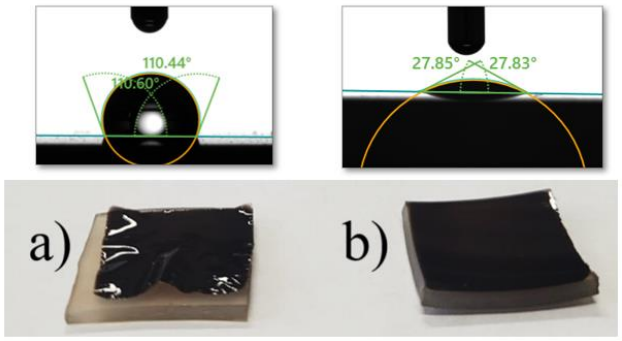

Fig. 2. Visual and wettability comparison between untreated and plasma-treated PDMS samples. *(a) High water contact angle (110°) before plasma activation and poor coating adhesion and (b) reduced contact angle (28°) after plasma treatment and uniform coating, demonstrating improved surface hydrophilicity.*

4. References

[1] Chen et al., Materials, 15 (2022) 839.
[2] Barros et al., Appl. Sci., 13 (2023) 6365.

Acknowledgments

The authors thank Claudia M. da Silva, Vinicius L. Ruschel, and João V. Kellner for technical support, Dr. Carmen Donaduzzi and Dr. Luiz Donaduzzi for guidance throughout the project.
*Corresponding author: francisco.alfaro@bpkedu.com.br

TiO_2 COATINGS OBTAINED BY MAO ON Ti-25Ta-xNb ALLOYS: EFFECT OF VOLTAGE VARIATION

Fernanda de Freitas Quadros[1]*, Diego Rafael Nespeque Corrêa[1] and Carlos Roberto Grandini[1]
[1]*UNESP – Univ. Estadual Paulista, Anelasticity and Biomaterials Laboratory, Bauru, SP, Brazil*

1. Introduction

Titanium-based alloys stand out among the materials used in orthopedic implants due to the productivity of their modulus in modeling cortical bone compared to pure titanium, as well as their high corrosion resistance and proven biocompatibility [1]. However, despite these specific properties, revision surgeries are still frequent [2]. In this context, strategies have been used to improve the performance of metal implants, including surface modification, which aims to extend implant life and reduce complications associated with biotribocorrosion and contamination. Among the available techniques, micro-arc oxidation (MAO) proves to be an efficient alternative for obtaining porous and bioactive oxide coatings on metal alloys [3]. In this study, we evaluated the effect of varying the applied voltage (200, 250, and 300 V) on the properties of TiO_2 layers formed by MAO on Ti-25Ta-xNb alloys (x = 10, 20, and 30%).

2. Experimental

To obtain the Ti-25Ta-xNb alloys (x = 10, 20, and 30%), the precursors were melted in a water-cooled copper crucible in an electric arc furnace under high vacuum (10^{-2} mBar) and argon atmosphere, using a non-consumable tungsten electrode. After melting, the ingots were rolled to obtain regular shapes, followed by homogenization heat treatment in high vacuum, heating at 10°C/min to 1000°C for 6 h, and cooling in air, in order to reduce residual stresses. The alloy surfaces were functionalized by micro-arc oxidation (MAO), applied in an electrolytic solution containing calcium acetate monohydrate (CaA), disodium β-glycerophosphate pentahydrate (β-GP), magnesium acetate tetrahydrate (MgA), and silver nitrate ($AgNO_3$). The process was carried out with anodic direct current on the substrate immersed in the solution, using platinum sheets as the cathode, with voltages of 200, 250, and 300 V, a current of 2.5 A, a time of 60 s, and magnetic stirring of 500 rpm.

3. Results and Discussions (bold face Times New Roman 11 pt)

Higher voltages were observed to increase the energy of electrical discharges, promoting the formation of homogeneous coatings with greater porosity. Electron micrographs reveal that the alloy containing 10% Nb, whose microstructure is predominantly formed by the α″ phase, exhibited greater porosity compared to alloys with a body-centered cubic structure (20% and 30% Nb), indicating that the predominant phase of the alloy influences the final coating morphology [4]. XRD analyses identified the anatase and rutile phases in the coatings, with the proportion of rutile being higher at higher voltages, associated with increased discharge energy. Regarding adhesion, all samples showed good integration between the coating and the metal substrate, regardless of the processing conditions [4]. The results indicate that the voltage applied during the MAO process directly influences the morphology, porosity, and composition of the TiO_2 layers. Thus, MAO-functionalized Ti-25Ta-xNb alloys show promising potential for biomedical implants with bioactive surfaces.

4. References

[1] Pesode, P. and S. Barve, *A review—metastable β titanium alloy for biomedical applications.* Journal of Engineering and Applied Science, 2023. **70**(1): p. 1-36.
[2] Kurtz, S., et al., *Projections of primary and revision hip and knee arthroplasty in the United States from 2005 to 2030.* Jbjs, 2007. 89(4): p. 780-785.
[3] Li, G., et al., *Review of micro-arc oxidation of titanium alloys: Mechanism, properties and applications.* Journal of Alloys and Compounds, 2023. 948: p. 169773.
[4] Quadros, F.d.F., et al., *Surface Characteristics of TiO2 Coatings Formed by Micro-Arc Oxidation in Ti-25Ta-x Nb Alloys: The Influence of Microstructure and Applied Voltage.* Coatings, 2025. **15**(6): p. 730.

Acknowledgments

The authors thank CAPES, CNPq and FAPESP (grant #2022/15205-6) for their financial support.
*Corresponding author: ff.quadros@unesp.br

KINETIC ANALYSIS OF *ESCHERICHIA COLI* ATCC 25922 GROWTH UNDER OXIDATIVE STRESS CONDITIONS USING UV-VIS SPECTROPHOTOMETRY

Eduardo Ferreira Martins[1]*, Marina Clara Ribeiro dos Santos[1], Michaela Shiotani Marcondes[1], Julianna Osses Pinto[2], Alvaro Busquet de Sant'Anna Junior[1], Anelise Osorio Cesar Doria[2], Sonia Khouri Sibelino[1], Argemiro Soares da Silva Sobrinho[1], Rodrigo Sávio Pessoa[1]

[1]*Plasmas and Processes Laboratory (LPP), Aeronautics Institute of Technology (ITA), 12228-900, São José dos Campos-SP, Brazil*

[2] *Research and Development Institute (IP&D), University of Vale do Paraíba (UNIVAP), 12244-000 - São José dos Campos-SP, Brazil*

1. Introduction

Quantitative growth-curve analysis with high temporal resolution is essential to resolve lag, exponential, and stationary transitions and to benchmark bacterial responses to stress [1,2]. Optical density at 600 nm (OD600) is the standard readout, but instrument/pathlength effects make condition-specific calibration advisable; recent workflows show that converting OD to cells·mL^{-1} preserves growth-rate estimates while improving comparability [3,4]. In *Escherichia coli*, hydrogen peroxide (H_2O_2) triggers the canonical oxidative-stress network (OxyR/SoxRS), with damage centered on Fe–S enzymes, DNA, and membranes—making H_2O_2 an informative, tunable stressor for kinetic assays [5]. In parallel, plasma-activated water (PAW) (produced by non-thermal discharges such as dielectric barrier discharge (DBD) and surfatron) accumulates long-lived ROS/RNS (e.g., H_2O_2, NO_2^-, NO_3^-, O_3) and acidifies the medium, jointly underpinning antimicrobial activity [6]. Building on these foundations, we report 24 h growth kinetics of *E. coli* ATCC 25922 at 10-min intervals under graded H_2O_2 (0/50/100 ppm) as a validated benchmark; ongoing work extends the same protocol to PAW generated by DBD and surfatron sources.

2. Experimental

Bacterial growth was monitored for 24 h in Mueller–Hinton broth (MHB), with optical density (OD600) recorded every 10 min on a Thermo Scientific GENESYS 180 UV-Vis spectrophotometer equipped with a Peltier-controlled 10-mm cuvette holder and continuous magnetic stirring. Cultures of *E. coli* ATCC 25922 were inoculated at low initial density to capture the lag phase. For each condition, three independent replicates (2 mL per semi-micro cuvette) were run simultaneously; the instrument was blanked with MHB at the experimental setpoint before acquisition. Tested conditions comprised: (i) control (no stressor) and (ii) H_2O_2 at 0, 50, and 100 ppm, prepared from a fresh stock and mixed directly in MHB immediately prior to monitoring. The acquisition sequence was automated (10-min sampling interval) and the temperature was kept constant at 37 ºC by the Peltier unit throughout the run. Raw OD traces were processed without smoothing; summary curves are presented as mean ± standard deviation (n=3). PAW arms (DBD and surfatron) are being conducted under identical monitoring parameters and will be reported in ongoing work.

3. Results and Discussions

OD_{600} kinetics resolved the canonical phases and showed a clear H_2O_2 dose–response: 25 ppm caused a modest lag with a slight reduction of the plateau, whereas 50–100 ppm produced strong inhibition with pronounced delays and lower final OD (100 ppm most impactful). Replicates were consistent; these curves will serve as the benchmark for forthcoming PAW (DBD/surfatron) assays under identical conditions.

4. References

[1] Pletnev, P. et al. *Survival guide: Escherichia coli in the stationary phase.* **Microbiology** (2015).
[2] Rolfe, M.D. et al. *Lag Phase Is a Distinct Growth Phase That Prepares Bacteria for Exponential Growth.* **mBio** (2012).
[3] Mira, P.M. et al. *Estimating microbial population data from optical density.* **PLOS ONE** (2022).
[4] Stevenson, K. et al. *General calibration of microbial growth in microplate readers.* **Sci. Rep.** (2016).
[5] Imlay, J.A. *The molecular mechanisms and physiological consequences of oxidative stress: lessons from a model bacterium.* **Nat. Rev. Microbiol.** (2013).
[6] Wong, K.S. et al. *Plasma-Activated Water: Physicochemical Properties and Applications.* **Processes** (2023).

Acknowledgments
CAPES (Code 001) and FAPESP (Process: 19/05856-7)
*Corresponding author: eduardomartins@ita.br

PROCESSING OF MULTICOMPONENT TITANIUM METAL MATRIX COMPOSITE BY ARGON ARC MELTING: A NEW HORIZON TO METALLIC BIOMATERIALS

Carlos Eduardo da Silva[1], Jhuliene Elen Muro Torrento[1], Carlos Roberto Grandini[1], Vinícius Richieri Manso Gonçalves[2], Conrado Ramos Moreira Afonso[2], Gerson Santos de Almeida[3], William Fernando Zambuzzi[3], Diego Rafael Nespeque Correa[1]*

[1]*São Paulo State University (UNESP), School of Sciences, Laboratório de Anelasticidade e Biomateriais, Bauru, Brazil*
[2]*Federal University of São Carlos (UFSCar), Department of Materials and Engineering, São Carlos, Brazil*
[3]*São Paulo State University (UNESP), Institute of Biosciences, Laboratório de Bioensaios e Dinâmica Celular, Botucatu, Brazil*

1. Introduction

Metallic biomaterials are conventionally used as hard tissue replacements and surgical instruments, even though the current materials do not match all the clinical needs [1]. Titanium matrix composites (TMC) have demonstrated promising properties for biomedical applications, but the lack of bonding between the matrix and reinforcement during the powder metallurgy processing has resulted in limitations [2]. The goal of this study was to exploit the processing of TMCs using conventional argon arc melting, focusing on evaluating the effect of in situ reactions on the microstructure and properties of interest.

2. Experimental

The TMCs were produced in a two-step argon arc melting. Firstly, two multicomponent TMCs (TiNb and TiNb-ZrTaMo) were produced from raw metals and previously submitted to a vacuum cleaning purge procedure. Then, the ingot was positioned in the crucible with B_4C powder, where the electrical arc was used to melt the metals and induce in situ reactions with the powders. The produced samples were characterized in terms of phase proportion, microstructure, chemical segregation, selected mechanical properties, tribological behavior, and cytotoxicity.

3. Results and Discussions

The results indicated that the argon arc melting technique successfully induced in situ reactions between the B_4C powder and the matrix, resulting in the formation of TiC and TiB precipitates (Fig. 1). The precipitates had distinct morphologies (elongated and round shapes) and had a smooth interface with the matrix, indicating considerable bonding strength. As a result, the samples possessed promising properties, such as high hardness, a relatively low elastic modulus, considerable wear resistance, and no adverse effect on cell viability and proliferation. Thus, the production of TMCs by using argon arc melting can give new perspectives for the next generation of metallic biomaterials that address the current clinical needs for long-term implantation.

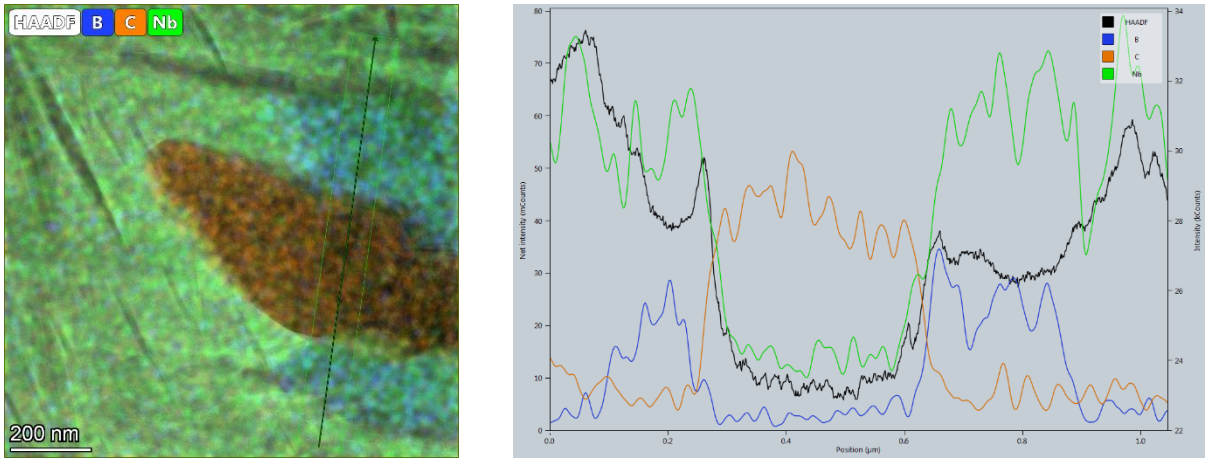

Fig. 1. *Line scan throughout the TiB and TiC precipitates in the Ti-15Nb alloy matrix acquired by STEM (left) and corresponding semi-quantitative result (right).*

4. References

[1] D. C. Maurício *et al.* J. Mat. Res. & Tech., **35**, 4009 – 40019, (2025).
[2] V. R. M. Gonçalves *et al.* J. Mat. Res. & Tech., **30**, 879 – 889, (2024).

Acknowledgments

The authors thank the Brazilian funding agencies CNPq and FAPESP for the financial support.
*Corresponding author: diego.correa@unesp.br

ATOMIC LAYER DEPOSITION OF AL_2O_3 ON PLA: IMPROVING RESISTANCE TO ATOMIC OXYGEN IN LOW-EARTH ORBIT

T. M. Vieira[1], M.P. Gomes[1], N.K.A.M. Galvão[2], F.C. Dalan[1], A.S.S. Sobrinho[1], H.S. Maciel[1*] and R.S. Pessoa[1]
[1]*Plasmas and Processes Laboratory (LPP), Aeronautics Institute of Technology (ITA), 12228-900, São José dos Campos-SP, Brazil*
[2] *Instituto Nacional de Pesquisas Espaciais (INPE), 12227-010, São José dos Campos-SP, Brazil*

1. Introduction

Polylactic acid (PLA) is a biodegradable polymer widely used in additive manufacturing due to its low cost and easy processing [1]. Despite its potential for Aerospace application, PLA has poor thermal stability, low environmental resistance, and degrades under harsh conditions. In low-Earth orbit, atomic oxygen (AO) accelerates surface erosion of PLA [7]. To mitigate this effect, protective coatings such as aluminum oxide (Al_2O_3) deposited by atomic layer deposition (ALD) was studied. Results show ALD Al_2O_3 provides lightweight, uniform protection, improving PLA durability in space.

2. Experimental

PLA samples (20 × 20 × 2 mm³) were 3D-printed with PLA PREMIUM HT filament and coated with Al_2O_3 films by thermal ALD at 100 °C using trimethylaluminum (TMA) and deionized water as precursors. Five coating thicknesses (100, 250, 500, 750, and 1000 cycles) were prepared and immersed into low-pressure oxygen plasma, so being exposed to neutral AO and energetic ion conditions. AO density was measured by optical emission actinometry, while SEM, ellipsometry, and gravimetric analysis evaluated structural and mass changes.

3. Results and Discussions

Even ultrathin films (16.5 nm) effectively protected against neutral AO exposure, while thicker coatings (101 nm) prevented erosion entirely, even under energetic ion conditions. These findings highlight ALD-deposited Al_2O_3 as a lightweight and efficient strategy to enhance PLA durability in harsh LEO environments.

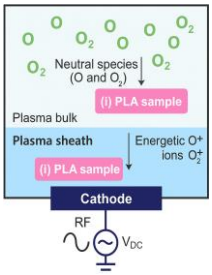

Fig. 1. *Schematic of the RIE setup with PLA samples in two positions.*

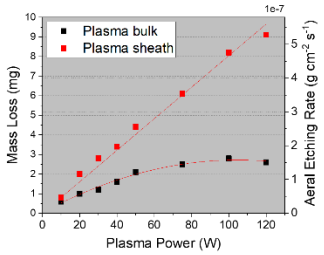

Fig. 2. *Δm (left) and etching rate (right) of uncoated PLA after 1800 s O_2 plasma vs. RF power, for bulk (black) and sheath (red).*

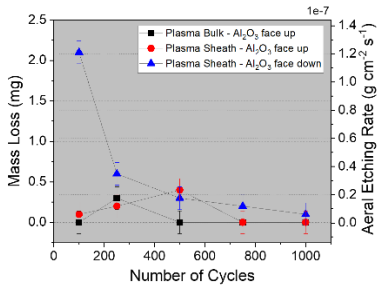

Fig. 3. *Δm (left) and etching rate (right) of Al_2O_3-coated PLA vs. ALD cycles (100–1000). Conditions: 100 W, 1800 s, O_2 plasma at 2×10^{-2} Torr.*

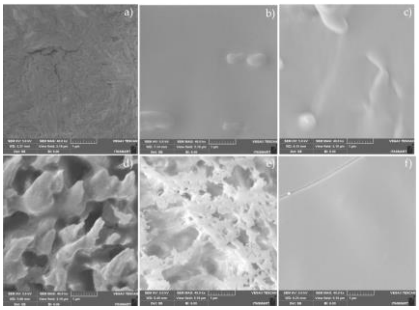

Fig. 4. *SEM micrographs of PLA: (a–c) uncoated, 100 ALD cycles, 1000 ALD cycles; (d–f) same samples after O_2 plasma (100 W, 1800 s, 2×10^{-2} Torr).*

4. References

[1]- P. Favia and R. D'Agostino, Surf. & Coat. Tech., **98**, 1102-1106, (1998).
[2]- H. Yasuda *"Plasma Polymerization"*, 2nd edition, Academic Press, USA, (1980).

Acknowledgments

FAPESP (2022/11544-0), CNPq AEB–Uniespaço (405637/2022-5), CAPES, CNPq and CNPq PCI (300217/2024-2).

EFFECT OF PLASMA COMPOSITION ON THE SURFACE PROPERTIES OF N95 RESPIRATORS

Emily da Silva Belchior[1], Maria Cláudia Batista[2], Elidiane Cipriano Rangel[2]
[1] *ETEC Rubens de Faria e Souza (Sorocaba), Av. Comendador Pereira Inácio, 190 - Jardim Vergueiro, Sorocaba - SP, 18030-005*
[2]*São Paulo State University (UNESP), Institute of Science and Technology (Sorocaba), Av. Três de Março, 511, 18087-180 Sorocaba, SP, Brazil*

1. Introduction

The large-scale disposal of N95/PFF2 respirators during the COVID-19 pandemic has generated significant environmental and economic concerns as well as interest in disinfection methods that enable reuse or safer disposal. Low-pressure plasmas have emerged as a promising alternative for mask disinfection and reuse, as they can inactivate microorganisms by physico-chemical processes, without substantially degrading the supporting material. In this study, the effect of a possible new chemical disinfection route on the properties of commercial N95 respirator fabrics was investigated. Specifically, the influence of varying Ar/O_2 gas ratios in plasmas, in the presence of sodium chlorite powder within the reactor, was evaluated in relation to the physicochemical properties of the respirators.

2. Experimental

The treatments were performed in a low-pressure stainless-steel reactor [1] equipped with a lower electrode, where sodium chlorite powder was placed, and a parallel upper electrode, to which the mask fabric samples were attached. The base pressure of the system was set to 2.0×10^{-2} Torr using a mechanical rotary pump. Argon and oxygen gases were then introduced to reach a working pressure of 7.0×10^{-2} Torr, and the plasma was ignited by applying a radiofrequency signal to the lower electrode. All treatments were carried out for 600 s, varying the Ar/O_2 proportion from 0 to 1. The effect of plasma composition was investigated in terms of the morphology, chemical structure, elemental composition, and wettability of the fabrics, as well as the composition of the plasma phase.

3. Results and Discussions

Argon, oxygen, and chlorine were identified in the plasma, with the relative concentration of Cl-containing groups decreasing with increasing argon proportion. The samples treated in plasmas containing 2% Ar exhibited the least alteration in the fiber morphology. The functional groups detect in the fabrics allowed their identification as polypropylene (PP, white) and polyester (PE, blue) and indicated that the PP functionalities remained stable after treatment. In contrast, PE fibers were more susceptible to modification. Pronounced changes were detected in the hydrophobic (PP) and hydrophilic (PE) characteristics of the fabrics, which tended to recover over time upon exposure to ambient air. The treatment with 2% Ar proved to be the most effective, preserving fiber integrity while promoting the generation of active species. These findings suggest that plasma treatment under low argon concentrations is a promising approach for respirator disinfection and reuse, contributing to waste reduction, cost savings, and environmental benefits.

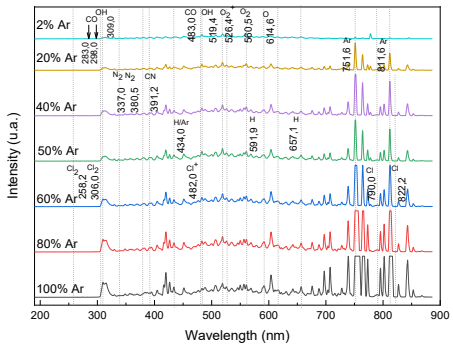

Fig. 1. *Optical emission spectra of the plasmas containing different Ar proportions.*

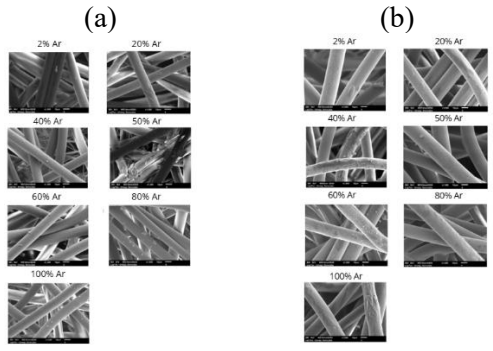

Fig. 2. *Secondary electron micrographs of (a) white and (b) blue fabrics exposed to plasmas with different Ar proportions, along with their respective control samples.*

4. References

[1] Kolowrotkiewicz, J. et ali. (2025), Plasma Processes and Polymers, 22: 70010.

Acknowledgments

The authors would like to thank the FAPESP (2017/21034-1), CNPq-PQ (1929/2021) and CNPq-PIBIC 2024/2025 for its financial support (process #17940).
*Corresponding author: emibelchior2007@gmail.com

STUDY OF SYNGAS PRODUCTION FROM SEWAGE SLUDGE TREATMENT WITH THERMAL PLASMA TECHNOLOGY

Alvaro Busquet de Sant'Anna Junior[1], Felipe de Souza Miranda[2], Pedro William Paiva Moreira Junior[1], Eduardo Petraconi Prado[1], Antonio Carlos da Cruz[1], Alexei Essiptchouk[2], Antônio Ferreira[3], Marcio Fuji[3] and Gilberto Petraconi[1]
[1] *Division of Fundamental Sciences—Technological Institute of Aeronautics*
[2] *Institute of Science and Technology, São Paulo State University*
[3]*Department of Execution of Research, Development and Innovation Project, Sabesp*

1. Introduction

An increase in sewage sludge production has been observed in many countries, and due to organic pollutants and heavy metals present in it, the disposal of this by-product of wastewater treatment has become a major issue for environmental conservation [1]. Traditional methods mitigate the problem but face operational drawbacks. Contrastingly, thermal plasma operates at high temperatures and energy densities, enhancing condensate volume reduction, and energy recovery by syngas [2]. In this context, computational modeling of plasma treatment offers a safe and cost-effective way to parametrize operating conditions to map optimal windows for syngas generation. This accelerates design–optimization cycles and guides scale-up by focusing experimental campaigns on the most promising regions of the parameter space. In this work, we conducted a computational study of sewage sludge treatment in a DC-arc thermal plasma reactor to assess syngas (H_2 and CO) production.

2. Theory

Sewage sludge samples were provided by the Basic Sanitation Company of São Paulo State (Sabesp), and their compositions were determined using X-Ray Fluorescence analysis (XRF). From this characterization, the composition of the resulting gaseous phase was predicted using a non-stoichiometric method based on the maximization of the system's entropy. Different conditions of operation were considered: pyrolysis and gasification with oxygen, air (22% O_2, 78%N_2), and steam.

3. Results and Discussions

A graph containing compound concentration curves for each treatment condition was made, as shown in Figure 1. Figure 2 shows curves for syngas concentration for each condition. The highest syngas production occurs between 1150 and 2000 K in pyrolytic conditions.

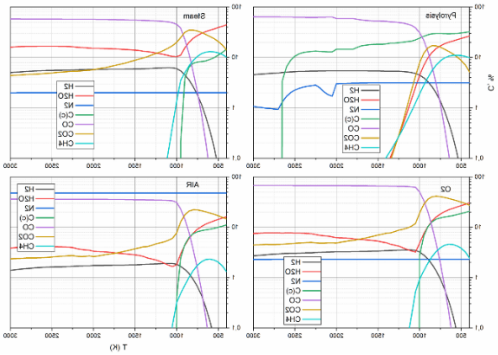

Fig. 1. *Concentration curves of the main compounds as a function of temperature for each type of thermal treatment: pyrolysis and gasification with steam, oxygen, and air.*

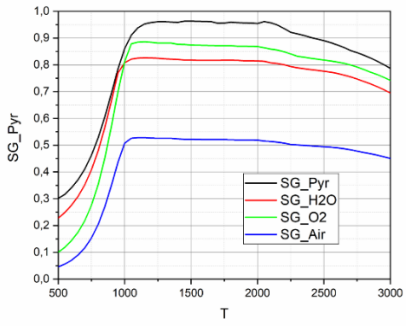

Fig. 2. *Concentration curves of syngas as a function of temperature for each type of thermal treatment.*

4. References

[1] D. Barry, C. Barbiero, C. Briens, and F. Berruti, "Pyrolysis as an economical and ecological treatment option for municipal sewage sludge," *Biomass and Bioenergy*, vol. 122, no. January, pp. 472–480, 2019, doi: 10.1016/j.biombioe.2019.01.041.

[2] X. Cai, X. Wei, and C. Du, "Thermal Plasma Treatment and Co-processing of Sludge for Utilization of Energy and Material," *Energy and Fuels*, vol. 34, no. 7, pp. 7775–7805, 2020, doi: 10.1021/acs.energyfuels.0c00572.

Acknowledgments

Conselho Nacional de Desenvolvimento Científico e Tecnológico (CNPq) (Grant No. 162119/2022-4). Fundação de Amparo à Pesquisa do Estado de São Paulo (FAPESP) (Grant Nos. 2022/03522 7 and 2023/02273-6). Collaboration and material supply: Companhia de Saneamento Básico do Estado de São Paulo—Sabesp.

*Corresponding author: alvaroabsj@ita.br

THE ROLE OF Nb_2O_5-BASED COATINGS IN IMPROVING THE CORROSION RESISTANCE OF FRICTION STIR WELDED 2198-T8 ALUMINIUM ALLOY IN NaCl ENVIRONMENTS

Renato Matos Francoi[1], Murilo Oliveira Alves Ferreira[1], Uriel Darhe Oudinot Dias Rangel[1], Rogério Valentim Gelamo[2], Natália Bueno Leite Slade[2], Haroldo Cavalcanti Pinto[1], Witor Wolf[1], João Carlos Salvador Fernandes[3], Jéferson Aparecido Moreto[1*]

[1]*São Carlos School of Engineering, University of São Paulo (USP), São Carlos, São Paulo, Brazil.*
[2]*Federal University of Triângulo Mineiro (UFTM), Uberaba, Minas Gerais, Brazil.*
[3]*Instituto Superior Técnico, University of Lisbon, 1049-001, Lisboa, Portugal.*

1. Introduction

Friction stir welding (FSW) has emerged as an alternative to conventional joining processes for high-strength metal alloys, offering advantages in material efficiency and cost-effectiveness [1]. However, the microstructural changes induced by FSW influence the mechanical and corrosion properties of aluminium alloys. To address these issues, anticorrosive coatings based on niobium pentoxide (Nb_2O_5) deposited via the physical vapour deposition (PVD) technique appear as a promising strategy to mitigate corrosion in the FSW-affected regions. This study aims to understand the corrosion behaviour of the 2198-T8 alloy post-FSW (nugget zone – NZ) and evaluate the protective efficacy of Nb_2O_5 coatings.

2. Experimental

The material employed in the development of this study was the 2xxx series aluminium alloy, specifically designated as 2198, in the T8 heat-treated condition, intended for use in aircraft fuselages. The deposition of Nb_2O_5 thin films was conducted using the PVD technique on the NZ region as well as the base material. Global electrochemical analyses, including open circuit potential (OCP), potentiodynamic polarisation curves (PPc), and electrochemical impedance spectroscopy (EIS), were conducted in 0.6 mol L^{-1} NaCl solution for the 2198-T8, 2198-T8/FSW, and 2198-T8/FSW/Nb_2O_5 specimens. An extensive morphological and structural analysis was carried out before and after the corrosion tests.

3. Results and Discussions

A comparative analysis of the uncoated samples revealed that NZ exhibited reduced corrosion resistance compared to the base material. However, the Nb_2O_5 coating produced using the PVD technique was able to delay the appearance of pitting on the surface of the 2198-T8/FSW alloy in 0.6 mol L^{-1} NaCl solution. The results demonstrate the efficacy of Nb_2O_5 coatings in safeguarding the 2198-T8/FSW aluminium alloy against aggressive chloride environments, thereby enabling a more effective application of innovative joining techniques such as the FSW process.

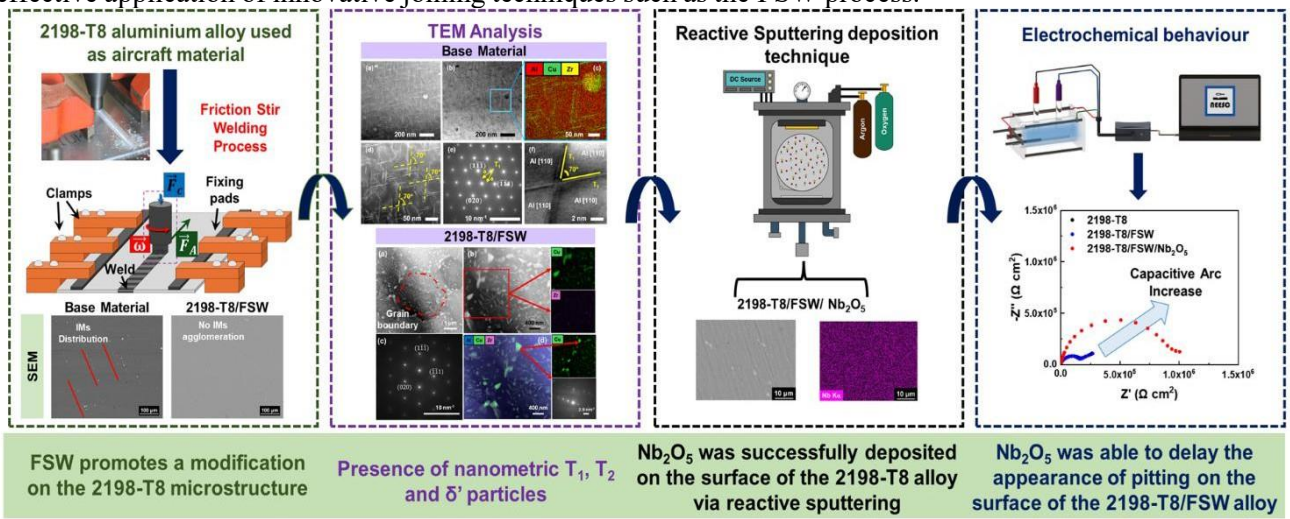

4. References

[1] J.A. Moreto *et al*. Applied Surface Science, 556 (2021), 149750. https://doi.org/10.1016/j.apsusc.2021.149750

Acknowledgments

CNPq-Brazil (402988/2021-3 and 302770/2022-4) and FAPESP (2024/02504-0).
*Corresponding author: jamoreto@usp.br

STRUCTURAL CHARACTERIZATION OF THERMAL BARRIER COATINGS UNDER EXTREME THERMAL LOADING IN SUBSONIC PLASMA FLOW FOR ATMOSPHERIC REENTRY APPLICATIONS

Nazir M. Santos[1], Roberson J. Silva[1], Agatha C. Corrêa[1],Vera L. O. Brito[1]
[1]*Institute of Advanced Studies (IEAv),São José dos Campos, São Paulo,Brasil*

1. Introduction

The development of advanced materials and protective coatings has been critical to the continuous improvement of gas turbines and aerospace propulsion systems, enabling higher operating temperatures, increased efficiency, and extended component lifespans [1]. Among these technologies, thermal barrier coatings (TBCs) play a fundamental role by providing both oxidation resistance and thermal insulation. A conventional TBC system typically consists of three interdependent layers: a metallic bond coat (commonly MCrAlY), which enhances resistance to oxidation and corrosion; a thermally grown oxide (TGO), primarily composed of α-Al_2O_3, that forms during operation; and a ceramic top coat, usually composed of yttria-stabilized zirconia (YSZ), which ensures thermal insulation and resistance to thermal shock [2,3]. These coatings are most commonly applied using atmospheric plasma spraying (APS) due to its versatility and cost-effectiveness [4].

2. Experimental

Thermal barrier coating (TBC) samples were deposited on Ti-6Al-4V (Ti64) substrates using the Atmospheric Plasma Spraying (APS) technique. The coating system consisted of a NiCrAlY bond coat and a yttria-stabilized zirconia (YSZ) top coat. To investigate the microstructural evolution of the TBC system, the samples were exposed to a plasma torch under varying heat fluxes and exposure times. The coatings were characterized before and after exposure using scanning electron microscopy (SEM) equipped with a field emission gun (FEG), energy-dispersive X-ray spectroscopy (EDS), and X-ray diffraction (XRD).

3. Results and Discussions

The correlation between microstructure and performance underscored the critical importance of porosity control, splat cohesion, and interface integrity in optimizing the efficiency of TBCs. Ablation tests conducted under atmospheric plasma exposure demonstrated that the TBC maintained its structural integrity at heat fluxes up to 2.0 MW·m^{-2} for 20 seconds, exhibiting minimal mass loss. This performance was attributed to the coating's low thermal diffusivity, stable emissivity, and high resistance to oxidation and ablation. In contrast, uncoated Ti64 substrates experienced rapid degradation due to oxidation and thermal damage when exposed to a heat flux of 1.5 MW·m^{-2} for 15 seconds.

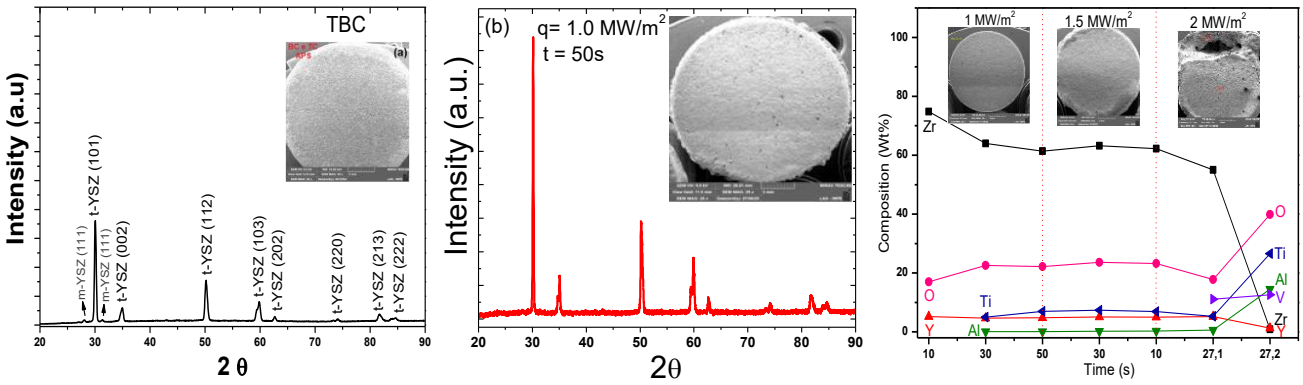

Fig.1. XRD patterns of APS-YSZ coatings before (a) and after (b) ablation at a heat flux of 1.0 MW·m^{-2} for 50 s, and (c) surface composition as a function of exposure time under different heat flux conditions.

4. References

[1] Miller RA. Cleveland: NASA; 2009.
[2] Clarke DR, Phillpot SR. 2005;8(6):22-29. doi:10.1016/S1369-7021(05)70934-2
[3] Liu Q, et al. Journal of Thermal Spray Technology. 2024;33:2723-2733. doi:10.1007/s11666-024-01782-0
[4] Jaworski R, et al. Journal of the European Ceramic Society. 2020;40:3745-3762.

Acknowledgments

COMAER - Ed. CAPA IEAV- PropHiper (Proc. 67720.
*Corresponding author: nazirmonteiro@gmail.com

EXPLORING THE INDIVIDUAL AND COMBINED EFFECTS OF LONG-LIVED REACTIVE SPECIES ON PLASMA-ACTIVATED WATER

Júlia Karnopp[1]*, Helen Caroline de Souza Barros[2], Thais Macedo Vieira[2], Mohammad I Hasan[3], Julio César Sagás[1] and Rodrigo Sávio Pessoa[2]

1 Laboratory of Plasmas, Films and Surfaces, Universidade do Estado de Santa Catarina, CCT-UDESC, Joinville, SC 89219-710, Brazil

2 Laboratory of Plasmas and Processes, Instituto Tecnológico de Aeronáutica, São José dos Campos, SP 12228-900, Brazil

3 Department of Electrical Engineering and Electronics, The University of Liverpool, L69 3GJ Liverpool, United Kingdom

1. Introduction

Plasma-activated water (PAW) is enriched with reactive oxygen and nitrogen species (RONS), which modify its physicochemical properties and broaden its applications in materials science, biomedicine, and agriculture. Among long-lived RONS, hydrogen peroxide (H_2O_2), nitrate ions (NO_3^-), and ozone (O_3) are thought to play key roles in PAW's activity. However, their individual and combined contributions to the unique characteristics of PAW remain unclear. This study aims to elucidate how these species influence PAW's properties and to identify potential additional factors responsible for its distinctive behaviour.

2. Experimental

PAW was generated using a pin-to-liquid plasma system and characterized via UV–Vis spectroscopy, Raman spectroscopy, Fourier-transform infrared (FT-IR) spectroscopy, and measurements of pH, electrical conductivity, total dissolved solids (TDS), and oxidation-reduction potential (ORP). To isolate the effects of individual RONS, aqueous solutions of H_2O_2, NO_3^-, O_3, and a composite solution containing all three at concentrations matching PAW were prepared and analyzed with the same techniques [1].

3. Results and Discussions

The results shown that H_2O_2, led to slight acidification and increased conductivity; NO3− significantly increased conductivity and TDS; O_3 had minimal measurable effects due to low solubility and rapid decomposition. The composite solution showed more pronounced modifications, including enhanced acidification, increased conductivity, and a positive ORP, reflecting partial oxidative conditions similar to PAW. However, none of the individual or combined solutions fully replicated PAW's physicochemical profile, and UV–Vis spectra revealed unique absorbance features in PAW absent in the RONS solutions. Raman and FT-IR analyses suggest that structural reorganization of the hydrogen-bond network and possible contributions from unidentified long-lived species or electrode-derived products are critical for the full activity of PAW.

These findings demonstrate that while H_2O_2, NO_3^-, O_3, each influence specific water properties, their effects alone or in combination do not fully account for PAW's unique characteristics. The enhanced reactivity of PAW arises from both the synergistic action of multiple long-lived RONS and structural alterations at the molecular level, which cannot be reproduced by simple addition of RONS or acidification.

4. References

[1]- Júlia Karnopp et al 2025 J. Phys. D: Appl. Phys. 58 275202

Acknowledgments

Júlia Karnopp, Thais Vieira thank to Coordenação de Aperfeiçoamento de Pessoal de Nível Superior—CAPES for doctorate grant (Finance Code 001). Helen Barros thanks to Fundação de Amparo à Pesquisa de São Paulo (FAPESP) for master grant (Process 2023/10449-7). The author M I Hasan thanks CAPES-Print program version 41/2017.

*Corresponding author: julia_karnopp@outlook.com

STUDY OF ALUMINUM NITRIDE FILMS FOR APPLICATIONS IN SUPERCONDUCTING DEVICES

Agatha Sandes Dutra[1]*, Francisco Rouxinol[2]
[1]*Gleb Wataghin Institute of Physics, State University of Campinas (UNICAMP), Campinas, SP, Brazil*
[2]*Gleb Wataghin Institute of Physics, State University of Campinas (UNICAMP), Campinas, SP, Brazil*

1. Introduction:

Piezoelectric materials have attracted significant attention over the past two decades due to their applicability in various technologies such as oscillators, filters, sensors, and transformers. Aluminum Nitride (AlN) stands out for its non-centrosymmetric crystal structure with a polarized c-axis and a fabrication process compatible with complementary metal-oxide-semiconductor (CMOS) technology. Its crystal structure generates polarization when the material is subjected to mechanical stress — or conversely — characterizing the piezoelectric effect. Thin films with piezoelectric properties will be employed for application in electromechanical resonators.

2. Experimental:

AlN thin films were deposited by Reactive Magnetron Sputtering with an Ar/N_2 flow of 80/30 sccm at different deposition times to generate incremental film thicknesses (Samples A2), enabling the study of deposition rate. These samples were characterized using techniques for chemical composition analysis (Raman Spectroscopy, FTIR, EDS), topology and surface mapping (Profilometry, SEM, and AFM), crystal structure (XRD), and optical properties (Ellipsometry). Subsequently, the nitrogen flow during deposition was varied to produce the A4 samples. Ellipsometry and X-ray diffraction techniques were employed to obtain information on refractive index, crystal planes, and grain size of the samples. The data from A4 and A2 samples were then combined and analyzed.

3.Results and Discussions:

In profilometry (Figure 1), it is observed that increasing the nitrogen flow reduces the film deposition rate. This effect can be explained by the increased collisions between Al atoms and nitrogen after being ejected from the target during the deposition process. The results are consistent with those reported in the literature [2]. In ellipsometry, it is observed that as the N_2 flow increases while maintaining a constant Ar flow, the refractive index of the film decreases, deviating from the expected value when the Ar/N_2 ratio is 1/4. The Ar/N_2 ratios at which reference values of the AlN refractive index were obtained are A4-B and A4-C, corresponding to 1/2 and 1/3, respectively [3].

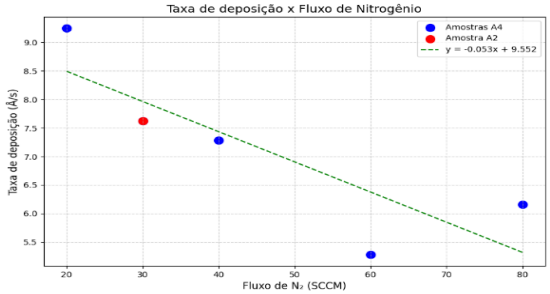

Fig. 1: *Deposition rate as a function of nitrogen flow. In blue, A4 samples. In red, A2 sample. In green, linear fitting of the data by least squares.*

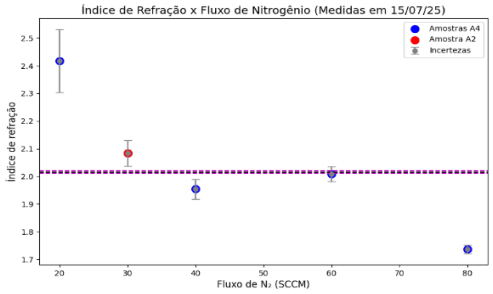

Fig. 2. *Refractive index of A4 and A2 samples as a function of nitrogen flow. In pink, the refractive index of AlN for red light (2.015).*

The XRD (X-ray Diffraction) technique was applied to the A4 samples. The generated spectrum was analyzed in the 2θ range from 30° to 60°, based on reference data and previous studies of earlier samples. In Figure 3, the presence of AlN(101) peaks can be observed in samples A2, A4-C, and A4-D. Peaks corresponding to the AlN(110) crystal structure are visible in all samples [4]. Uniquely in sample A2, a peak associated with AlN(002) is observed, which approaches the background noise level in this measurement [5]. A decrease in the FWHM of the AlN(101) peaks is observed with increasing nitrogen flow. Additionally, the AlN(110) peaks decrease (with increasing FWHM), indicating a reduced presence of this orientation.

4. References:

[1] - O'Connell, A. D. et al. Nature 464, 697–703. 2012
[2] - Chen, Y. et al.. Chinese Journal of Semiconductors 31, 34–35 (2010).
[3] - Choudhary, R. K., et al.,. ISRN Materials, 2015

SIMULATION AND DEVELOPMENT OF HUMIDITY SENSOR TECHNOLOGIES FOR PAPER-BASED DEVICES

Luiz Antonio Rasia[1]*, Carlos Eduardo Andrades[2], Mariana Amorim Fraga[3] and Humber Furlan[4],
[1,2]*UNIJUI- Universidade Regional do Noroeste do Estado do Rio Grande do Sul,*
[3]*MACKENZIE - Universidade Presbiteriana Mackenzie,*
[4]*FATEC – Faculdade de Tecnologia de São Paulo*

1. Introduction

The development of graphite-based sensors on cellulose substrates constitutes a strategic advancement in the field of green electronics, emphasizing the adoption of biodegradable and environmentally sustainable materials. The study demonstrates that cellulose paper is a viable platform for electronic device fabrication, owing to its widespread availability, low production cost, and inherent biodegradability. Additionally, its mechanical flexibility and low mass density render it particularly suitable for integration into wearable systems and Internet of Things (IoT) applications, where lightweight and conformable components are essential.

Materials' mechanical properties, such as resilience and modulus of elasticity, are crucial for the design of sensor devices. Paper's properties vary depending on the orientation of its fibers, so mechanical tensile testing is essential to determine its limits and provide design parameters for sensor devices.

The potential of graphite as a piezoresistive material was validated through electron microscopy, X-ray diffraction, and electromechanical characterization, supporting its application in humidity sensing. This study emphasizes a multidisciplinary methodology that integrates material analysis, mathematical modeling, and cost-effective fabrication processes to enable the development of high-performance graphite-based humidity sensors on paper substrates [1,2].

2. Experimental

The devices were produced in a laboratory at a controlled temperature of 23°C using A4 paper, 2B pencil graphite, copper wire, epoxy glue, and a final encapsulation made of 3D-printed PLA – polylactic acid. The manufacturing process is detailed in stages, from substrate preparation to sensor encapsulation, including graphite deposition on the paper (GoP method) and contact attachment, as shown in Fig. 1 [1].

Fig.2 shows the arrangement for mechanical tensile and humidity testing in a controlled environment and the mounting of the humidity sensor.

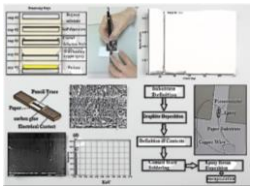

Fig. 1. *Processing steps, SEM of paper and graphite and EDS, flowchart and photograph of a cantilever structure.*

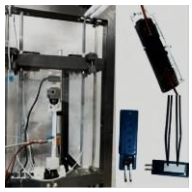

Fig. 2. *Mechanical tensile tests and sensor device encapsulated in PLA, using 3D printing.*

3. Results and Discussions

The experimental data were compared with the proposed mathematical model and show that the model represents the electrical, mechanical and hygroscopic behavior of the graphite sensor element on a polymeric substrate, paper, as illustrated in Fig. 3 and Fig. 4.

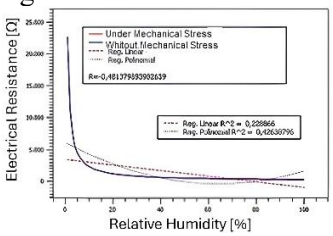

Fig. 3. *Características do comportamento do piezoresistor sem aplicação de tensão mecânica e com tensão mecânica.*

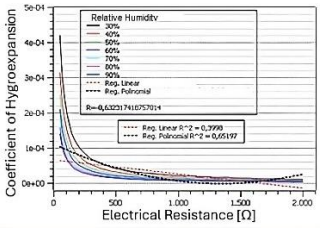

Fig. 4. *Coeficiente de higroexpansibilidade do Sensor de humidade caracterizado.*

4. References

[1]- P. C. Pedrali, L. A. Rasia, A. C. Valdiero and M. A. Fraga. Graphite piezoresistive sensors in polymeric substrates. Int. J. Adv. Eng. Res. Sci., AI Publications, v. 5,**10**, 2456 - 1908, (2018).

[2]- S. K. Mahadeva, K. Walus and B. Stoeber. Paper as a Platform for Sensing Applications and Other Devices: A Review. ACS Appl. Mater. Interfaces, **7**, 8345 – 8362, (2015).

Acknowledgments

The authors thank FAPERGS for financial support through call 06/2023 - PqD.

*Corresponding author : rasia@unijui.edu.br

DEVELOPMENT OF AN EDGE PROTECTIVE DEVICE FOR IMPACT-ABRASION WEAR TESTING

Omar Maluf[1*], Mauricio Angeloni[1], Rosamel Melita Munoz Riofano[1], Marcos Dorigão Manfrinato[2],
[1]*FATEC SERTÃOZINHO*
[2]*FATEC SOROCABA*

1. Introduction

Impact-abrasion wear involves the effects of abrasive particles colliding with a solid surface and causing scratching movements. Other factors, such as particle size, shape, environment, and impact and abrasion rate, together make this a complex problem [1]. This phenomenon is important in wear-resistant steels and welded hardfacing used in mining operations. The objective of this work is to verify the effectiveness of an edge protection device for impact-abrasion wear testing of welded tubular wire overlays using the FCAW process.

2. Experimental

The tubular wires (chemical composition in Table 1) were deposited on the ASTM A36 steel with a two-layer overlap using CO2 as shielding gas. After welding, the specimens and the edge protector device were machined for the impact-abrasion test (Fig. 1). The wear test parameters were: brown corundum (granulometry 5 to 10 mm) as the abrasive; drum rotation was 360 RPM and shaft rotation was 240 RPM, both counterclockwise; test time was 30 minutes (abrasive was changed every 10 minutes), and the impact angle was 90°. Triplicates were performed for the condition with and without the edge protector. The specimens were weighed before and after the test.

3. Results and Discussions

The developed sample holder effectively eliminated the wear effect on the edges of the specimens, transferring this effect to the sample holder. Fig. 2 shows the mass loss graph for the two hard coatings, and it can be observed that with the use of the device, the mass loss is lower because the edge effect does not occur on the coating sample, but on the device. The use of the edge protector device reduced mass loss by 58% for both coatings, thus allowing the observation of tribological phenomena on the surface, eliminating edge wear and masking the results of impact-abrasion wear. The surface hardness of the coating welded with NCSW247CrNbT and NCSW3265T were, respectively, 60.5 ± 0.8 HRC and 58.7 ± 0.6 HRC.

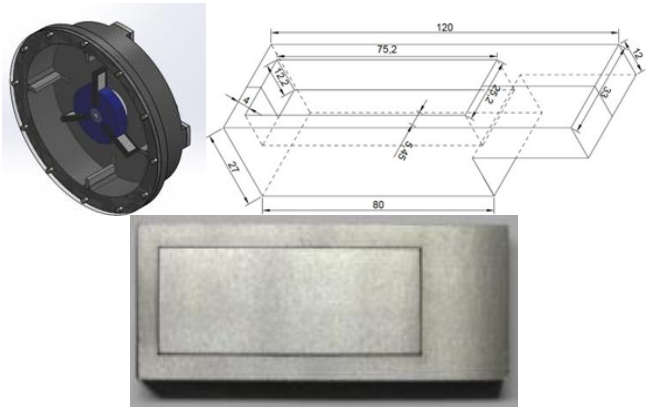

Fig. 1. *Sample holder device*

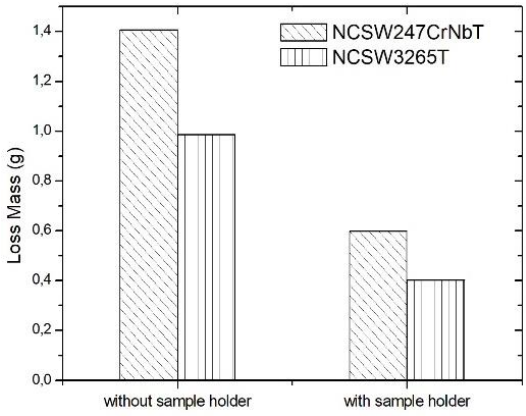

Fig. 2. *Impact-abrasion mass loss*

Tab. 1. *Chemical composition (%wt) of tubular wires*

	ϕ (mm)	C	Si	Cr	Nb	V
NCSW247CrNbT	2,0	3,9	1,4	17,2	2,9	0,6
NCSW3265T	1,6	4,4	0,7	17,0		

4. References

[1]-. BHANSALI, K. MILLER, A.E. Resistance of pure metals to low stress abrasive wear. Wear, v.71, n.3, p. 375 379, 1981.

Acknowledgments
CBMM for financing the project and FATEC Sertãozinho for using the equipment.
*Corresponding author: omar.maluf@fatec.sp.gov.br

SURFACE CHARACTERIZATION OF THE $Ti_{25}Ta_{25}Nb_3Sn$ ALLOY SUBJECTED TO PLASMA ELECTROLYTIC OXIDATION (PEO) TREATMENT

Juliana Layber Mota Engelhardt[1,2], Henrique Engelhardt[1,2], Rafael Resende Lucas[1], Rogério Pinto Mota[1], André Luiz Reis Rangel[1], Ana Paula Rosifini Alves Claro[1]

[1]*São Paulo State University (UNESP), School of Engineering and Sciences, São Paulo, Brazil*

[2]*Fluminense Federal Institute of Education, Science and Technology (IFF), Campos dos Goytacazes, Brazil.*

1. Introduction

The Ti25Ta25Nb3Sn alloy shows great potential in the biomedical field, particularly for bone implant applications, due to its biocompatibility and osseointegration properties. The presence of elements such as tantalum (Ta) and niobium (Nb) helps stabilize the β-phase of titanium, providing a favorable combination of mechanical strength and low stiffness, which is desirable for these devices [1;2]. Surface treatment by plasma electrolytic oxidation (PEO) has emerged as an effective technique to modify titanium alloy surfaces, promoting the formation of stable and adherent oxide layers, including TiO_2. These oxides play a key role in the material's bioactivity, enhancing cell adhesion, an essential aspect for osseointegration [3].

2. Experimental

The alloy, produced from commercially pure Ti, Ta, Nb, and Sn (99.99 wt%), was shaped into discs (10 mm × 4 mm) and surface-treated by plasma electrolytic oxidation (PEO) under direct current (0–550 V). A stainless steel beaker acted as counter-electrode, with mechanical stirring to maintain electrolyte circulation. The electrolyte contained calcium glycerophosphate (0.02 mmol/L), calcium acetate (0.2 mmol/L), and sodium phosphate (9.5 mmol/L), and the treatment lasted 6 minutes. In this work, the oxide layer was characterized through contact angle measurements and Energy Dispersive X-ray Spectroscopy (EDS), which can also be used to estimate the coating thickness, to evaluate the surface properties.

3. Results and Discussions

The results indicated that the variation in voltage during the PEO treatment influenced the surface wettability of the alloy. The contact angles of the samples ranged from 53.2° to 90.2°, with Sample 3 (549 V) showing the most hydrophilic surface, favorable for cell adhesion and osseointegration, while Sample 2 (460 V) exhibited hydrophobic behavior, which may be advantageous in applications requiring reduced initial contact with body fluids. Coating thicknesses ranged from 3.8 to 4.0 µm, showing no direct correlation with wettability, suggesting a complex interaction between processing parameters and surface morphology. These findings highlight the importance of detailed characterization of treated surfaces and indicate that adjusting the PEO voltage can be a strategy to optimize the hydrophilic and hydrophobic properties of the samples, tailoring their performance for specific biomedical applications [1,2].

Fig. 1. *Treated Ti25Ta25Nb3Sn disc, 10 mm × 4 mm.*

Sample	Voltage (V)	Contact angle (°)	Coating thickness (µm)
AM1	350	73,9	3,9
AM 2	460	90,2	3,8
AM 3	549	53,2	4,0

Table. 2. *Measured parameters of Ti25Ta25Nb3Sn samples.*

4. References

[1] - C. Bortolini Jr, et al. Journal of Manufacturing and Materials Processing, **7**(6), 201, (2023)

[2] - G. Beilner, et al. Matéria, **26**(01), e12933, (2021)

[3]- P. Kuroda, et al. Materials, **16**(6), 2352. (2023).

Acknowledgments

The authors thank UNESP-FEG and the Graduate Program in Engineering for their support and the opportunity to participate in academic conferences.

*Corresponding author: juliana.mota@unesp.br

VIOLOGEN-BASED FILMS ELECTRODEPOSITED ON ITO: A STABLE AND CONDUCTIVE PLATFORM FOR IMMOBILIZING MOLECULAR CATALYSTS

Thaisa Brandão Ferreira de Moraes [1*], Eduardo Rezende Triboni[1], Denis Frath [2], Grégoire Jean-François Demets[1] and Christophe Bucher [2]
[1]*Universidade de São Paulo*
[2] *École Normale Supérieure de Lyon*

1. Introduction

Scientific interest in viologen-based polysilsesquioxanes (VG-PS) has grown because of their electroactive properties and stable polymer structure.[1,2] The VG-PS architecture features a 4,4'-bipyridinium core coupled with trimethoxysilane groups (–Si(OMe)$_3$). Viologen components are dicationic in the ground state, but they can undergo reduction to first produce radical cations and then neutral species.[2]

2. Experimental

This study details the fabrication of VG-PS-modified electrodes through electrodeposition, employing various electrochemical methods such as voltammetry and chronocoulometry. The film thickness was controlled by varying the number of voltammetric cycles or adjusting the deposition time. The cationic nature of these films was subsequently used to incorporate anionic species relevant to CO_2 catalysis, including an iron-porphyrin complex. The films were characterized by AFM, spectroelectrochemistry, and electrochemical techniques [3]

3. Results and Discussions

Our results demonstrate that the resulting VG-PS films exhibit high stability, conductivity, and electrochromic properties. Furthermore, we established the feasibility of functionalizing these VG-PS platforms with catalytic molecules, thereby creating films with potential electrocatalytic capabilities.

4. References

[1] L. Chenbao, S. J. Tong, B. Zhang, Y. Chen, G. Zhai, J. Ding, C. Zheng, L. Wang, C. Lu, M. Li, X. Zhuang, Journal of Materials Chemistry A, **7**(41), 23337–23360(2019).
[2] J. G. Croissant, X. Cattoën, J. O. Durand, M. Wong Chi Man, N. M. Khashab, Nanoscale, **8**(48), 19945–19972(2016).
[3] I. Hod, M. D. Sampson, P. Deria, C. P. Kubiak, O. K. Farha, J. T. Hupp, ACS Catalysis, **5**(11), 6302–6309(2015).

Acknowledgments
We thank the financial support from FAPESP (grant n° 2019/27157-3 and 2025/12403-0) and CNPQ (grant n° 402907/2024-8).
*Corresponding author: thaisabrandao@usp.br

BORAX-CROSSLINKED PECTIN FILMS: INSIGHTS INTO THEIR MECHANICAL PERFORMANCE AND THERMAL BEHAVIOR

Natália Vitória Garcia Mendes[1]*, Luís Fernando Zitei-Baptista[2], Delia Rita Tapia-Blácido[2], Eduardo Rezende Triboni[1]
[1] *Lorena School of Engineering, University of São Paulo*
[2]*Faculty of Philosophy, Sciences, and Letters, University of São Paulo*

1. Introduction

Biofilms are commonly developed from proteins, polysaccharides, lipids, or mixtures of these substances. Pectin, a water-soluble polysaccharide, is one of the main materials used for film formation and is typically derived from sources such as citrus peels, apple residues, sunflower seeds, or beet pulp [1]. The water solubility of films made from natural polymers can represent a drawback, One strategy to overcome this limitation involves introducing crosslinks between polymer chains. Such crosslinking also improves its thermal stability and physical properties.

2. Experimental

The experiments were conducted using a base film-forming solution with the same biopolymer (pectin) concentration in water (~0.02 g/mL). For the samples, different concentrations of the crosslinking agent, borax, were added (1.33%, 2.66%, and 4% w/w). The samples were designated as PB 133/100, PB 266/100, and PB 400/100, respectively. A control sample (P), prepared without the addition of the crosslinker, was used for comparison. Finally, the films were prepared by casting method.

3. Results and Discussions

The results demonstrated that the addition of the crosslinking agent led to an increase in the thermal stability of the pectin films crosslinked with borax (Fig.1). Table 1 shows that films showed reduced moisture absorption (52.55→22.68%) and an initial ~30° drop in contact angle, followed by an increase with higher borax levels. Thickness rose (0.09→0.27 µm), while tensile strength, Young's modulus, and elongation significantly decreased. The crosslinker first increased hydrophilicity by introducing OH-interacting groups, but higher concentrations caused electrostatic repulsion, reducing this effect. Overall, borax proved to be a promising crosslinking agent for improving the thermal and physicochemical properties of pectin films

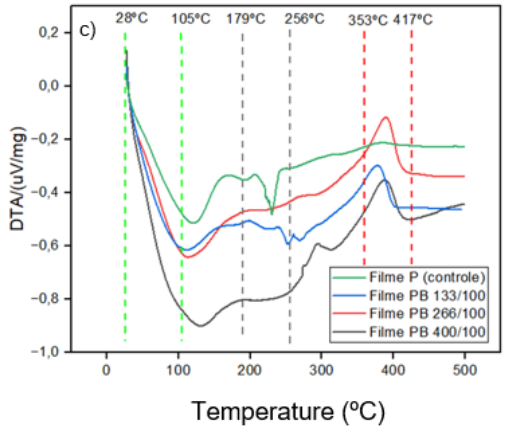

Fig. 1. *DTA analysis of the samples .*

Table. 1. *Mechanical properties of the samples.*

Film	Moisture (%)	Thickness (µm)	Tensile break (MPa)	Elongation (%)	Young Modulus (MPa)	Contact Angle (°)
P	52.55±0.31a	0.09±0.06c	20.36±0.18a	21.09±0.36a	269±6a	61.95±0.08a
PB 133/100	26.66±0.64b	0.10±0.01bc	9.50±0.51b	12.52±0.14c	141±9b	31.93±0.23c
PB 266/100	26.26±0.85b	0.27±0.02a	1.87±0.12d	19.93±0.32b	23±2d	32.28±0.07c
PB 400/100	22.68±0.35c	0.21±0.01b	2.32±0.19c	6.67±0.34d	69±8c	38.39±0.44b

4. References

[1]- B.R. Thakur, R.K. Singh and A.K. Handa, Crit. Rev. Food Sci. Nutr., 37, 47-73, (1997).
[2]- S. Young, M. Wong, Y. Tabata and A.G. Mikos, J. Control. Release, 109, 256-274, (2005).

Acknowledgments

Thanks Truly Nolen and FAPESP 2024/09719-2.
*Corresponding author: natalia_mendes@usp.br

COMPOSITE DEVELOPMENT FOR REUTILIZATION OF METAL CONTAMINATED POLYMER

Alana M. Corá[1]*, Jane M. F. de Paiva[2], Elidiane C. Rangel[3], Silvia P. Irazusta[1]
[1]*Faculdade de Tecnologia de Sorocaba (Fatec)*
[2]*Universidade Federal de São Carlos (UFSCar) - Campus Sorocaba*
[3]*Instituto de Ciência e Tecnologia (UNESP) - Campus de Sorocaba*

1. Introduction

In the field of civil construction, the reuse of waste materials in the production of composites is a common practice. With the increasing use of polymers for soil remediation, another type of waste is generated. Thus, the development of composites as a means of reusing this waste has become a growing practice, in which residues are incorporated into a different matrix and employed as reinforcement in the composite [1].

2. Experimental

The potential application of the sodium polyacrylate (PAS) after its use in a soil remediation of metallic contaminants was conducted by evaluate its incorporation in a composite as constructive material. For the preparation of the specimens, samples were produced with and without PASe, in triplicate, using cement and sand (1:3) with 2% PAS. The samples were molded into PVC cylinders measuring Ø5×10 cm and cured for 7, 14, and 28 days. The tests followed the ABNT 7215 standard for Portland cement to compressive strength test and were analyzed by Scanning Electron Microscopy (SEM).

3. Results and Discussions

The control preparation without PAS addition, exhibited a progressive increase in compressive strength (Fig. 1), as curing time advanced. In contrast, the PAS composite showed a reduction in strength,as compared with the control cement. However, when comparing the compressive strength of the composite at 28 days with the control at 7 days, the values were comparable. These findings suggest that composite with the PAS may require extended curing times in order to achieve compressive strength levels equivalent to those reached by standard preparation at shorter curing times. The SEM analysis, represented by the Fig. 2, 3, and 4, of the control and composite samples (40x) reveals differences in microstructure over time. In the 7 and 14 day samples, the composite (Fig. 2b and 3b) exhibits greater heterogeneity and porosity compared to the control (Fig. 2a 3a), associated with the presence of PAS. After 28 days, the composite surface becomes similar to that of the control samples. In short, the reuse of the waste generated in remediation in another production process, such as the one presented here, offers the closing of the PAS cycle, in accordance with the principles of circularity.

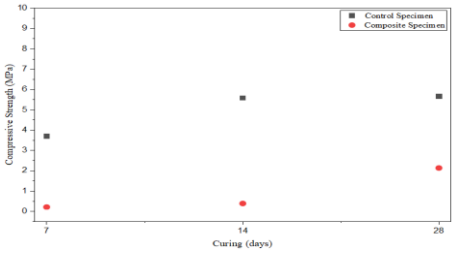

Fig. 1. *Compressive strength of control and composite samples at different curing times.*

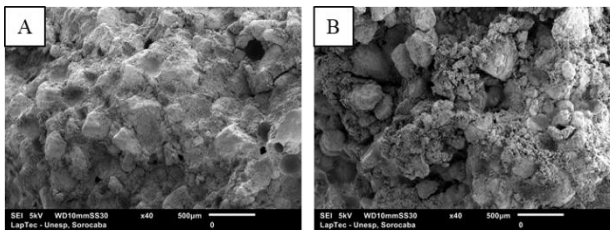

Fig. 2. *SEM images of the 7 days specimens, where A. represents the control and B. the composite*

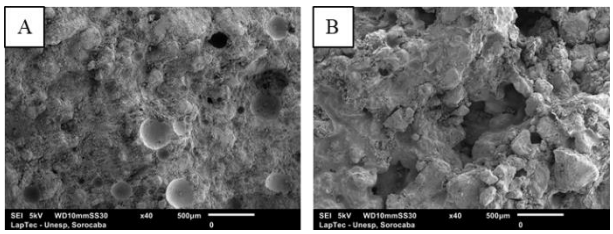

Fig. 3. *SEM images of the 14 days specimens, where A. represents the control and B. the composite*

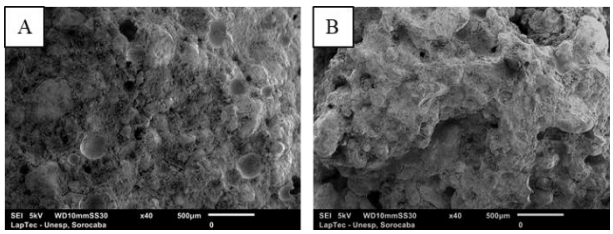

Fig. 4. *SEM images of the 28 days specimens, where A. represents the control and B. the composite*

4. References

[1] – N. T. A, Filho *et al*. Rev. Bras. de Eng. Agrícola e Ambiental, **16**, 894-902 (2012).

Acknowledgments

To FAPESP for the Process No. 2022/49136-3.
*Corresponding author: alana.cora@gmail.com

PROCESSING OF TI-33ZR-33NB BETA ALLOY PROCESSED BY CASTING, LASER 3D PRINTING, AND SEVERE PLASTIC DEFORMATION

Conrado R. M. Afonso[1], Mariana L. Lourenço[1], Marcio Sangali[2], Athos Plaine[3], Rubens Caram[2]
[1]*Universidade Federal de São Carlos (DEMa /UFSCar), 13565-905, São Carlos/SP, Brazil,*
[2] *Universidade Estadual de Campinas (FEM/Unicamp), Campinas - SP, 13083-970, Brazil*
[3]*State University of Santa Catarina (UDESC),Malschitzki, 89219710 Joinville, SC, Brazil*

1. Introduction

β-type titanium alloys have attracted considerable attention for biomedical applications due to their good properties. The Ti-Nb-Zr system stands out for its ability to tailor properties through compositional control and thermomechanical processing. Severe plastic deformation techniques have been employed to refine the microstructure of various metal alloys, thereby enabling the formation of ultrafine grains and enhancing their mechanical performance [1-2]. The LPBF technique guarantees samples with precise geometry, in addition to having a very high cooling rate, favoring the formation of refined microstructures and metastable phases, which can result in good mechanical properties.

2. Experimental

The alloy was synthesized under three conditions: i) as-cast (AC) and subjected to hot rolling; ii) additive manufacturing using laser powder bed fusion (LPBF) with a power of 200 W and laser speeds ranging from 500, 750, and 1000 mm/s; and iii) severe plastic deformation by ECAP at two temperatures (25 °C and 350 °C). Microstructural characterization was studied by OM, SEM, TEM, EBSD, and ASTAR. Mechanical and physical characterization was performed by determining micro- and nanohardness and the modulus of elasticity. Thus, the objective is to evaluate the effect of grain refinement using different techniques on the multiprincipal β Ti-33Nb-33Zr alloy as a candidate for biomaterials for implants.

3. Results and Discussions

The microstructure revealed that rolling promotes dynamic recrystallization, while ECAP intensely refines the grains, especially after two passes. Microhardness increased after rolling and remained stable after ECAP, a balance between grain refinement and stress relief. Among the LPBF samples, a slight downward trend in microhardness (316-312-309 HV) was observed, due to the increase in porosity in the alloy as the laser scanning speed (500-750-100 mm/s) increased. The elastic modulus was approximately 80 GPa in all treatments, a result attributed to the stable structure of the β phase and the unchanged chemical composition, revealing values comparable to those of cortical bone. Overall, the results demonstrate that controlled application of ECAP, combined with thermal regulation, and LPBF-printed samples can effectively optimize β-Ti alloys for biomedical implants, increasing mechanical strength while maintaining elastic compatibility with bone.

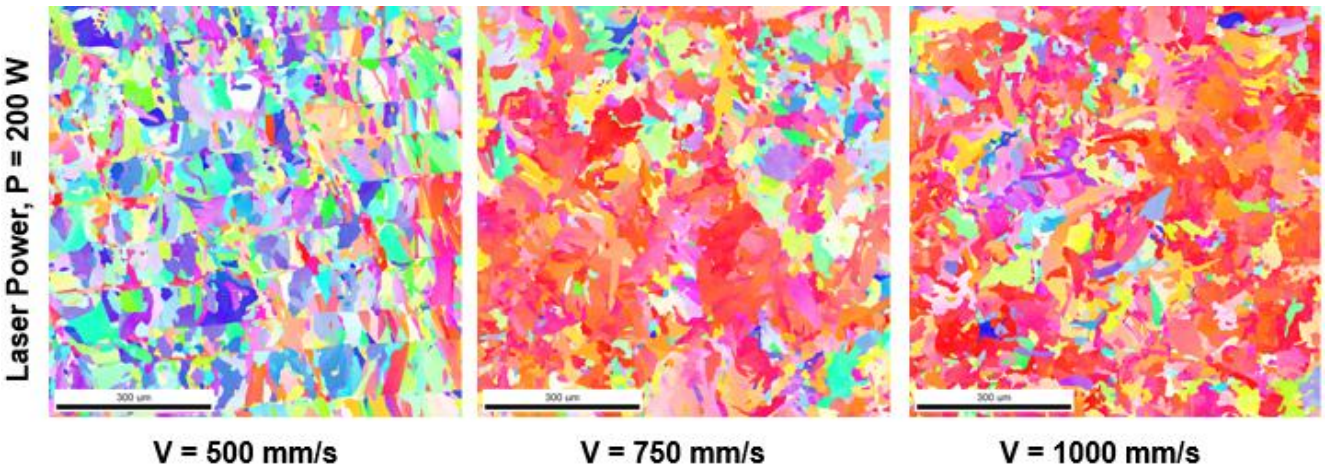

Figure 1 – SEM-EBSD analysis showing 3D Print multiprincipal β Ti-33Nb-33Zr alloy under P = 200 W and varied speed of 500, 750 and 1000 mm/s, from ultrasonic atomized powder.

4. References

[1] R. Silva, et.al., Journal of Materials Research and Technology, **35**, 2055-2067, (2025).
[2] R.F.M. dos Santos, er.al. Journal of Materials Research, **40**, 548-559, (2025).

Acknowledgments

The authors would like to thank FAPESP, CAPES, and CNPq for their financial support.
*Corresponding author: conrado@ufscar.br

STUDY OXIDATION AND FATIGUE AT HIGH TEMPERATURES OF THE MAR-M247(Nb) ALLOY

Rogério Varavallo[1]*, Cassius Olivio Figueiredo Terra Ruchert[2], Marcos Dorigão Mnafrinato[3]
[1]*Centro Universitario Unica*
[2]*Escola de Engenharia de Lorena (EEL-USP)*
[3] *FATEC Sorocaba*

1. Introduction

The design of jet engines was theoretically possible at the beginning of the 20th century, but their practical application only became feasible with the development of superalloys. This term emerged after World War II to describe high-performance materials that maintain their mechanical properties above 540°C in corrosive environments. Composed mainly of nickel, iron, and cobalt, and elements such as chromium, nickel superalloys have become the most widely used in various high-temperature applications, such as aircraft turbines. Their excellent mechanical strength over a wide temperature range is the main reason for their predominance, with no substitutes to date[2]. The objective of this work was to determine the fatigue limit of the MAR-M247(Nb) alloy and the mass gain at high temperatures of the MAR-M27 and MAR-M247(Nb) alloys.

2. Experimental or Theory

The MAR-M247 (Nb) alloy was tested using high cycle fatigue, in accordance with ASTM E466-07, at temperatures of 700 and 900°C, and oxidation testing in accordance with ASTM G54-84, carried out at temperatures of 500 and 1000°C for 470 and 360 hours, respectively. For comparison purposes, SAE 1020 steel and AISI 304 austenitic stainless steel test specimens were added to the oxidation test. Table 1 shows the chemical composition in weight percentage of the MAR-M247 and MAR-M247(Nb) alloys.

3. Results and Discussions

Fig. 1 shows the mass gain of each material for each temperature of the oxidation test. Fig. 1 shows the exponential mass gain that 1020 carbon steel exhibited at both temperatures. At a temperature of 500°C, the MAR-M247 and MAR-M247(Nb) alloys were close to the mass gain of AISI 304 stainless steel. At a temperature of 1000°C, however, the MAR-M247 and MAR-M247(Nb) alloys showed a lower mass gain due to their resistance to high temperatures. The SN curves in Fig. 2 show that the increase in temperature reduces fatigue life when comparing the same amplitude levels. For example, at 500 MPa at 700°C, a life close to 10^4 cycles was determined, while at the same stress at 900°C, the life found was below 10^3 cycles.

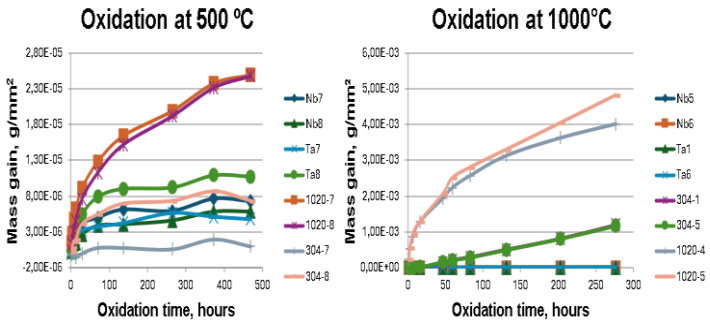

Fig. 1. *Oxidation test for 500°C and 1000°C.*

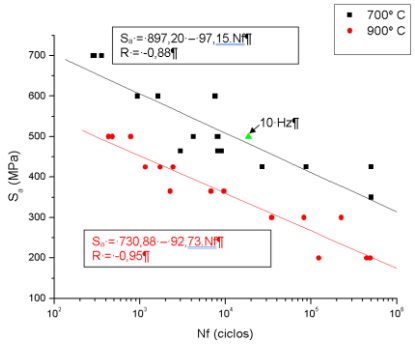

Fig. 2. *SN curve MAR-M247(Nb) for 700°C and 900°C.*

Tab. 1. *Chemical composition (%wt) of MAR-M247 and MAR-M247(Nb) alloys*

	C	Si	Cr	Mo	Fe	V	W	Cu	Al	Co	Nb	Ti	Ni	Hf	Ta	Zr
MAR-M247	0,11	0,062	8,38	0,64	0,07	0,03	9,55	0,0125	5,9	10	<0,02	1,06	59,7	1,32	3,12	0,051
MAR-M247(Nb)	0,12	0,035	8,49	0,64	0,08	0,03	9,48	<0,005	6	10	1,76	1,08	60,6	1,38	0,09	0,054

4. References

[1]- BRADLEY, E. F. (1988). **Superalloy:** a technical guide. Materials Park: ASM International, 280 p.
[2]- HUSSAIN, N. et al. (2004). **Oxidation of Metals**, New York, v. 61, n. 5-6, p. 355-364.
*Corresponding author: rogeriovaravallo@gmail.com